Contribution to understanding the formation process and corrosion protection of the PEO coating on AM50 magnesium alloy

Dissertation

Zur Erlangung des Grades eines Doktors der Ingenieurwissenschaften

vorgelegt von

Alireza Ghasemi Abyazani

aus Teheran / Iran

genehmigt von der

Fakultät für Natur- und Materialwissenschaftlichen

der Technischen Universität Clausthal

Tag der mündlichen Prüfung
07.06.2011

Die Arbeit wurde durchgeführt am

Institut für Nichtmetallische Werkstoffe
der Technischen Universität Clausthal

Hauptberichterstatter……...Prof. Dr.-Ing. Jürgen. G. Heinrich
Berichterstatter……...Prof. Dr.-Ing. Karl U. Kainer
Vorsitzender der Prüfungskommission…… Prof. Dr. rer. nat. Winfried Daum

Acknowledgments

I would here like to express my thanks to the people who have supported me during the time it took me to complete my PhD. It would not have been possible to fulfil this work without their help and financial support of the German academic exchange service (DAAD) and Helmholtz-Zentrum Geesthacht.

I gratefully acknowledge Prof. Dr.-Ing. Karl U. Kainer and Prof. Dr.-Ing. Jürgen G. Heinrich for their precious comments and supervision. Their attitude showed me how to approach the scientific subjects by the systematic way of thinking and organized method of researching.

I wish to express my sincere gratitude to Dr. Wolfgang Dietzel who has always been very approachable and helpful to me and never withheld his support and encouragement from the preliminary to the concluding level of my work in Helmholtz-Zentrum Geesthacht. It is also a pleasure to convey my gratitude to Prof. Dr. V. S. Raja of the Indian Institute of Technology who taught me the new analyzing methods and patiently answered my questions.

I would extend my thanks to all my colleagues in material research institute, who helped me in various technical and personal matters during my stay in Helmholtz-Zentrum Geesthacht. It is a pleasure to thank Dr. C. Blawert for his comments and advice. Moreover I am very thankful to Dr. N. Scharnagl, Dr. P. Bala Srinivasan and Dr. J. Liang who gave me interesting feedback and valuable suggestions. I would also like to be grateful for the technical support and assistance extended by Mr. U. Burmester and V. Heitmann.

I would like to offer my regards and blessings to my father and mother for their infinite kindness and support which I am continuously receiving from them.

Lastly but above all, I gratefully appreciate my beloved wife, Sepideh whose love and kindness offered me confidence and endurance in hard moments of life. I am thankful, not only for her spiritual support but also for the scientific suggestions and discussions she offered me during completion of the work.

I thank God by standing by me.

Zusammenfassung:

Die plasmaelektrolytische Oxidation (PEO), die auch unter der Bezeichnung Micro Arc Oxidation (MAO) bekannt ist, ist ein Prozess, mit dem stabile und gut haftende Oxidschichten auf der Oberfläche von Metallen, wie Aluminium, Titan und Magnesium, erzeugt werden. Durch das Aufbringen einer PEO-Beschichtung insbesondere auf der Oberfläche von Magnesiumwerkstoffen kann das Substrat vor Korrosion und Verschleiß geschützt werden. Der PEO-Prozess basiert auf der anodischen Oxidation der Oberfläche des Metallsubstrates, das dazu an eine Hochspannungs-Stromversorgung angeschlossen und in einen geeigneten Elektrolyten getaucht wird. Durch das Anlegen einer hohen elektrischen Spannung wird auf der Oberfläche des Substrates nach dem Überschreiten einer Durchbruchspannung ein Plasma erzeugt, das mit dem Entstehen von Funken an der Substratoberfläche einhergeht. In der vorliegenden Arbeit wurden vor allem der Entstehungsprozess und die Struktur der sich dadurch bildenden PEO-Beschichtungen sowie der Einfluss der Zusammensetzung des Elektrolyten auf die Stabilität der Passivschicht und auf die Korrosionsbeständigkeit von PEO-Beschichtungen auf Substraten aus der Magnesiumlegierung AM50 untersucht.

Der Mechanismus der Schichtbildung auf jeder der Substratphasen, d.h. Al_8Mn_5, $Mg_{17}Al_{12}$ (β-Phase) und α-Mg, wurde jeweils für sich betrachtet. Dabei wurden der Einfluss der Konzentration der Lösung und der Prozessdauer auf den Entstehungsprozess durch die Erzeugung von Beschichtungen in verdünnten, mittel und stärker konzentrierten Elektrolytlösungen bei kurzen, mittleren (vor und nach dem Erreichen der Durchbruchspannung) und langen Beschichtungszeiten untersucht. REM-, XRD-, XPS- und EDAX-Untersuchungen ermöglichten eine detaillierte Analyse der Schichtmorphologie, der Phasenbildung und -verteilung sowie der Schichtzusammensetzung.
Der Einfluss der Zusammensetzung des Elektrolyten auf die Stabilität der Passivschicht und die Korrosionsbeständigkeit der PEO-Beschichtung wurde in Silikat-, Phosphat- und Aluminat-Lösungen untersucht. Grundlegende Parameter der Lösung, wie pH und Leitfähigkeit, wurden gemessen und die Beschichtungen im Hinblick auf ihre Oberflächenmorphologie, den Querschnitt und die Phasenzusammensetzung charakterisiert. Die Ermittlung der Stabilität der Passivschicht und der Korrosionsbeständigkeit der PEO-Beschichtungen erfolgten durch elektrochemische Impedanzspektroskopie (EIS) und Polarisationsmessungen, wobei die Struktur und das Korrosionsverhalten der Beschichtung sowohl anhand ihrer Morphologie als auch durch einen Vergleich der gemessenen Impedanzkurven mit anhand elektrischer Ersatzschaltkreise simulierten Kurven charakterisiert wurden.

Es zeigte sich, dass die verschiedenen Phasen des Substrates Auswirkungen auf den Entstehungsprozess, die Morphologie und die Zusammensetzung der Beschichtung haben. Dabei wurde davon ausgegangen, dass die Schichtbildung auf der Al_8Mn_5-Phase an der Partikel/Matrix-Grenzfläche beginnt und dass die Oberfläche dieser Phase dem Überschreiten der Durchbruchspannung in gleicher Weise an der Schichtbildung beteiligt ist. Die Beschichtung auf diesen Partikeln erwies sich jedoch als abweichend von derjenigen auf der Matrix. Der Schichtbildungsverlauf auf der β-Phase zeigte, dass hier die Durchbruchspannung im Vergleich zur Matrix später überschritten wurde. Die Poren auf den β-Partikeln waren größer und die Beschichtung besaß eine andere Zusammensetzung als diejenige auf der Matrix. Die Schichtbildung auf der α-Mg-Matrix begann mit einem netzartigen Abscheidungsmuster, im weiteren Prozessverlauf wurde die gesamte Oberfläche gleichmäßig bedeckt. Diese Bedeckung der Oberfläche führte zum Überschreiten der Durchbruchspannung, mit dem die Bildung der PEO-Beschichtung einsetzte. Die Analyse der Phasenverteilung über den Querschnitt zeigte, dass die Phasenbildung in der Beschichtung in einer bestimmten Reihenfolge erfolgte, wodurch verschiedene Schichten mit speziellen Zusammensetzungen entstanden. Es erwies sich ferner, dass eine Abweichung von einer mittleren Konzentration der Lösung diesen Effekt verstärkte.

Die Ergebnisse zeigten außerdem, dass sich die Stabilität der Passivschicht unmittelbar auf die Korrosionsbeständigkeit der endgültigen PEO-Beschichtung auswirkte. Unter den gewählten Beschichtungsbedingungen ergab eine Na_2SiO_3 + KOH-Lösung eine stabilere Passivschicht und damit eine PEO-Beschichtung mit höherer Korrosionsbeständigkeit als die übrigen verwendeten Elektrolyten.

Stichworte: plasmaelektrolytische Oxidation, Beschichtung, Magnesium, Korrosion

Abstract:

Plasma Electrolytic Oxidation (PEO), known also as Micro Arc Oxidation (MAO), is a process which is capable of producing stable and adherent oxide layers on the surface of metals such as aluminium, titanium and magnesium. Application of the PEO coating, particularly on the magnesium surface, can protect the substrate against corrosion and wear. The process takes place on the basis of anodic oxidation of the metal which is connected to a high voltage power supply and immersed in a proper electrolyte. Application of high potential gives rise to a plasma environment which appears as scatter sparks on the surface during the process. The present work mainly studies the "formation process and structure of the PEO coating" as well as the "influence of the solution composition on the stability of the passive layer and corrosion resistance of the PEO coating" on the AM50 magnesium alloy.

The coating formation on each substrate phases, namely Al_8Mn_5, $Mg_{17}Al_{12}$ (β-phase) and α-Mg, was individually studied. The influence of solution concentration and coating duration on the formation process was also considered by preparing the coatings in diluted, medium and concentrated solutions within short, intermediate (Pre and post breakdown) and long durations of coating periods. The SEM, XRD, EDAX and XPS methods were employed to study the coating morphology, phase evaluation, layer composition and phase distribution, respectively.

The influence of the solution composition on the stability of the passive layer and the corrosion resistance of the PEO coating was studied in silicate, phosphate and aluminate base solutions. Basic properties of solution such as pH and conductivity were measured and the coatings were characterized by considering the surface morphology, cross section and phase composition. The stability of the passive layer and the corrosion resistance of the PEO coatings were determined by different evaluation methods i.e. impedance and a polarization test. The structure and corrosion behaviour of the coating was studied by considering the coating morphology and fitting the proper curves to the impedance data. The curve fitting method can provide more information about the coating layers and the corresponding corrosion resistance.

The study of the formation process showed that the components of the substrate affect the formation process, morphology and composition of the coating layer. It was considered that the formation process on Al_8Mn_5 initiated from the particle/matrix interface and the surface of this phase involved in the PEO coating concurrent with the breakdown phenomenon. However the coating formed on this particle showed discontinuity with that on the matrix area. The formation process on the β-phase showed that breakdown phenomenon occurred on the β-particle with a delay compared to that on the matrix. The size of the pores was bigger and the coating had a different composition compared to that on the matrix. The layer formation on the α-Mg matrix was initiated with a net like deposition pattern which covered the whole area as the process proceeded. Coverage of the surface gave rise to the breakdown phenomenon and subsequently the PEO coating started to form. The results regarding the distribution of the phases through the cross section showed that the phases form in the coating by following a sequential order. This effect generates different layers which have specific compositions. It was also seen that deviation from an intermediate solution concentration intensifies the latter effect.

The results showed that the stability of the passive layer has a direct influence on the final corrosion resistance of the PEO coatings. Under the conditions employed, the Na_2SiO_3+KOH was the solution which formed a more stable passive layer and therefore produced a PEO coating showing higher corrosion resistance compared to the other solutions.

Keywords: Plasma electrolytic oxidation, coating, magnesium, corrosion

TABLE OF CONTENTS

1 Introduction

Growing concern about the green house effect and increasing fuel costs have been major driving motivations to develop light weight materials for different applications. Many manufacturing industries today face a common objective of reducing the weight of their products. This is particularly relevant to those manufacturing organisations serving the transportation industry in for example the automotive and aerospace areas.

Magnesium, being one of the lightest engineering metals, remains a potential candidate material for such applications. There has been a surge in the recent years, in the development of a variety of magnesium alloys which can exhibit more appropriate mechanical properties such as strength and creep resistance. Improvements in mechanical properties to weight ratios can justify the growing demand for magnesium and its alloys.

Nevertheless, large volume usage of magnesium is constrained, mainly because it is highly susceptible to corrosion. Magnesium and its alloys are prone to corrosion, by virtue of magnesium being one of the most reactive metallic elements. Unlike aluminum and titanium, the oxide forming on the magnesium surface is not able to protect the substrate. So, in order to derive benefit from the several advantages offered by magnesium and its alloy, development of an effective corrosion protection technology seems to be imperative.

Among different protective methods, plasma electrolytic oxidation (PEO) is an effective process which is able to produce a stable oxide layer on the surfaces of magnesium and its alloys. The PEO coatings possess unique physical and mechanical properties providing both a high degree of hardness and a strong adhesion to the substrate. Subsequently it can effectively improve the corrosion and wear resistance of the base metal [1-3]. During the PEO treatment, many different processes occur at the electrode surfaces, such as dissolution of substrate, dielectric breakdown and formation of an oxide ceramic layer [4]. These make it a complex process which is not trivial to study. In the PEO process, the substrate forms the anode which is

immersed in a suitable electrolyte and is connected to the positive terminal of a high voltage power supply. By increasing the voltage over a certain value (i.e. breakdown voltage), some dispersed discharges can be observed on the metal surface. The plasma chemical reactions occurring in the region of each discharge leads to conversion of the surface to a stable and protective oxide layer [5].

With the aim of improving the corrosion resistance of the PEO coating, several studies have so far been done. The final performance of the coating has been related to the thickness [6,7], morphology [8-10] and phases of the coating [11-13] which are known as the effective parameters. However these parameters were taken into account without considering the formation process which is the factor determining the final characteristics of the effective parameters. The formation of the coating is the process which is influenced by the *microstructure* of the substrate and the *concentration* of the solution. The *microstructure* of the substrate is usually composed of different particles which have different compositions and specific crystallographic arrangements [14-17]. Different characteristics of the particles impose direct influence on the formation process and results in a different morphology and composition of the PEO coating. The *concentration* of solution is the parameter which determines the abundance of the constructive species in the solution which are required for formation of the coating. The concentration is the only factor which influences the formation process of the coating by changing the breakdown value.

The role of the passive layer in the PEO process is another issue which has not been studied in detail. It was mentioned that high potential is required to be applied for the formation of the PEO coating. High potential provides enough energy for a current to pass through the surface by breaking down the resistance of the dielectric layer on the surface. It is believed that this resistance originates from the passive layer formed on the surface during the first steps of the PEO process [18,19]. The existence of the passive layer after the breakdown phenomenon, the influence of the passive layer on corrosion resistance of the PEO coating, the stability of the passive layer in different solutions are still among the open questions in the study of the PEO process.

The influence of the solution composition on the corrosion resistance of the PEO coating will be considered in the present study. According to the literature, a suitable solution for the PEO process usually consists of two or more components, i.e., a salt and a hydroxide. Each component introduces different cations and anions into the solution which consequently influences the resultant coating [3]. The chemical composition of the electrolyte is the factor influencing the final properties of the coating. Many works have been studied the influence of the different electrolytes on the properties of the PEO coatings. The aim of these works was optimization and improvement in the performance of the coating [11,12,20]. However there are still contradictory results which need to be made clear by appropriate explanation. Ma et al. [7] reported that on the pure magnesium, the coating prepared in a phosphate solution has better corrosion resistance compared to the oxide films grown from a silicon based solution. However, the conclusions of Cai et al. [2] indicate that the silicon based coatings show better corrosion performance than the phosphorous based coatings.

The study of the formation process on each substrate phase and the effect of concentration on the formation process are among the basic issues which have not been considered systematically and they are incompletely understood. Understanding the way the PEO coating forms, grows and covers the surface of each component in different concentrations can provide better knowledge about the PEO process. The lack of detailed information regarding the influence of the solution composition on the passive layer and PEO coating necessitates a study of the electrolyte and its effect on the coating properties. This aim cannot be reached without conducting a systematic study of different solutions under similar conditions.

2. Background and Literature review

Engineering applications aside, it is interesting to note that magnesium is the fourth most abundant mineral in the structure of the human body. Approximately 50% of magnesium is found in the bones, the other half is predominantly located inside the cells [21]. From an engineering point of view, magnesium is an excellent choice which provides feasibility of production of light structures.

New life styles, environment concerns and limited energy resources demand the application of lighter materials to fulfil the needs of the near future. This is what has convinced most industries and research centres to invest in basic studies directed towards reaching an imperative target. This target is nothing except the weight reduction of new products, which is a common objective pursued by many industries such as transportation, electronics and so on.

2.1 Magnesium and magnesium alloys

Among the light engineering metals, magnesium, with its good mechanical properties to weight ratio, has high potential for use in different applications such as the automotive and aerospace industries as well as those which produce electronic equipments. There has been a surge in the development of various alloys of this metal such as AZ and AM series. Therefore, the demand for magnesium alloys has increased worldwide [22].

Magnesium is the 8th most abundant element on the land surface of the earth and in the oceans with approximately 1.3 Mt/km^3 magnesium ions as sources for magnesium. It makes Mg a comparatively inexpensive material. The density of magnesium alloys (~1.8 g/cm^3) is 35% lower than that of aluminium and only two-ninths of stainless steels [23,24,25]. Two basic processes are currently used to produce magnesium metal. The first is electrolysis of the fused anhydrous magnesium chloride ($MgC1_2$) obtained from magnesite, brine or seawater and the second is thermal reduction of magnesium oxide (MgO) by ferrosilicon obtained

from carbonate ores. Another process has been recently developed that uses electrolysis of fused anhydrous $MgC1_2$ derived from serpentine ores [22].

2.1.1 Consumption and Market

Consumption of magnesium is summarized in Fig. 2.1. It shows that magnesium was mostly used in die cast products and also as an alloying element in the production of aluminium alloys. A further 12% was added to ferrous alloys to desulfurize steel or to produce nodular cast iron. 10% of magnesium was consumed in titanium sponge production and the remainder was used in different applications [26].

2.1.2 Application

Magnesium has been employed in different applications, including metallurgical, electrochemical, and structural applications. In metallurgical field, magnesium is used in the manufacturing process of nodular cast iron as graphite spherodizer, for steel production as desulfurizer and for copper base alloys as deoxidizer. However it is highly used in aluminium alloys production where it is added to aluminium as alloying element to improve strength and corrosion resistance [22].

Electrochemical applications of magnesium and magnesium alloys include cathodic protection and production of batteries. Sacrificial anodes of magnesium are widely employed to protect the household and industrial structures especially in marine environments. Structure of dry cell and reserve-cell types get also benefit from electrochemical properties of the magnesium. Therefore it is widely is being used in the construction of batteries [22].

High strength to weight ratio of magnesium is a very important factor made it to be selected in the structural applications. However some other attractive properties of magnesium such as fatigue strength in wheels, damping in electronic housings of aircrafts, dimensional stability in electronic housing, machinability in tooling plate and alkaline resistance in the concrete industry has given it suitable characteristics to be applied in several industries. The magnesium alloy components are also used in different products of automobiles. An examples of which is the seat frame for

Mercedes Benz, which has been produced from AM20 and AM50 magnesium alloy die castings and weighs just 8.4 kg. It is claimed that a comparable steel seat design would weigh an estimated 35 kg [22].

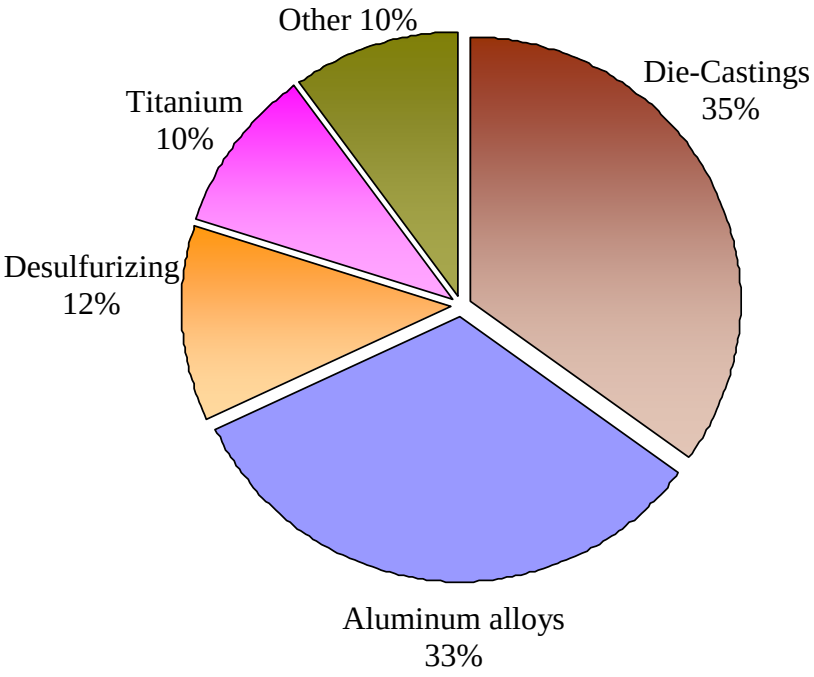

Fig. 2.1. Consumption of magnesium by sectors in 2006 [26].

2.1.3 Magnesium alloys AM series

The AM-series are among the most widely used commercial magnesium alloys due to their adequate strength and good cast ability [14]. Specific properties of this class of alloys, such as excellent energy absorption and ductility together with reasonable yield and tensile properties make them suitable for use in die casting processes to produce parts which require good ductility and toughness, such as automotive wheels [22].

AM-series alloys belong to Mg–Al system, where manganese is usually added to reduce the harmful galvanic effects of iron in the alloy. Small additions of manganese with a high tendency to bind with iron and aluminium, decreases the iron concentration in the melt through the formation of Al–(Fe,Mn) intermetallic

particles. Part of them settles at the bottom of crucibles and the others remain embedded in castings during solidification. This improves the corrosion behaviour of the AM-series [14,27]. It is seen that in addition to possessing many advantages, magnesium is also associated with high corrosion susceptibility, which puts a big constraint on magnesium being employed on large scale. Unlike aluminium and titanium, the oxide film forming on the surface of the magnesium and its alloy is not durable enough to protect the substrate [66]. So an effective protection method is required to improve the weakness of the magnesium and its alloy.

2.2 Plasma Electrolytic Oxidation

Various types of protective methods, namely organic and conversion coatings as well as plasma electrolytic oxidation (PEO) are already known to demonstrate effectiveness in preventing the corrosion of magnesium [23,3]. Among these, the plasma electrolytic oxidation technique, known also as micro-arc oxidation (MAO), is a process with the capacity to produce chemically stable and adherent oxide layers on surfaces of metals such as aluminium, titanium and magnesium.

Plasma electrolytic oxidation can be categorized under electrochemical surface treatment but it is actually an advanced form of anodization in which higher range of voltage is applied. During the treatment, different processes such as dissolution of substrate, formation of oxide layer and dielectric breakdown occur which make it a complex process to study [4].

The schematic of the process shown in Fig. 2.2 is based on the oxidation of the substrate in the anode connected to a high potential power supply and immersed in a proper electrolyte. High potential provides enough energy for a current to pass through the surface by breaking down the resistance of the dielectric layer (i.e. passive layer and continuous gaseous vapour envelope) on the surface. The breakdown of the layer occurs together with some scattered sparks on the metal surface (Fig. 2.2). The event is known as a sparking phenomenon. The sparks on the surface, besides providing an attractive display, also provide a plasma environment in which complex reactions take place. Very high temperature and very short lifetime

are the other characteristics of the sparks which provide suitable conditions for the formation of a stable and protective oxide layer on the surface [5].

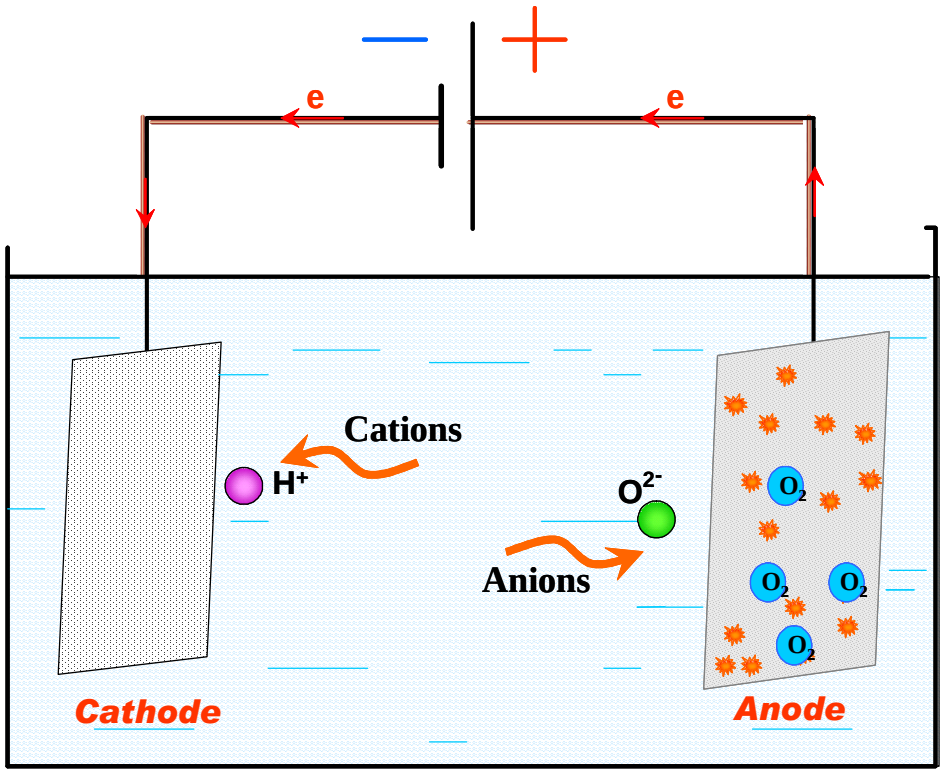

Fig. 2.2. Schematic of the PEO process shows liberation of gas and sparks on anode and moving direction of the ions.

What is happening during the layer formation is a kind of chemical conversion of the metal into the oxide phase which forms in two opposite directions; inwards and outwards from the original metal surface [28]. As the layer forms by this conversion mechanism it has better adhesion to the substrate metal compared to those resulting from processes such as plasma spraying and polymer coatings. The applied layer is largely crystalline and enhances the surface properties of the metals by offering high degrees of hardness and of wear and corrosion resistance, as well as of insulation against heat and electricity [3,25,29].

2.2.1 History and development of the PEO process

The discharge phenomena in an electrolysis process were discovered by Sluginov in 1880s [30]. However, the first step of a scientific investigation of the spark phenomena was conducted in the 1930s by Gunterschultze and Betz [31].

In 1953 the studies by Huber on the anodic film formed on magnesium during the anodizing process in NaOH showed that with potentials over 50 V the process reaches an intensive sparking. This phenomenon was attributed to the breakdown of the thin layer of $Mg(OH)_2$ formed on the surface during the anodizing process [32].

Detailed study on the anodizing process of magnesium alloys by Dow Chemical Company led to a patent in the 1950s [33]. The process was named as the DOW17 method in which the electrolyte consists of sodium bichromate, ammonium acid fluoride (NH_4HF_2) and phosphoric acid with approximate pH value of 5. The produced coating shows very low corrosion resistance in salt spray testing but it can be used as a proper base for a top coating like paints. However the electrolyte had a toxic composition and polluted the environment [34].

In 1955 the anodic oxidation was considered as a method for the surface treatment of magnesium and led to the issue of patent by Harry A. Evangelides [35]. The process, known as the HAE process, consists of a surface treatment applying a coating layer on the surface by the usage of an alternating current. The electrolyte is made of potassium permanganate, potassium fluoride, trisodium phosphate, potassium hydroxide and aluminium hydroxide with an approximate pH level of 14. The produced coating is highly porous and has a low ability to protect the magnesium against corrosion. However it provides a good base for painting on the surface [34]. Like the DOW17 process, the HAE electrolyte had composition that was harmful for environment but together they established a suitable foundation for further research which attempted to improve the properties of magnesium by coatings produced from an environmentally friendly electrolyte.

McNeill and Grussin the 1960s understood that the films formed in aluminate and silicate solutions consist of a mixture of crystalline MgO plus $MgAl_2O_4$ and Mg_2SiO_4 respectively. It was concluded that electrolyte composition influences the chemical composition of the coating by the contribution of the electrolyte species in the formation process. More improvements in the coating properties, such as corrosion resistance, were also achieved which led to the submission a patent titled "Anodic spark reaction processes and articles" [36].

After that, several works have been done on the effects of electrolytes on physical and chemical properties of the anodized coatings. With the objective to improve properties of the HAE coating process, Kotler et al. in 1970s [37,38] studied the magnesium anodizing process and named it the MGZ process. The MGZ process employs an alternative current in an aqueous solution containing chromate, vanadate, phosphate and fluoride. The final results showed that the corrosion and wear performance of the MGZ coating on magnesium alloys was better than that of both DOW17 and HAE.

Investigations by Technology Application Group Inc. resulted in the invention of a new coating known as Tagnite [39]. The coating was based on a patent issued in the 1990s and was formed in two steps [40]. In the first step of the process, the sample is immersed in an heated (40-100°C) ammonium fluoride solution with a concentration of 0.2 to 5 molar and a pH ranging from 5 to 8. During the immersion period, two processes take place on the metal surface including cleaning and then formation of fluoride layer. In the second step, the substrate is anodized in a chromium free solution operating below room temperature. The chemical composition of the electrolyte was a soluble hydroxide plus fluoride and silicate with a pH of about 12.5. The major part of the coating was composed of MgO but formation of hard fused silicate in the coating was also reported [39,41]. To produce a Tagnite coating a high DC voltage of up to 340V should be applied which results in the formation of a coating with a corrosion resistance better than that of the Dow and HAE processes [23]. The coating can resist 480 hours in salt fog test (according to ASTM Bl17 and

evaluated by ASTM D1654). However, existence of fluoride in the electrolyte causes an environmental concern.

In 1998 the Magnesium Technology Ltd. produced a coating by employing Anomag method with a electrolyte composed of ammonia (NH_3) and sodium ammonium hydrogen phosphate ($NaNH_4$ $HPO_4.4H_2O$) [42]. This anodizing process is more environmentally friendly but there are still concerns about usage of toxic compounds like ammonia. The main difference of the process lay in the fact that it is a method applying a coating layer on magnesium alloy without sparking. As a result it is a process with lower energy consumption and higher efficiency [34,41]. Based on an agreement in 2007, the Anomag technology is nowadays used by Keronite Ltd [43].

The Magoxid-Coat is a method invented in Russia and developed by AHC coating company (AHC Oberflächentechnik GmbH) in Germany [44]. The Magoxide process produces a hard anodic coating on magnesium base substrates by using external power supply producing discharges in alkaline solutions mainly consisted of phosphate, borate, silicate, aluminate or fluoride anions but free of chloride. The applied ceramic coating on the surface improves the corrosion and wear properties of the substrate. The optimum thickness of the layer is between 15-25µm which increase the hardness of the coating to a level between 7 (Quartz) and 8 (Topaz) in the Mohs scale of scratch test. It is reported that the coating resists about 500 hours in salt fog without any corrosion evidence, however it is not mentioned with or without a post treatment. According to structure analysis of the coating, it consist of three layers ; a thin layer laying directly on the metal surface, a middle layer with compact structure acting as a barrier layer against corrosion, and an outer porous layer which can be used as a good base for a post treatment like painting or polymer coating [23,45].

Keronite Ltd has recently developed a PEO coating method which is also available commercially. As well as Magoxide the Keronite technology originated form Russia but it has been developed in the UK. It is claimed that it is an environmentally friendly process applying a coating layer on the aluminium and magnesium surface with high ability to resist against corrosion and wear. A pulsed alternating current is

employed through the oxidation bath with low concentrate alkaline electrolyte and chrome-free. It is reported that the protective ceramic coating grow partly above and partly below the surface at the rate of 0.3 to 1 µm per minute on aluminium and up to 2 µm per minute on magnesium surfaces [43].

Different tests have demonstrated that magnesium alloy AZ91D, coated with 25-35 µm of Keronite only, survives one month immersed in a saline solution, or 1000 hours in a salt spray environment with very little evidence of corrosion attack. Further tests showed that hardness of the coating is over 700 HV on the same substrate. This makes the coating harder than the most hard anodized aluminium, and provide wider use of magnesium and its alloy [43,46,47].

2.2.2 Basics and theories

2.2.2.1 PEO process before Breakdown

The PEO process follows the classic anodizing reactions before the breakdown point [48]. During the anodizing of a magnesium substrate in alkaline electrolyte, due to the dissolution of magnesium, Mg^{2+} enters the electrolyte under the effect of the electric field. High volumes of gas liberated on the anode can also be seen which mainly consists of the oxygen generated by oxidation of the OH^- [18]. Equations 2.1 and 2.2 show the anodic reactions.

$$Mg \rightarrow Mg^{2+} + 2e^- \quad (2.1)$$

$$4\,OH^- \rightarrow O_2 + 2H_2O + 4e^- \quad (2.2)$$

As soon as the amount of anions and cations reach a high enough concentration around the electrode / electrolyte interface, a uniform passive layer starts to form on the surface. Depending on the anion types, different reactions may take place on the surface which subsequently leads to different compositions of the layer. However, the formation of $Mg(OH)_2$ is a common reaction taking place due to equation 2.3.

$$Mg^{2+}(aq) + 2\,OH^-(aq) \rightarrow Mg(OH)_2\,(s) \quad (2.3)$$

In the next step, dehydration of $Mg(OH)_2$ takes place and magnesium oxide (MgO) forms, as the sample is taken out of the electrolyte due to equation 2.4.

$$Mg(OH)_2 \rightarrow MgO + H_2O \quad (2.4)$$

These are the reactions which would occur on the magnesium electrode in alkaline solutions, so that a thin and uniform layer covers the whole surface of electrode [48]. The formed layer has high dielectric characteristics and acts as a barrier against the passing current. When the surface is completely covered by the barrier layer, only the local collapse of the layer can provide a possibility for a current to pass through the surface. This phenomenon is known as the breakdown effect in the PEO process, which gives rise to the sparks on the surface.

2.2.2.2 Breakdown theory

Since the 1960s, different theories and models have been developed to explain the breakdown mechanisms and to clarify the generation of the sparks at local sites [49,50]. According to the first studies, the breakdown process was generally considered a consequence of an avalanche of electrons injected at the electrolyte/oxide interface. Wood and Pearson (1967) [49] developed a dielectric breakdown model caused by the damage of the insulating property and an electron avalanche in anodic film. Vijh (1971) [51] proposed injection of electrons by a tunnelling mechanism across the electrolyte/oxide barrier. He suggested that micro cracks and impurity of the initial oxide film were conducive to the generation of a leak current and a dielectric breakdown.

The first attempt to develop a quantitative theory was made by Ikonopisov in 1977 [52]. He believed that the breakdown voltage (V_{BD}) depends fundamentally on the nature of the anodized metal, composition and resistivity of the electrolyte. Many other factors like current density, surface topography of the electrode, history of the film formation and so on do not affect V_{BD} noticeably. According to the model, sparking was considered an electron avalanche from the electrolyte to the anodic film. This model quantitatively predicts the dependence of the breakdown voltage on the electrolyte resistivity and explains that it is independent of the current density. Equation 2.5 shows the relation between breakdown voltage and resistivity of the

solution where a_B and b_B are constants depending on metal and electrolyte composition and (ρ) is electrolyte resistivity.

$$V_{BD} = a_B + b_B \log(\rho) \quad (2.5)$$

Albella et al. (1987) [53,54] proposed a breakdown model during anodic oxidation of valve metals. The model clarifies that the incorporation of the electrolyte species into the oxide layer occurs at the electrolyte/oxide interface and it is determined by the nature and concentration of the anodizing electrolyte. Therefore, in contrast to the earliest theories that attribute the breakdown to the electron injecting properties of the electrolyte, the breakdown properties are directly related to the electrolyte species incorporated in the anodization process. From this point of view it can be concluded that the oxide breakdown properties are mainly controlled at the electrolyte/oxide interface by the ability of electrolyte species to be incorporated into the oxide layer during the anodization process.

Another model developed by Klapkiv (1999) [55] indicates that the oxide coating forms in four main stages: (i) formation of the primary oxide film; (ii) breakdown of the primary oxide film and appearance of the discharge channel; (iii) formation of intermediate and final products in the gas phase; and (iv) condensation and polymorphic transitions in the oxide phases. Based on this model shown in Fig. 2.3, different temperature layers arise in a discharge tunnel where the metal and electrolyte serve as an anode and cathode respectively. An oxide layer and an electric double layer form on the electrolyte/oxide boundary. And the main drop of the potential occurs across the oxide layer. The discharge tunnel within the oxide layer which forms because of charge transfer between cathode and anode can be divided to different temperature zones. Different reactions are possible depending on the temperature of each zone.

In the central zone of the discharge tunnel the temperature could reach about 7000 to 10000 K. At such a high temperature the matter is partially ionized and the rest is in a mono atomic state. Therefore, a suitable environment is provided for reaction between mono atoms of metal and oxygen. In the next layers which have lower

temperatures the non-dissociated molecules or radicals would exist on the peripheral sections. The temperature of the outer layer with side boundaries to the oxide material and bottom boundary to the metal surface drops to low values close to room temperature.

From the electrolyte side, a vial of steam and gas forms during the lifetime of the discharge channel. The steam and gas vial is understood as the zone where the matter is in the plasma state. The temperature of the vial in direct contact with the discharge tunnel reaches high values similar to that of the discharge environment, but the outer layer connecting with the electrolyte is at a relatively low temperature close to the solution temperature. In this zone, dissociation of water and formation of mono atomic oxygen and hydrogen can take place. Here is the opening from which oxygen, hydrogen, OH radicals, and other components of the electrolyte get into the discharge channel.

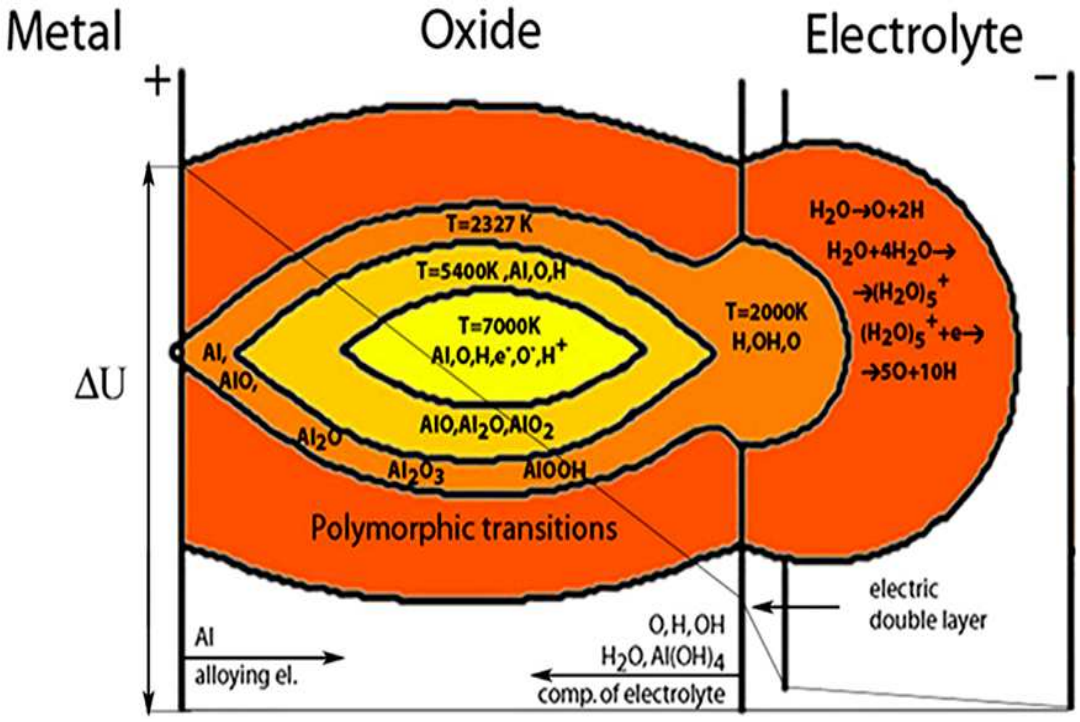

Fig. 2.3. Schematic representation of the oxide synthesis process in the discharge channel [55].

Yerokhin et al in 2003 [56] proposed another model in which gas bubbles forming on the surface play a more important role. As Fig. 2.4. shows, the electrons emit from the electrolyte surface (partial cathode) into a gaseous phase, rather than a dielectric breakdown of the growing oxide film. In other words, instead the free electrons entering directly to the oxide layer, which leads to breakdown of the layer, the electrons enter the gas phase. Combination of the gas phase and a high electric field develop the plasma environment. The free electrons would then immediately participate in a series of reactions with water resulting in the formation of gaseous products such as H_2 and O_2, providing the necessary conditions for the maintenance of a stable plasma discharge environment.

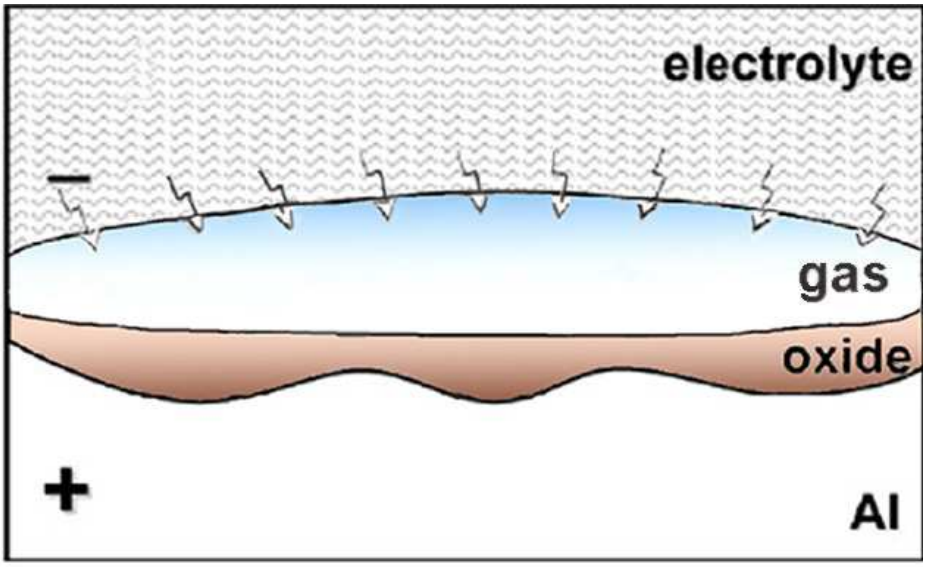

Fig. 2.4. Schematic model of contact glow discharge electrolysis adapted for the presence of an oxide film on the Al surface [56].

Guo et al. (2005) [18] proposed a new model describing what happens on the Mg-Al alloy during the PEO process in a sodium aluminate solution. According to the model, the PEO process begins with the dissolution of the substrate when the metal loses its brightness within a few seconds. Subsequently, a thin transparent passive film forms on the anode surface and oxygen gas resulting from oxidation of water (eq. 2.6) or hydroxide (eq. 2.2) covers the anode surface uniformly. A dielectric layer made of a thin passive layer and a continuous gas envelope enfolds the anodic surface.

$$2H_2O \rightarrow O_2 + 4H^+ + 4e^- \quad (2.6)$$

When a 'conventional' electrolytic process is studied (e.g. electroplating, electrochemical machining, anodising, etc.), the electrode processes are usually considered as simplified models, where the electrode/electrolyte interface can be represented by a two-phase system (i.e. metal–electrolyte or oxide–electrolyte couple) with a single phase boundary consisting of a double-charged layer and concurrent by-product processes such as gas liberation are neglected [19]. Compared with the simplified models the new model is more complex, with four-phase systems including electrode/dielectric film/gas/electrolyte. Fig. 2.5 shows a number of possible chemical, electrochemical and thermo-chemical processes which occur concurrently on the electrode surface.

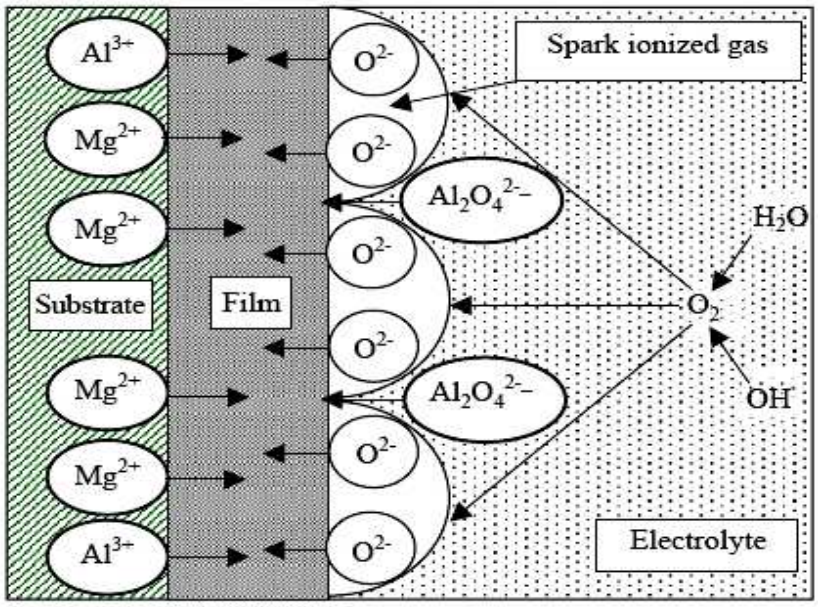

Fig. 2.5. Schematic diagram of a four-phase electrode system for MAO process [18].

The dielectric properties of a thin dielectric layer and gas envelope are very high and the drop of the voltage happens mainly at these regions near an electrode. As soon as the intensity of the electrical field reaches a value in the order of 10^6-10^8 V/m in the dielectric region, the electrons are directly injected into the oxide film through the electrolyte/oxide interface and then get accelerated in the electric field. This

produces an electron avalanche by impact ionization and the breakdown of the thin dielectric film or ionization of the gas envelope occurs. So a route develops on the layer through which the electrons transfer to the film. At the film/electrolyte interface, the oxygen forms by oxidation of the OH^- ions or water molecules adsorbed on the anode surface according to the equations 2.2 and 2.6. Thermal decomposition of water also could be another possible reaction for the formation of oxygen at the film/electrolyte interface due to the equation 2.7.

$2H_2O \rightarrow H_2 + 2\,OH$ subsequently $2\,OH \rightarrow H_2O + 1/2\,O_2$ (2.7)

The breakdown of the dielectric layer results in the sparks and liberation of high amount of gas composed mainly of oxygen. Initial sparks are high in number but small in size with a white light colour moving rapidly. As process proceeds, the sparks change to less number with orange sparks moving slowly across the surface [18]. With regard to the anions existing in the solution, the MgO and $MgAl_2O_4$ can form on the coating layer based on the equations 2.8 and 2.9.

$Mg^{2+} + 2OH^- \rightarrow MgO + H_2O$ (2. 8) [57]

$Mg^{2+} + 2AlO_2^- \rightarrow MgAl_2O_4$ (2. 9) [6].

Rakoch et al. (2006) [50] developed a model based on the fact that formation of a dielectric layer is required for occurrence of a discharge. The dielectric layer is a continuous organic or oxide coating covered with a vapour-gas phase in a pore (VGPP). The VGPP forms as a result of oxygen evolution according to equation 2.2.

The electrons originated from electrolyte anions (including OH^-) inject into the vapour-gas layer. The anodic reactions lead to dissolution of substrate according to the equation 2.10

$M \rightarrow M^{n+} + ne$ (2. 10)

The complex reactions taking place in the plasma lead to interaction between oxygen and the elements in the plasma (e.g. metallic ions or electrolyte anions) to produce oxide phases. Fig. 2.6 demonstrates different stages of the process occurring after breakdown of dielectric coating [50]. Fig. 2.6-a schematically illustrate a VGPP in

oxide layer through which the metal ions introduce to the solution. Fig 2.6-b shows that the exchange of the electrons and ions takes place through the VGPP and the plasma environment with high temperature comes up. The reactions happening in the plasma environment lead to formation of the coating layer. Fig 2.6-c illustrates the oxide layer formed on the substrate. Because of the thermal stress some defects or gaps could be appear in the interface of the layer and the substrate.

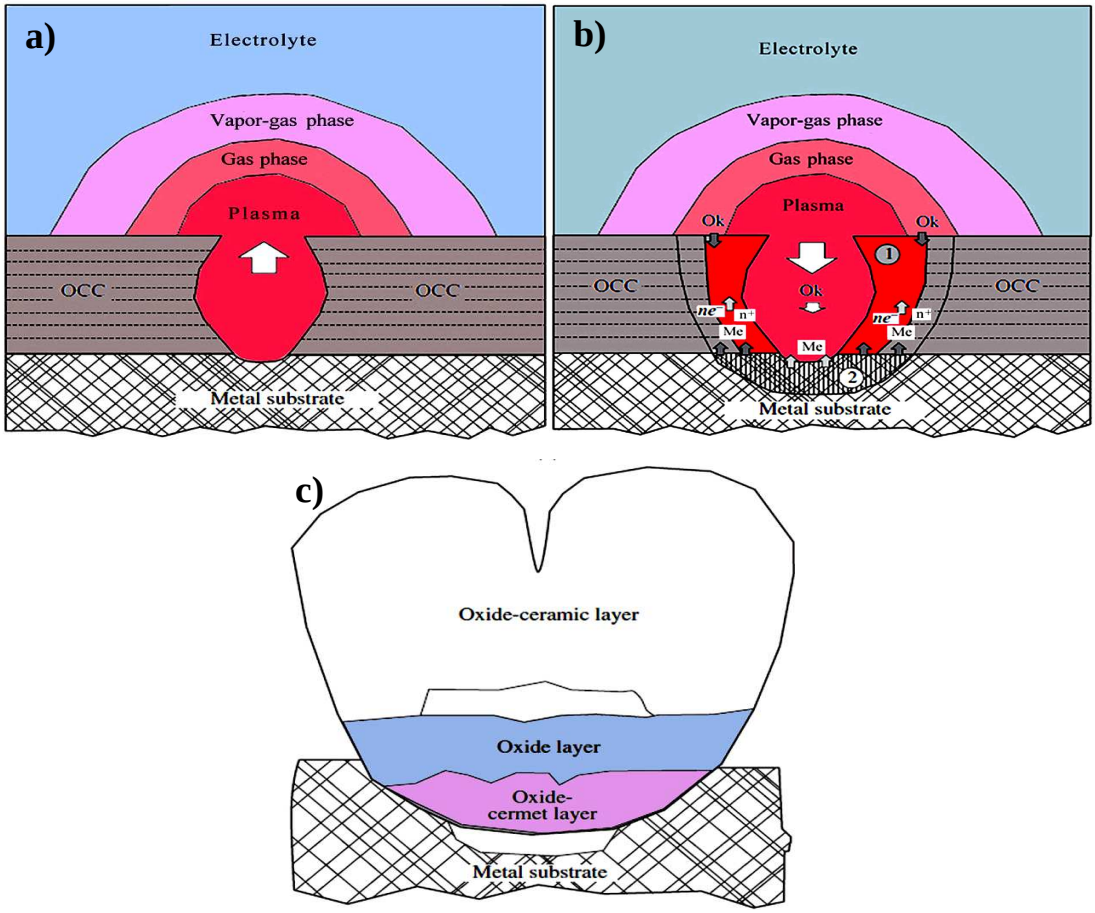

Fig. 2.6. Stages of processes occurring after the micro plasma breakdown of dielectric coating: (a) micro plasma breakdown, (b) high temperature oxidation zone, (1) thermal effect zone, (2) fused metal substrate, (c) a local area fragment of the oxide ceramic coating (OCC) formed after micro plasma breakdown [50].

2.2.2.3 Discharge characteristics

According to the proposed models, a discharge appears on the surface when resistance of the dielectric layer breaks down by the potential applied. Yerokhin et al. [56] have studied discharge characterization throughout the oxidation process. The results indicate that at initial steps the sparking size of the events is smaller than those happening later in the process. The cross-sectional areas and life time of the sparks fluctuate in the range of 0.01–1.35 mm^2 and 10^{-4}–10^{-3} second respectively. Long et al. also believe that the life time of a single spark could be about 10^{-5}–10^{-4} seconds [58]. The temperature produced by the sparks can reach to a maximum of $(4–10)\times10^3$ K [4,55,59,60]. Such high temperatures together with high intensities of the electric field give rise to a plasma environment in which dissociation and excitation of the atoms and ions occurs.

2.2.3 Constituent elements of the PEO process

So far the basic concepts of the PEO process have been explained. However the aspects influencing the process should also be taken into consideration in order to produce an improved coating. Taking a broad view, three different constituent elements have an essential influence on the PEO process; these are substrate, electrolyte and power supply. Several studies have focused on each of these elements to reveal how the coating gets affected by each of them.

2.2.3.1 Substrate

Magnesium and its alloy show poor corrosion resistance. This could be understood by considering the corrosion reactions and passive behaviour of the metal during the corrosion process. The corrosion process of magnesium in an aqueous solution has been considered in several studies. It is believed that the following equations show the possible reactions taking place during the dissolution of magnesium leading to the formation of corrosion product [61-63].

$Mg \rightarrow Mg^{2+}(aq)+2e$ (anodic reaction) (2. 11)

$2H_2O+2e \rightarrow H_2+2OH^-(aq)$ (cathodic reaction) (2. 12)

$Mg^{2+}(aq)+2OH^-(aq) \rightarrow Mg(OH)_2\ (s)$ (corrosion product) (2. 13)

$Mg + 2H_2O \rightarrow Mg(OH)_2\ (s)+H_2$ (corrosion process) (2. 14)

Based on equation 2.13 and due to the limited solubility of Mg^{2+} in water [63,64], the $Mg(OH)_2$ forms on the surface of the magnesium in pH values higher than 10.5 [63]. It is known that in humid environments, a hydroxide layer [65] with Pilling-Bedworth ratio (R_{PB}) of 1.77 [66] forms on the magnesium surface. According to the $R_{PB,}$ the hydroxide layer can show protective ability however it has poor pitting resistance in aqueous solutions containing aggressive anions such as chloride and so on [66]. Therefore the process continues due to the equation 2-4 which is a summary of the reactions 2-1 to 2-3. In dry conditions, the hydroxide film converts to an oxide film with R_{PB} lower than one (~0.81) [24,67]. The oxide layer is not stable enough to protect magnesium against future corrosion because of a misfit between the lattices of the cubic oxide and the hexagonal metal [65].

The literature review indicates that aluminium, titanium and magnesium are the most PEO treated metals. However, the number of magnesium-based references is increasing. For example, some publications deal with development of PEO coatings on AZ91 [1,11] and AZ31 [68] alloys. Studies have also been done on AM-series [12,69] but many aspects of the coating behaviour like structure of the coating and formation mechanism during the PEO process still remain unknown. The way an alloy behaves during the PEO process depends on the nature of the substrate [52]. The microstructure and passive behaviour of the substrate which are related to the composition of the alloy are two main inherent parameters which determine the behaviour of the substrate during the PEO process. Therefore the way these parameters influence the coating process should be studied in greater detail.

2.2.3.1.1 Microstructure

Intermetallic phases, grains and sub-grains are components which represent the microstructure of a metallic alloy. Several studies reported the characteristics of intermetallic particles and morphology of the grains and sub grains of different magnesium alloys [14-16]. As the influence of the microstructure constituents on the coating formation process will be considered in this study, the following sections provide more detail information regard to the alloy employed in this study, i.e. AM50 magnesium alloy.

Wang et al. [17] studied the microstructure of the AM50 magnesium alloy which is composed of about 5% Al and 0.5% Mn. The results show that the microstructure of the alloy consists of α-Mg (mainly magnesium), β-phase ($Mg_{17}Al_{12}$) and Al_8Mn_5 phases. The α-Mg regions and $Mg_{17}Al_{12}$ particles have a wide variety of morphologies while Al_8Mn_5 particles have a typical polygonal shape. The Al_8Mn_5 is composed of 4.98% Mg, 37.08% Mn and 57.94% Al while the β-phase has about 67.14% Mg, 32.76% Al and α–Mg is composed of 94.65% Mg, 5.25% Al and 0.1% Mn.

The backscatter studies of Kadiri et al. in Fig. 2.7 [16] showed that the microstructure of the AM50 consists of α-Mg grains surrounded by Al-rich eutectic layers. The figs 2.8 clearly shows the morphology of the β-phases and Al_8Mn_5 particles in the microstructure of the alloy.

Jonsson et al. [27] studied the electrochemical properties of different phases existing in the microstructure of the magnesium alloys. According to the findings, the regions and particles which are rich of aluminium (β-phase) or contain manganese (η-Al_8Mn_5 phases) show more noble potential than that of α-Mg and nobility of the phases decrease in the order of η-Al_8Mn_5 > β-$Mg_{17}Al_{12}$ > α-Mg (Table 2.1).

It is clear that the $Mg_{17}Al_{12}$ phase and the Al_8Mn_5 phase work as local cathodes when coupled to the α-Mg. The higher potential of the β-$Mg_{17}Al_{12}$ and η-Al_8Mn_5 phases compared to that of the magnesium matrix could be related to the higher Al content

which builds up a more stable passive layer than that of the magnesium. In addition to those of Jonsson, the results of Arrabal et al. [70] showed that the potential of β-phase is higher than α-Mg.

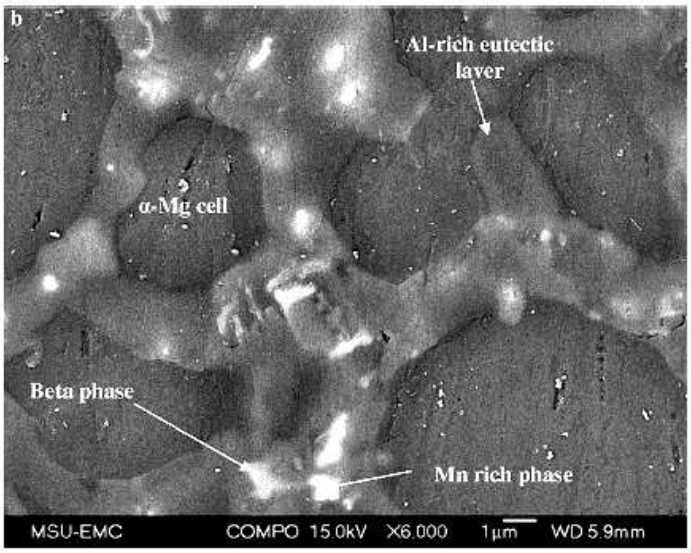

Fig. 2.7. Backscatter micrographs of a polished AM50 sample showing the formation of the beta phase and Mn-rich phase inside the Al-rich eutectic layer [16].

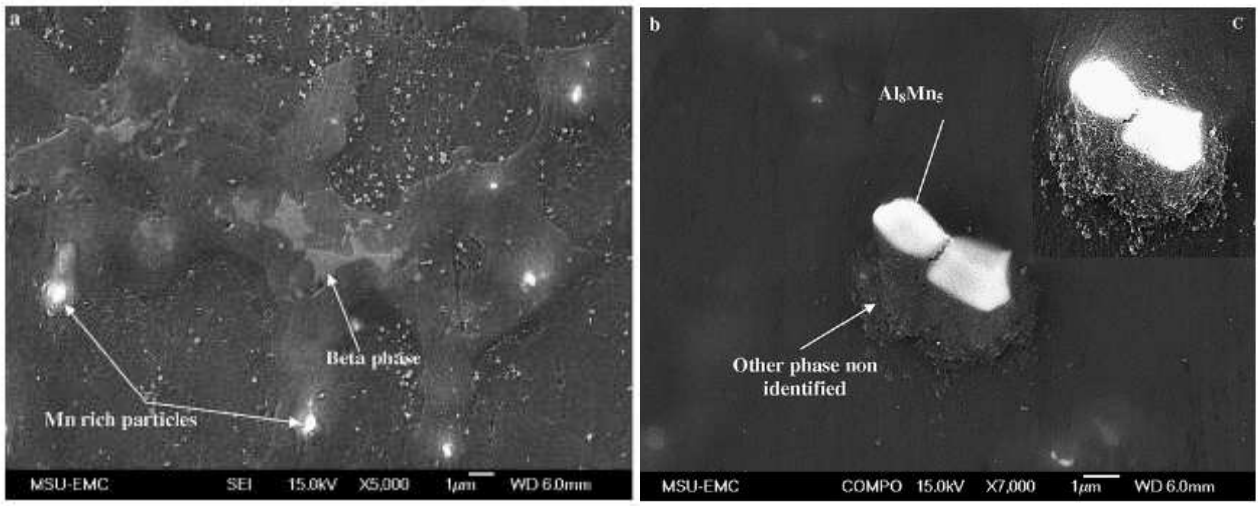

Fig. 2.8. Backscatter micrographs of a polished AM50 sample showing a) β-phase. (b) Al_8Mn_5 phase, and (c) a secondary electron image of the same particles shown in (b) [16].

Table 2.1. Composition and Volta potential of different phases in magnesium alloy [27].

Concentration (at.%)			phase	Volta potential (mV/SHE)
Mg	Al	Mn		
15.8	53.8	30.4	Al_8Mn_5	-640
71.2	28.7	0.1	β-$Mg_{17}Al_{12}$	-760
93.8	6.1	0.1	α-Magnesium	-1025

The effect of the microstructure on PEO coating process was studied by Duan et al. who applied a coating layer on magnesium alloy substrate. The results show that the structure and growth rate of the PEO coating on α and β-phase are different [48]. It is reported that during the PEO process α-Mg has higher reactivity and tends to release more Mg^{2+} to take part in the coating formation reactions. The higher concentration of Mg^{2+} around α-Mg provides more active sites for plasma sparking. From the other side, the β-phase is relatively more stable and consequently needs higher breakdown voltage for sparking than α-phase. Therefore the pore size formed on β-phase is larger than that on the α -phase [48,71].

2.2.3.1.2 Passive behaviour

The way a substrate reacts with an electrolyte depends on the intrinsic characteristics (physical-chemical properties) of the metal and electrolyte species. The reactions between the substrate and the electrolyte lead to the formation of a passive layer whose degree of stability determines whether it is a protective layer or not. The passive layer which forms on the magnesium surface is magnesium hydroxide, which is not as stable as the aluminium oxide which forms on the aluminium surface. This is why aluminium shows better performance against corrosion compared to magnesium [61]. According to the Pourbaix diagram shown in Fig. 2.9, formation of a passive layer on the magnesium surface can be expected only in relatively strong alkaline environments.

Khaselev et al. [72,73] studied behaviour of the passive layer and PEO coating on magnesium and its alloys with different aluminium content. The results obtained

showed that although the passive layer on pure Mg, Mg alloys and β-phase shows similar behaviour, those with a higher Al content such as β-phase needs a higher breakdown voltage compared to that of α-Mg. He has also stated that the PEO process starts on α-Mg and continues on β-phase.

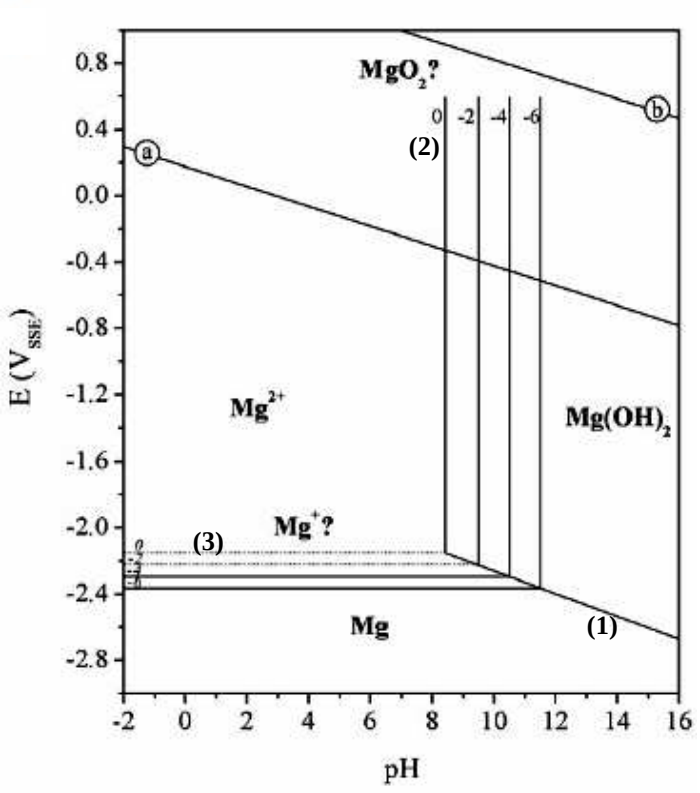

Fig. 2.9 Pourbaix diagram for the Mg-H_2O system at 25 °C . The region of water stability lies between the lines marked a) and b). The different regions are separated by the following reactions: (1) $Mg+2H_2O \rightarrow Mg(OH)_2+H_2$; (2) $Mg^{2+}+H_2O \rightarrow MgO+2H^+$; (3) $Mg \rightarrow Mg^{2+} +2\ e^-$. [61,62].

According to the obtained results the higher breakdown voltage of the β-phase is attributed to the higher aluminium content of the alloy which is beneficial for the passivity of the Mg-Al alloys. However no details have been reported on the role of Al-Mn phases during the PEO process.

2.2.3.2 Electrolyte

The chemical composition of electrolyte plays a very important role in the PEO process. It is why most of the recent works in the field of PEO coating have studied the effect of the electrolyte on the coating by checking different electrolytes. These studies are trying to optimize and improve the coating performance by finding a suitable solution and examine the influence of the electrolyte on the obtained PEO coating [11,12,20,74].

It was previously shown that based on the Pourbaix diagram, a passive layer forms on the magnesium surface in an alkaline solution. This accounts for why electrolytes for a magnesium substrate have a high pH value (usually more than 12). Different hydroxides such as KOH [13] or NaOH [75] with a high pH value were employed to apply a coating layer on the magnesium surface without any additive. However, simple hydroxide electrolytes are not able to produce a proper coating because of high energy consumption and low growth rate. Fukuda et al. [13] studied the formation of anodic films on Mg alloys in KOH solutions with and without the addition of Na_2SiO_3 in low potential. Reduction in the anodic current upon the addition of Na_2SiO_3 indicated that anodic dissolution was suppressed because an anodic film forms on the surface and it improves the formation process of the PEO coating. It was also reported that a denser, thicker and more uniform anodic film formed on the surface when Na_2SiO_3 was used.

Examination of the literature revealed to the point that any suitable solution for the PEO process usually consists of two or more components such as alkaline and salt solutions [3,29,76-78]. The salts, such as aluminate [6], phosphate [2], silicate [1], fluorides [79], chromates [80] and ammonia [81], in combination with an alkaline solution were employed in different studies. These solutions are able to produce successful coatings with different properties. However the growth rate and the energy efficiency of the process still need to be improved [82]. Another concern that should be taken into consideration is the environmental issue. The evolution trend of the PEO process shows that more studies have recently concentrated on the

aluminate, phosphate and silicate base solutions as these are more environmentally friendly than toxic solutions such as fluorides, chromates and ammonia.

It is clear that each part of the solution (i.e. hydroxide or salts) introduces different cations and anions to the solution. Consequently the characteristics and final performance of the produced coating change. Ma et al. [6] prepared a PEO coating on a magnesium alloy with solutions composed of $NaAlO_2$ (1-20g/l) and KOH (0.5-1.5g/l). The results showed, besides the formation of MgO, that the electrolyte introduces $MgAl_2O_4$ to the coating. Studies by Guo et al. [83] also confirmed the formation of $MgAl_2O_4$ in the coating when $NaAlO_2$ was employed in the solution. Liang et al. [69] introduced different amount of $NaAlO_2$ to a KOH+Na_3PO_4 solution and prepared several coatings. The results showed that $NaAlO_2$ is beneficial for coating properties as it improves the corrosion resistance of the coatings. Improved properties of the coating are attributed to the formation of $MgAl_2O_4$ in the coating structure.

The studies show that the presence of phosphate and silicate in the electrolytes leads to the formation of $Mg_3(PO_4)_2$ [70] and Mg_2SiO_4 [84] phase in the coating structure. Arrabal et al. studied the role of phosphate and silicate species during the PEO process on magnesium alloy. According to the results, the phosphate elements are located mainly in the inner region of the coating, while silicate elements are distributed almost homogeneously across the coating [85]. Preferential distribution of elements through the PEO coating is also reported by Lv et al. for phosphate and silicate solutions [86].

The influence of electrolyte on corrosion properties of the PEO coated magnesium alloys was studied by Blawert et al.[87]. The study is considering the influence of the electrolyte concentration and composition on the corrosion properties of the PEO coatings. Three solutions were prepared in different concentrations and composition namely standard and high concentration as well as high concentration plus additive (i.e. CrO_3). The results showed that the corrosion resistance of the coatings are changing depend on the concentration and composition of the solutions. So that the

high concentration solution is able to produce a higher corrosion resistance coating compared to the rest of the solutions. So it can be seen that the composition of the electrolyte is an important parameter which influence the final properties of the coating by determining the type and chemical composition of the phases in the coating.

As noted before, different studies have been done to find out an appropriate electrolyte which can improve the coating performance [3,8,88]. However in some cases literature review shows inconsistent results. For example Ma et al. [74] reported that on pure magnesium, the coatings deposited from phosphate solutions had a better corrosion resistance than those of silicate solutions. On the other hand the results of Cai et al. [2] are indicating that both phosphate electrolytes (P-film) and silicate electrolytes (Si-film) can enhance the corrosion resistance of magnesium alloy significantly, but the Si-film performs better than the P-film in corrosion resistance. It can be seen that both papers have compared corrosion properties of the PEO coatings prepared by the silicate and phosphate electrolytes on magnesium substrates. However due to the first paper phosphate solutions and according to the second work silicon solution resulted in the better corrosion resistance of the PEO coating. So when influence of electrolyte on performance of the coating is investigated the experiments under similar conditions should be conducted to draw an approved conclusion.

2.2.3.3 Power supply (Current and voltage)

Another aspect affecting the quality of the PEO coating is the power supply. The PEO process can essentially be controlled under constant current [89,90], constant voltage [58,72] or both methods in different steps, for example a constant current process in the first step and then a constant voltage in the second step. [11]. Typical behaviour of the voltage during the anodizing of magnesium under different current densities is demonstrated in Fig. 2.10 (a). The figure shows that in a constant current process, the voltage-time curve typically consists of three stages: (i) quick rise of the voltage because of the formation of a barrier layer on the surface before breakdown point; (ii) a slowing down of the increase rate after the breakdown point because a

stable PEO coating starts to form on the surface; and (iii) a steady state region in which the voltage remains almost constant for the rest of the process. The latter happens when the coating layer covers the surface [9].

The behaviour of the current under constant voltage processes is shown in Fig. 2.10. (b) [72]. It is clear that under a constant voltage process, the current immediately reaches a certain value and then starts to decline by further processing. The immediate increase of the current occurs because the formation of the coating layer still has not started. So the current can easily pass through the surface without any obstruction. Further process leads to the formation of a barrier layer, the occurrence of the breakdown phenomena and the commencement of the coating development. The coating layer puts an effective barrier against the current which makes it gradually approach a very small value as the coating develops. The current remains at an almost constant value for the rest of the process.

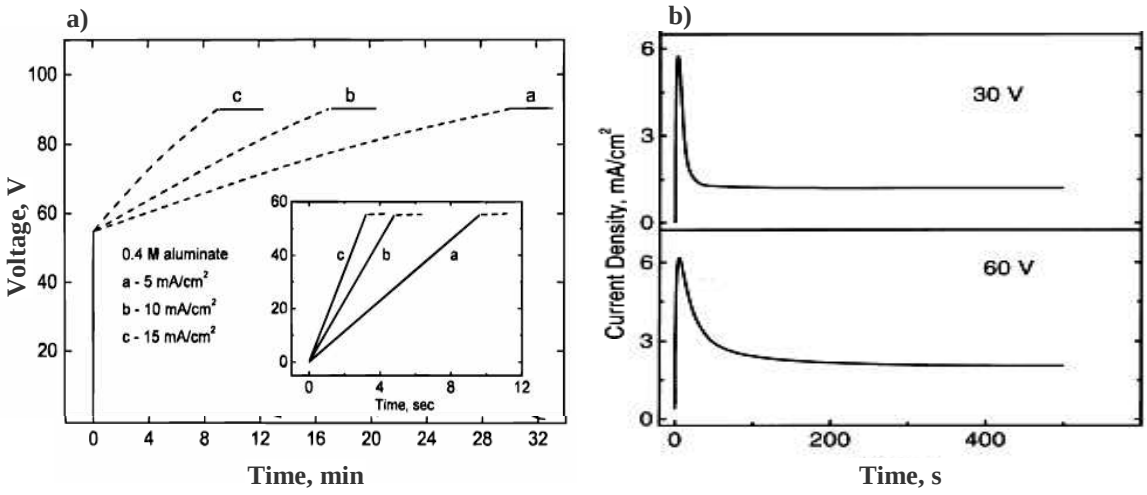

Fig. 2.10. Behaviour of a) Voltage[9] and b) Current [72] during anodizing of magnesium under different conditions.

Yerokhin et al. considered the behaviour of the current vs. voltage under different electrolytes which is shown in Fig. 2.11. It can be seen that the current responds differently to the applied voltage depending on the type of electrolyte employed. This could be attributed to the pH, conductivity and chemical composition of the electrolytes which influence the characteristics of the passive and coating layer. It can be seen that any change in the properties of the electrolyte lead to a main change

in the behaviour of the process, which subsequently influences the properties of the final result.

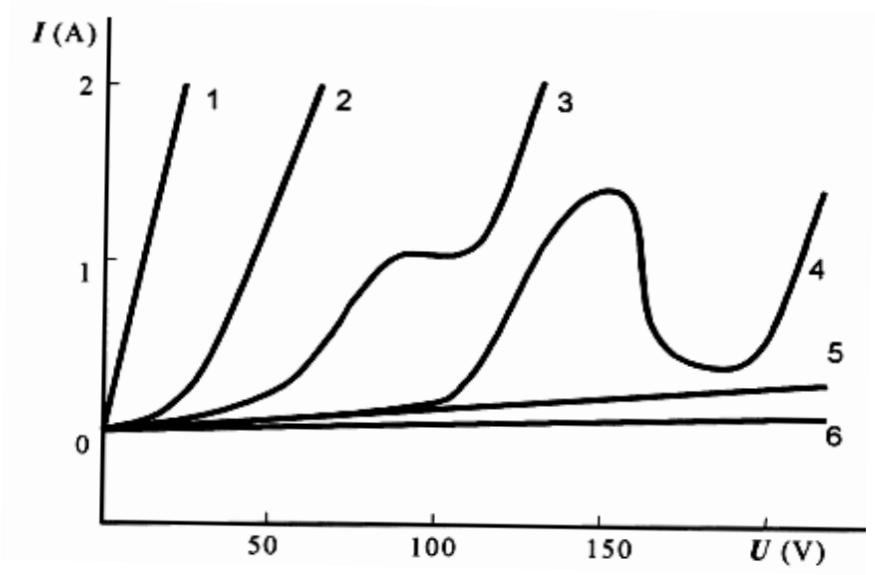

Fig. 2.11. The function *I=f*(*U*) of various electrolytes tested for treatment of (1) fast metal dissolution, (2) slow metal dissolution, (3) metal passivation in narrow voltage interval, (4) complex behaviour with a wide interval of passivation, (5) slight passivation and (6) strong passivation of the metal [19].

2.2.4 Characteristics and properties of the PEO coating

2.2.4.1 Surface morphology

The formation of the PEO coating is based on the sparks passing through the oxide layer and generating the discharge tunnels. So the nature of the coating formation introduces pores to the surface morphology of the coating. Typical porous surface morphology of the PEO coating on the AZ91 magnesium alloy can be seen in the Fig. 2.12. The coating of the Fig. 2.12-L is produced by the Na_2SiO_3 + NaOH + KF solution. The coating contains of the pores which have mainly irregular shapes and they are of different sizes. However the coating of the Fig. 2.12-R which is formed in a Na_2SiO_3+ KOH +$K_4P_2O_7$ solution mainly contains circular pores which have comparable sizes.

According to Curran et al. [91], porous structures form on the coating surface because of oxygen evolution during the PEO process. As the lifetime of the discharges is very short, ~10µs, the evolved oxygen can be trapped in the molten

material. Presence of the pores and cracks in the coating can facilitate a stable growth of oxide during the formation process although they cause deterioration in corrosion resistance of the coating. It should be kept in mind that the coating layer has the characteristics of a dielectric material and hence, the coating process would be stopped if a defect-free layer were to form on the surface [91]. The presence of holes with an opening on the free surface provides a route for the electrolyte to penetrate into the coating. So fine scale discharges can occur across a relatively thin barrier near the substrate interface. As a result the inner defects are recovered and a more compact coating results. Sundararajan et al. [92] also reached the conclusion that the discharge channels are continuously formed and closed all throughout the coating process. Thus a discharge channel has a finite lifetime.

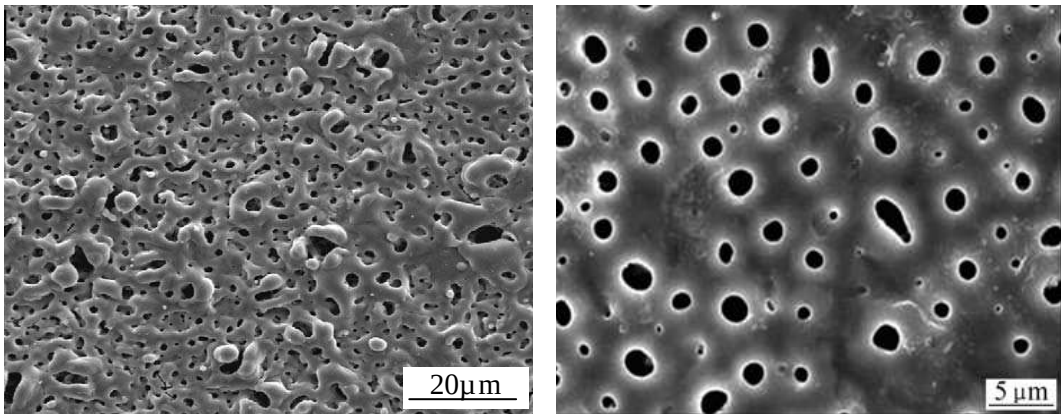

Fig. 2.12. Typical surface morphology of the PEO coating with L) irregular shapes and different sizes [93] R) circular shapes and comparable sizes [94]

Different parameters such as thickness and electrolyte influence the number, shape and size of the pores. Dissimilar appearance of the coatings could be related to variations in the characteristics of the micro-sparks such as the size and number of the sparks occurring during the process with regard to the employed solutions. Furthermore, the coating surface gets coarser and rougher as the process proceeds and the oxide layer gets thicker [12,58,95,96]. Essentially the charges require higher energy to pass through a thicker layer of coating. Because of this, the current concentrates on some weak points of the existing layer to find a way for discharging. This is why the number of the sparks decrease but their size increases as the layer gets thicker. In fact, an increase in the diameter of the discharge channels is the way

in which the process compensates for the resistance of the barrier formed against the passing current [92]. In this way, the size and number of the sparks are themselves affected by the thickness of the coating layer.

Apart from thickness, the chemical composition of the electrolyte is another parameter which influences the pore size. Results of Liang et al. showed that a change in the solution composition results in different pore sizes [97]. It is also reported that for the same thickness of the coating, the number of sparks in phosphate electrolyte is higher than in the silicate electrolyte during the PEO process, which leads to higher number of pores [12].

2.2.4.2 Cross section

2.2.4.2.1 Structure

The structure and thickness of the coating are characteristics which can be studied by considering the cross section of the coating. Studies regarding the structure of the PEO coating mainly assume that the PEO coating is composed of an outer and an inner layer. The outer layer is usually a porous layer which cannot provide effective corrosion resistance. Conversely, the inner layer is commonly dense and compact, acting as a barrier layer against the corrosion attacks. The outer layer is normally thicker than the inner layer [20,93,98,99]. Fig 2.13 shows a cross section of the PEO coating, including the inner and outer layers.

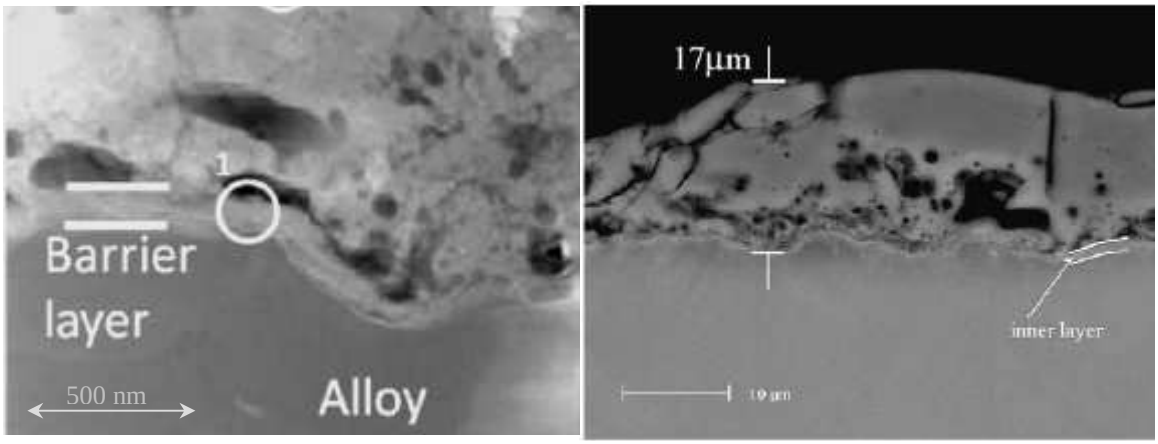

Fig. 2.13.Cross section of the PEO coating [20,99]

Several theories are proposed regarding the nature and characteristics of the barrier layer. It is stated that the barrier layer is a thin, nano-crystalline oxide layer adjacent to the substrate which is normally considered to provide resistance to corrosion [48] and forms in the end stage of the discharge events [99,100]. On the other hand, the relation between the passive layer and corrosion resistance of the PEO coating suggests the existence of a passive layer directly over the substrate [3,101].

It is also believed that the barrier layer originates from the formation of the passive layer at the bottom of the open pores [41,98]. In contrast, it is stated that no layer exists on the substrate at the bottom of the open pores and it is a place which can be easily corroded [102]. The barrier layer is also described as a thin compact layer through which the pores do not cross. [103]. Nevertheless, it should be kept in mind that the layer has the characteristics of a dielectric material. Therefore, the coating process would be stopped if a defect-free layer formed on the surface [91]. Sundararajan et al. suggest that the discharge channels have a finite life, i.e., that the discharge channels are continuously formed and closed throughout the coating process [92].

2.2.4.2.1 Thickness

The formation of a PEO layer with a specific thickness is a consequence of the reaction between metal ions, in this case Mg^{2+}, and anions existing in the solution. So the thickening process requires the anodic dissolution for subsequent reactions with the solution anions. The “rate of anodic dissolution” and the “rate of film formation” are two opposing factors which reversely influence the final thickness of the PEO coating. Essentially the coating starts to grow as the rate of the film formation gets higher than the dissolution rate of the substrate [4].

Time, current density and composition of the electrolyte are among the parameters influencing the growth rate of the coating. Duan et al. showed that the anions have a direct influence on the thickness and morphology of the PEO coating [20]. It is reported that under similar conditions of current and time the silicate solution results in a greater thickness of the coating than do the phosphate and aluminate solutions.

This provides supportive evidence for the beneficial influence of the silicate anions on the growth rate of the PEO coating. [2,19,77,92,101]. The effect of conductivity on the rate of the film formation process should also be considered. Guo et al. reported that the rate of film formation increased when anions with higher conductivity were introduced to the coating solution [83].

2.2.4.3 Corrosion resistance

The coatings produced by PEO show a high degree of hardness as well as strong adhesion to the base metal. Consequently the PEO process potentially enhances the surface properties by providing an effective barrier against corrosion and wear of the magnesium substrate [1-3].

The surface morphology of the PEO coatings seems porous however improvements in corrosion resistance of the magnesium substrate have been reported by application of the coating prepared under different conditions. Improvements in corrosion resistance by the PEO coating could be attributed to the inner barrier layer lying directly on the metal surface. According to cross section observation and EIS investigations [3,24,90], the structure of a PEO coating is composed of an inner compact (barrier) layer and an outer porous layer which is usually thicker than the barrier layer. The porous layer forms as a result of plasma interaction with the metal and electrolyte while, the barrier layer is formed as a result of the applied potential over the metal. Hence, the electrochemical property of the latter layer depends on the chemistry of the alloy and the environment to which it is exposed [52]. Formation of the barrier layer is a consequence of the reaction between metal ions, here Mg^{2+}, and anions existing in the solutions. Therefore, formation of the layer requires anodic dissolution to provide metal ions. The ions subsequently react with electrolyte species and result in the barrier layer. Formation of barrier layer gives proper ability to the PEO coatings to protect the substrate against corrosion [85,104].

The protection ability of the PEO coating is recently being determined by the Electrochemical Impedance Spectroscopy (EIS) method. The magnitude of the impedance value reported for bare magnesium alloys such as AM50, AZ91, WE43 in

3.5% NaCl solution normally is around 10^3 Ω.cm^2 [5,70,10,105]. However, a corrosion evaluation of the coated substrate in the same environment shows that the PEO coating effectively improves the corrosion resistance of the substrate.

Hsiao et al. [11] prepared a complex solution with the chemical composition of KOH+Na_3PO_4+KF+$Al(NO_3)_3$+Na_2SiO_3. The thickness of the coating was about 10µm on an AZ91 alloy. The maximum impedance value of the PEO coating in 3.5% NaCl reaches about 1.6×10^5 Ω.cm^2. The data reported by Arrabal et al. [70] for coatings prepared by Na_3PO_4+NH_4OH showed that the impedance of the coating in a 3.5% NaCl solution was about 1.2×10^5 Ω.cm^2 on WE43 with a thickness of ~30µm and 0.8×10^5 Ω.cm^2 on AZ91 magnesium alloys with a thickness of about 20 µm. Luo et al. [10] also added different concentrations of $(NaPO_3)_6$ to Na_2SiO_3+KOH+KF+Na_2B4O_7 solutions. His results based on a 3.5% NaCl solution showed that the maximum impedance data, namely 20×10^4 Ω.cm^{2,} was achieved when 5g/l of $(NaPO_3)_6$ was introduced to the electrolyte. These conditions led to a coating layer with about 35µm on an AZ91 alloy. Although the data clearly show improvements in corrosion resistance, it is clear that the composition of the electrolyte influences the final performance of the produced coating.

According to the literature, the protection ability of a PEO coating could mainly be attributed to the chemical composition of the coating. However the latter parameter by itself is determined by the chemical composition of the electrolyte. Different studies have reported beneficial effects of stable phases such as Mg_2SiO_4 [13,10] $Mg_3(PO_4)_2$ [20] and $MgAl_2O_4$ [6,9] to improve corrosion resistance of the PEO coatings. Liang et al. compared the corrosion resistance of two coatings. The first is mainly composed of MgO and Mg_2SiO_4, and the second is mainly composed of MgO. The results show that both coatings provide effective corrosion protection, however the coating consisting of Mg_2SiO_4 shows a better corrosion resistance property [12]. Comparison of the corrosion resistance of the coatings which are composed of MgO and $MgAl_2O_4$ also show that a higher amount of $MgAl_2O_4$ increases the corrosion resistance of the coating [69]. Therefore, the presence of

different anions in the electrolyte determines the chemical composition of the coating which leads to the different corrosion performance.

2.2.4.4 Wear resistance

Beside corrosion resistance, wear resistance of the Mg alloy also has been studied by several researchers. The obtained results indicate that high hardness of the PEO coating (as a ceramic material) enhances the wear resistance of the substrate. It was shown that the PEO coating increase the hardness of the magnesium five times more than that of the bare substrate. The wear rate of an uncoated AM-60 Mg alloy is reported to be about 3.81×10^{-4} mm^3/Nm, while that of the same substrate coated by silicate and phosphate solution are in range of 3.55×10^{-5} - 8.65×10^{-5} mm^3/Nm respectively [12]. The results of Zhang et al. showed that the mass loss of untreated AZ91D under wear test is 1.5 times more than that of coated by PEO process [25]. The latter results indicate that application of PEO coatings is an effective process by which it is possible to improve the wear resistant properties of the magnesium substrates.

2.2.5 Drawbacks

It was explained that the PEO coating improves some properties of the metallic substrates such as wear and corrosion resistance. However, it should be remembered that the nature of this process results in a porous coating which in some cases is together with the cracks. Porous structure is the feature which weakens the performance of the PEO coating especially from the corrosion point of view. The pores and holes on the surface reduce the performance of the coating although they could be employed as an appropriate base for a top coating. The holes and cracks act as the routes to conduct the corrosive medium into the coating structure which deteriorates the prevention properties of the coating.

The PEO process by itself, especially from the efficiency viewpoint, still needs to be improved. Calculations made by Guo et al. [18] during a PEO process on a magnesium alloy also showed low efficiency (9.31–61.51%) of the current depending on the concentration and composition of the electrolyte. The possible

reasons leading to the low current efficiency could be related to oxygen evolution in the anode, anodic dissolution of metal and chemical dissolution of pre-existing oxide films in the electrolyte. Among these reasons oxygen evolution (excessive oxygen) associated with the passing current during a sparking phenomenon is considered to be the most likely dominant one.

Snizhko et al. [4,106] have studied the efficiency of the current during the PEO process by attempting to understand the mechanisms underlying gas evolution and partial processes such as dissolution, oxide film formation and dielectric breakdown at the anode surface. The overall efficiency of the current lies in the range of 10-30%, depending on concentration of the solution. The evolution of the oxygen was shown to be the main electrochemical process which reduces the efficiency of the process.

2.3 Conclusion

A review of literature has showed that so far different aspects of the PEO process and the coating have been studied. Different theories and models have been proposed, several surface morphologies of the coatings have been recognized, several combinations of electrolytes have been tested, effective parameters have been studied, coating performance has been determined, and so on. However, as plasma electrolytic oxidation is a complex process and also because different parameters directly and indirectly influence the final performance of the coating, different aspects of the process still need to be studied. The studies can provide more information regarding the process leading to an improvement in the final performance of the coating.

The substrate microstructure which includes grains, grain boundaries and intermetallic phases, as well as the solution concentration, are the features whose role in the formation of the coating has rarely been studied. Each of these components influences the formation mechanism, structure and morphology of the coating and needs to be studied in detail under different conditions of the coating process.

On the other hand, the composition of the solution is one of the most important elements which has a great influence on the performance of the PEO coating. The type of the ions existing in the electrolyte is a factor which influences the stability of the passive layer and final properties of the PEO coating. Not much work has been dedicated to investigating the role of the passive layer in the PEO coating process, although breakdown in this layer is the basis of layer formation during the process. It has also been explained that there are still contradictory results regarding the optimum solution composition. The existing lack of information necessitates detailed studies on the electrolyte and its effect on the passive layer and coating properties. This aim will not be achieved without conducting systematic study of different solutions under similar conditions. So the main objectives of this work can be summarised as a detailed study of “the formation process and structure of the PEO coating” as well as “the influence of the solution composition on the stability of the passive layer and the corrosion resistance of the PEO coatings”.

3 Motivation and objectives

In the last chapter, some aspects of the PEO coating which still need to be further studied were mentioned. It was explained that the role of some parameters is still unknown and the results of some investigations show contradictions. The PEO coating process still lacks some information which could be clarified just by doing some systematic study. The open questions regarding the influence of the substrate microstructure on the formation process and the distribution of the phases in cross section are among those that should be answered. Different components of the microstructure like grain boundaries and secondary phases influence the formation process because of diverse arrangements or different compositions. The lack of information about the formation process on each component and the distribution of the phases in the coating structure are matters which needs to be considered and reasonable explanations found. This is one of the objectives of the present study. The present study clarifies precisely how the coating forms on each microstructure components during the coating process and how the phases are distributed in the coating structure. It also discusses and finds reasonable explanations for the observable incidences based on the experimental results and literature review.

In order to study the formation process and structure of the coating, the formation of the coating layers on each of the substrate phases were studied in different concentrations step by step. Diluted, medium and concentrated solutions were used to prepare coatings with very short, intermediate (pre and post breakdown) and long process durations. The behaviour of the layers formed on each phase was studied by SEM and the corresponding composition was analysed by EDAX. Type and distribution of the phases in the coating were also evaluated in XRD and XPS experiments. The results of this study reveal how the microstructure of the base metal and concentration of the solution influences the formation process. It provides more information regarding the initial stages of the formation process and shows which kind of morphology forms on the surface of each phase. As the surface morphology directly influences the final performance of the coating, the obtained results can provide a better understanding for future improvement of the process.

The lack of information or contradictory literature regarding the "influence of the solution composition on the stability of the passive layer and corrosion resistance of the PEO coating, as well as the role of the passive layer in the PEO process" is another issue which is addressed in this work. The present study answers the open questions regarding the influence of the different solutions on the stability of the passive layer and PEO coating. It clarifies how stability of the passive layer influences the performance of the PEO coating. It also explains how and why different solutions influence the performance of the PEO coating and which solution has a greater ability to improve the coating performance. So a detailed study to understand the influence of the solution composition on the stability of the passive layer and performance of the PEO coating is the next objective of this study.

To achieve this aim, different solutions were selected based on the literature review and some primary experiments. The solutions which are on the base of silicon, phosphorous and aluminium and different hydroxides were selected for the coating process. Chemical and physical characteristics of all solutions were determined by checking the solution properties such as conductivity and pH. The stability of the passive layer formed in different solutions was determined by impedance and polarization tests. Corresponding to each solution, the PEO coatings were applied on the substrate under similar conditions and the coatings were characterized. Surface morphology, cross section, chemical phases of the coatings were analysed and subsequently the corrosion resistance of the PEO coatings was evaluated by different test methods. The results of this study provide more information about the role of the solution composition in the PEO process. The relationship between the stability of the passive layer and the corrosion resistance of the PEO coating has also been explained in the present work. The outcomes of this study provide evidence on the relationship between the stability of the passive layer and the corrosion resistance of the PEO coating.

4 Experimental methods

This chapter will give information regarding the experimental methods employed in the thesis. The experiments mainly consist of "preparation and application of the PEO coatings on substrate", "characterization and description of the PEO coatings as well as the coating process" and "evaluation and analysis of the passive layers and the PEO coating". In order to give a clear explanation, different procedures are classified under three categories, i.e.:

1-Coating preparation,

2- Coating characterization,

3- Coating evaluation.

4.1 Coating preparation

In order to obtain a successful PEO coating, essentially three components should be considered which are: substrate, electrolyte and source of current/voltage. Each of these parts should be properly selected to get a successful coating on the surface.

4.1.1 Substrate

AM 50 magnesium alloy with chemical composition of "4.89 % Al, 0.30 Mn, 0.02% Zn, 0.002% Fe, reminder Mg" measured by optical emission spectrometer (OES), Spectrolab M9-2003, was used as substrate. It should be noted that in the present manuscript any phrases such as "substrate" or "bare metal" refer to AM 50 magnesium alloys. The specimens in size of 15×15×4 mm^3 were ground up to 2500 grade by silicon carbide papers. To get a stable current transfer through the sample and electrolyte, a threaded hole with a diameter of 2.5mm was applied on one of the lateral sides of the specimens and the specimens were screwed to a holder.

4.1.2 Electrolyte

4.1.2.1 Study of the formation process

Formation process of the PEO coating on each of the substrate components (i.e. η-Al_8Mn_5, β-$Mg_{17}Al_{12}$ and α-Mg) was studied in diluted (1 g/l), medium (10 g/l) and

concentrated (20 g/l) sodium silicate solution. 10g/l of potassium hydroxide were added to each solution and a constant current density of 3.6 mA/cm^2 was employed for the preparation of the PEO coatings. Such a low current density was employed to reduce the rate of coating formation and therefore provide appropriate conditions to study the layer development step by step.

For each concentration, five different samples were prepared in short (20s), intermediate (pre and post breakdown) and long (750 and 1500s) periods of the process. The intermediate period samples were prepared within the processing time in which the voltage reached to about ± %10 of breakdown voltage. The breakdown voltage (V_{BD}) is referring to the moment when some scatter sparks can be seen on the surface. It was seen that changes in the concentration of the solution influences the magnitude of the breakdown voltage. The diluted solutions require a higher voltage to acheive the sparking phenomenon. Hence this kind of sample preparation provides the proper conditions to study the layer formation in the initial stages, and before and after the break down phenomenon, as well as in the final stages of the coating process.

Table 4.1 and Fig. 4.1 show the variation of voltage and preparation conditions respectively. The coated samples were subsequently analyzed by EDAX, XRD, XPS and SEM in order to determine the point analysis, phase identification, phase distribution and surface morphology, respectively.

Table 4.1. Preparation condition of the samples in Fig. 4.1

Condition	**Voltage(V)**		
	1g/l (V_{BD}=195V)	**10g/l (V_{BD}=160V)**	**20g/l (V_{BD}=135V)**
20 sec.	38	38	38
V< V_{BD}	175	145	120
V> V_{BD}	215	175	150
750 sec.	300	270	225
1500 sec.	360	322	255

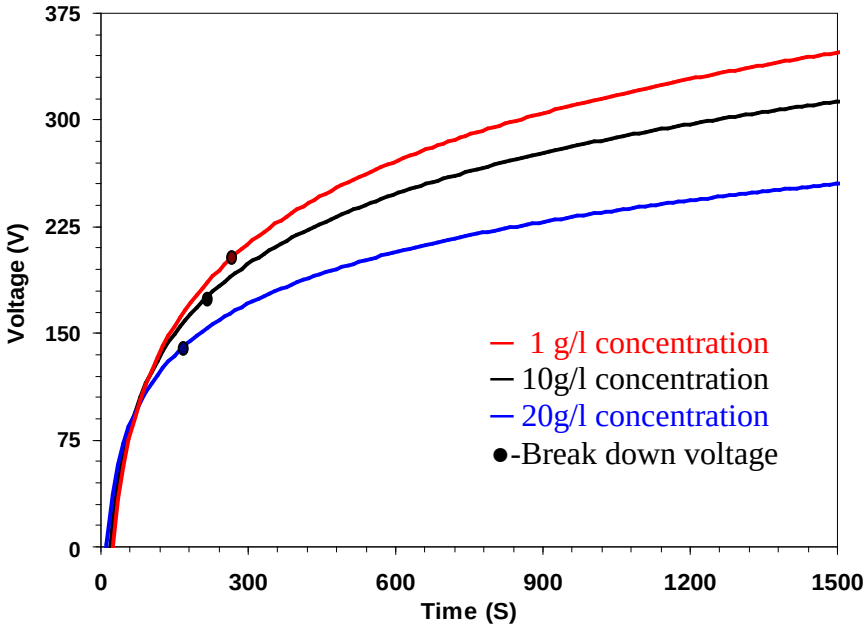

Fig. 4.1. Variation of voltage during the coating process in different concentration

4.1.2.2 Study of the role of solution composition

To study the role of the solution composition, different electrolytes were employed for the coating preparation. Table 4.2 shows the salt solutions which are based on the silicon, phosphorous and aluminum. The pH and conductivity of the solutions were measured by Metrohm pH meter 691 and Mettler toledo conductivity meter, respectively. These specific compounds were selected on the basis of the literature review and environment concerns. Therefore, instead of some toxic chemicals based on fluoride [79] chromium [80] and ammonia [81], more environmental friendly salt solutions were employed. The solubility, pH and conductivity of solutions were other parameters which were taken into consideration. Selection of the salt solutions with similar cation but dissimilar anions provides proper conditions to study the influence of the compound stoichiometry on the PEO process.

Table 4.2. The salt solutions.

Na_2SiO_3	K_2SiO_3	Na_3PO_4	$Na_5P_3O_{10}$	$Na_2H_2P_2O_7$	K_3PO_4	$K_4P_2O_7$	$NaAlO_2$

In order to perform a proper comparison, the coatings were classified in four groups based on the chemical composition of the solutions. Silicate, sodium-phosphate, potassium-phosphate and aluminate coatings are the four groups of the coating in the study. These solutions were employed to determine the stability of the passive layer and the corrosion resistance of the corresponding PEO coating.

To study the role of solution composition, the coating layer was applied on the substrate under a constant current of 36.2 mA/cm^2 for 5 minutes in 10g/l of each solution listed in table 4.2 with the addition of potassium hydroxide in the same concentration. Then the corrosion resistance of the PEO coatings was evaluated by both of impedance and polarization test methods.

The proper conditions of time, current density and concentration of the solutions were determined by performing some primary experiments. It should be born in mind that the solutions have dissimilar chemical compositions, conductivity, pH and solubility. Therefore it was necessary to find a condition which can be applied for all of the solutions without producing a problem. The results of the primary experiments showed that the application of a constant current density of around (36.2±5) mA/cm^2 within (5±1) minutes and of a concentration of (10±3 g/l) are the proper conditions that provide a successful PEO coating for all salt solutions. Significantly higher or lower deviation from these conditions could lead to different failures like early burning effect, not getting to the sparking phenomena, not achieving an acceptable thickness of the coating and so on. In this manuscript, the above conditions are referred to as the “common conditions” to avoid repetition.

in order to study the stability of the passive layers formed in each solution, two kinds of experiments were designed, namely *immersion* and *anodic polarization* methods. In the first set of experiments bare substrates were immersed in 100ml of salt solutions with a concentration of 10g/l in room temperature for about 525 hours. This period of immersion was required for the formation of a distinguishable passive layer on the surface. After this, the stability of the layers was determined by the impedance test method. In the second set of the experiments bare substrates were anodically polarized with a scan rate of 12 mV/min from -150 to 3500 mV with respect to the open circuit potential (OCP) by using each of the salt solutions with and without

hydroxide to consider the behaviour of the passive layers in different environments. Prior to the polarization, the substrate was immersed in the solutions for 30 min to reach a stable potential.

It is known that the coating solutions consist of at least two parts. The first part is usually a salt solution and the second part is normally a hydroxide solution. As well as the salt solutions, the effects of the hydroxide solutions on the stability of the passive layer and on the corrosion resistance of the PEO coatings were studied. Table 4.3 lists the chemical composition of the hydroxides which are used in the study. Similar to the salt solutions, the stability of the passive layer in different hydroxides and the corrosion resistance of the corresponding PEO coatings were evaluated. Sodium silicate as a salt solution was added to each of the hydroxides to prepare PEO coating under common condition. It should be mentioned that in case of the $Al(OH)_3$, $Mg(OH)_2$ their solubility is lower than 10 mg/l [107], and the saturated solution was used.

Table 4.3. The hydroxides

KOH	NaOH	$Al(OH)_3$	$Mg(OH)_2$

4.1.3 Source of current/voltage

Depending on the capabilities of the power supply, it is possible to use different types of currents, such as AC, DC and pulse DC, in a PEO process. Fig. 4.2 shows a schematic of different signals. The power supply employed in the project has the ability to produce AC and DC in ordinary and pulsed forms in frequency of 50Hz and up to 1000 V and 3A.

All the samples were prepared by applying the pulsed DC current with $t_{min} : t_{max} = 1$ ms : 4 ms. The temperature and agitation of the electrolyte were kept constant at 25^{oc} and 200 rew/min respectively. The set up used in the study can be seen in the Fig. 4.3.

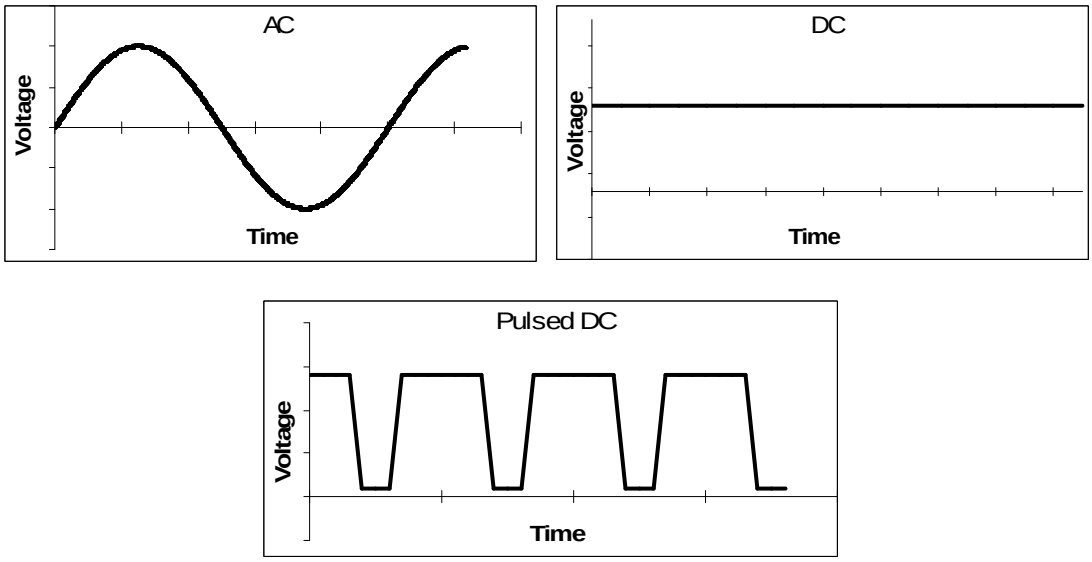

Fig. 4.2. Schematics of the AC, DC and Pulsed DC signals

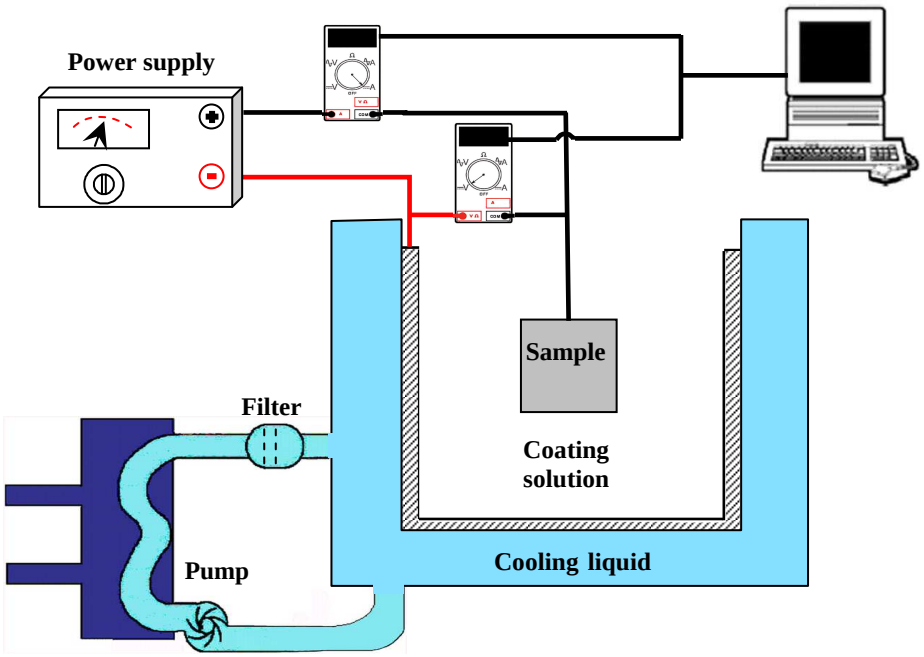

Fig. 4.3 Schematic of the coating facilities

4.2 Coating characterization

4.2.1 Corrosion resistance

The corrosion resistance of the coatings, with at least three measurements for each case and calculation of standard deviation for errors, was evaluated by

electrochemical impedance spectroscopy (EIS) and polarization test methods in 3.5%wt of sodium chloride (NaCl) solution. The data collected by impedance test methods theoretically forms a semicircle curve which is called as Nyquist curve. Fig. 4.4-L shows a typical Nyquist curve. The Rs equals the solution resistance and Rp equals the polarization resistance which is a proportional indicator of the corrosion resistance. An alternative method of data plotting is the impedance plot. Fig. 4.4-R schematically shows the impedance plot which is based on the logarithmic scale.

Before running the tests, the samples were immersed in the test solution for 30 min to reach a stable condition i.e. open circuit potential (OCP). The impedance test was set up on the frequency range between 0.1 and 10^4Hz with amplitude of ±10 mV.

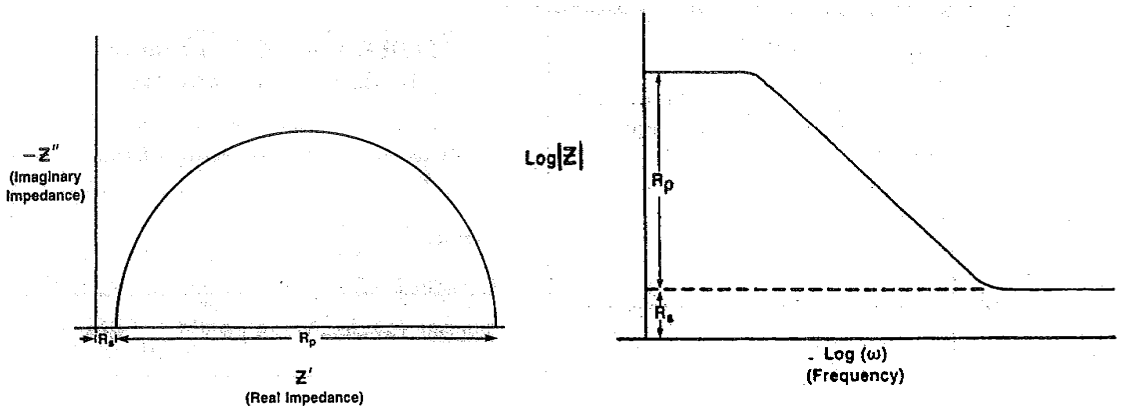

Fig. 4.4 Simple charge transfer corrosion process. Its L) Nyquist and R) Impedance curve.

The second method i.e. the anodic polarization test is one of the common electrochemical techniques which is on the basis of the two opposite reactions namely reduction and oxidation (redox reactions). In the anodic reaction a metal is oxidized and release the electrons. In the cathodic reaction the solution species which can accept electron (e.g. O_2 or H^+) are reduced by taking electrons from the metal. The equilibrium point of these two opposite reactions determines the rate of the corrosion. Fig. 4.5 shows the current-potential relationship of a redox system.

During the polarization test of a metal, it is expected that application of more positive potentials results in the higher value of the current density. The higher current

density is equal to higher rate of the corrosion. Under specific conditions, a resistive layer can forms on the surface of some metals which is able to protect the underlying substrate. This layer is called as "passive layer". The passive layer can also form on the surface of some metals in special range of potentials (or voltages). In this case, the current density remains constant and it doesn't increase as the potential increases. This current is known as "Passive current".

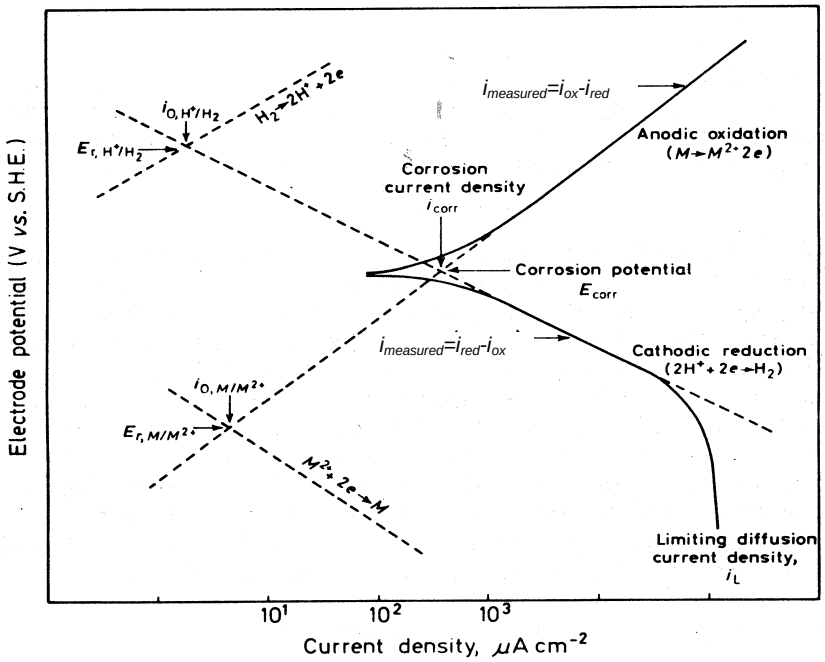

Fig. 4.5 Relationship between potential and current for redox reactions.

The anodic polarization test was done under a scan rate of 12 mV/min which starts from -150 to 3000 mV with respect to OCP. The sketch of the corrosion test facilities used in the study is shown in the Fig. 4.6. The corrosion cell, which has a volume of about 450 cm^3, consists of an Ag/AgCl (3mol/l KCl) reference electrode, a platinum counter electrode and a PEO coated specimen as a working electrode. An ACM Gill AC potentiostat in connection with a computer controlled the current and voltage applied.

4.2.2 Propagation of the corrosion pattern

The corrosion behaviour of the PEO coating immersed in a still solution of 3.5% NaCl was studied by taking photos with intervals of 7.5 min in room temperature.

The "progress of the corrosion process", "propagation pattern of the corrosion" and "required time for appearance of the first corrosion products" are among the items of information which could be studied by the dynamic corrosion observation.

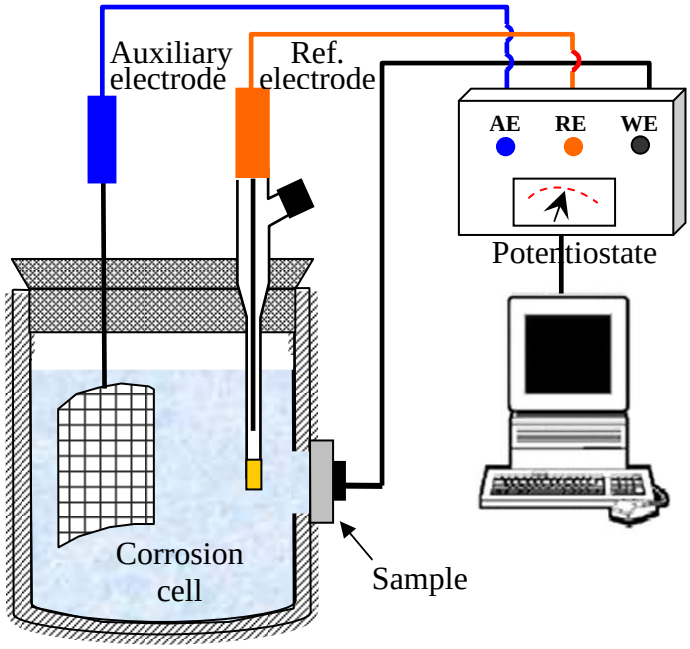

Fig. 4.6 Sketch of the corrosion test facility

4.2.3 XRD Phase determination

The phases of the coatings were determined by using x-ray diffraction (XRD) method. The experiments were performed by a Siemens diffractometer D 5000 using a Cu K_α radiation source. The step scanning range was set to between 20-80 degree with steps of 0.05º and a step time of 3 seconds.

4.2.4 SEM and LM study

Scanning Electron Microscopy (SEM), Cambridge stereoscan 250, was employed to observe the surface morphology and cross section of the coatings. For cross sectional observation the cut samples were mounted by methyl methacrylate, polished by silica powder aqueous suspension and gold sputtered.

The light microscopy (LM) samples were prepared by etching the polished specimens in "7 (ml) acetic acid + 40 (ml) distilled water + 140 (ml) ethanol + 5(gr)

picric acid" solution and the pictures were taken by means of a Leica DMI 5000M inverses Hellfeld microscope.

4.2.5 Thickness and pore measurements

Besides observation of the cross section by SEM, the thickness of the coatings was measured by using an eddy-current coating thickness measurement gauge (Minitest 2100, Electrophysik, Germany). The resolution of the gauge is about 0.1 µm with a measurement ability of the coatings in the range of 1-200 µm. It should be noted that the reported data are averages of at least three different measurements.

To identify the open pores, the coated samples were immersed in a solution containing 60 g/l CH_3COOH + 5 g/l $CuSO_4$. $5H_2O$ + 15 g/l $ZnCl_2$. $7H_2O$ for 30 seconds [108]. As a result of this immersion process, copper is deposited on the alloy and decorates the open pores. In order to count the open and total number of the pores, the LM and SEM pictures were used, respectively. The counting process and image analysis was performed by the Image Tool® software. Several measurements were done and the software was properly set up to reduce possible errors.

4.2.6 XPS study

The 2×2 mm^2 of the coating surfaces were analyzed by XPS examination to determine how the coating phases are distributed and how concentration of the elements changes through the coating thickness. The XPS study was performed by Kratos DLD Ultra spectrometer device with a Al K_α source (monochromator) as an anode. The concentration and chemical state of the elements were determined using argon sputtering with energy of 3.8keV.

4.3 Coating evaluation

4.3.1 Optical emission spectroscopy

Reactions which occur during the PEO process lead to some visible optical radiations. Optical emission spectroscopy consists of the collectors which are able to gather and analyze the radiations and illustrate the results as wavelength-intensity

patterns. The sources of the emissions are excited elements in the plasma environment. As the excited elements radiate on some specific wavelengths, the elements in plasma could be determined and possible reactions could be estimated. The emitted light from PEO coatings prepared under the "common conditions" was analyzed by an optical emission spectroscopy appliance provided by Plasus Company.

4.3.2 Characterization of the spark phenomenon

In order to characterize the behaviour of the sparks in 10g/l of sodium silicate and potassium hydroxide, the change of the feature, size and number of the sparks was studied during the PEO process. To achieve this objective, a constant current in the magnitude of 9 mA/cm^2 was applied and the behaviour of the sparks were recorded by taking continuous photos in different stages with intervals of 150 ms. The life time of the sparks in different stages were determined by following the events from first appearance to fading away in sequential pictures. Quantitative values such as number and size of the sparks were analyzed by using UTHSCSA Image Tool software.

4.3.3 Corrosion progress

The impedance data were employed for study of the coating layers (10g/l Na_2SiO_3+KOH, 36.2 mA/cm^2, 5 min) and corrosion progress by curve fitting method. This method, which is based on the electrochemical results, tries to fit a curve to the impedance data by employing a proper equivalent circuit. The curve fitting process, together with information coming from the cross section of the coating, provides some detailed information about the arrangement of different layers in the coating. Behaviour of different layers could be related to the circuit components of which the values are known. So, the structure and characteristics of the coating could be recognized by analyzing the values.

Fig. 4.7 shows the equivalent circuit which was used in this study. In general, an equivalent circuit can consist of different components such as capacitor, resistor, warburg element and so on. Each component of the equivalent circuit reflects the specific character of the coating layers. The employed equivalent circuit consists of

three resistance and two constant phase elements (CPE), each of which is parallel with a resistor. the combination of a CPE and a resistor is referred as a time constant. The circuit consists of two time constants, suggesting two different layers in the coating, namely outer and inner layer. The R_S, R_1 and R_2 represent the solution resistance, and the resistances of the outer and inner layers, respectively. CPE_1 and CPE_2 represent the capacitances of the outer and inner layers, respectively.

To get a better fit and also include a surface inhomogeneity factor and a possible diffusional factor, a more general constant phase element (CPE) was used instead of a rigid capacitive element. The capacity element is expressed by the following equation:

$$Z_{CPE} = 1 / [T (j\omega)^P] \qquad (4\text{-}5)$$

Where T is CPE constant, j is the imaginary unit ($\sqrt{-1}$), ω is the angular frequency (1rad/s) of the sine wave being considered as $\omega = 2\pi f$, f is the frequency in Hz; the value of P ranges between 0 and 1. The values 0, 0.5 and 1 of P imply the CPE of the circuit to be pure resistor, Warburg impedance and capacitor, respectively [109,110].

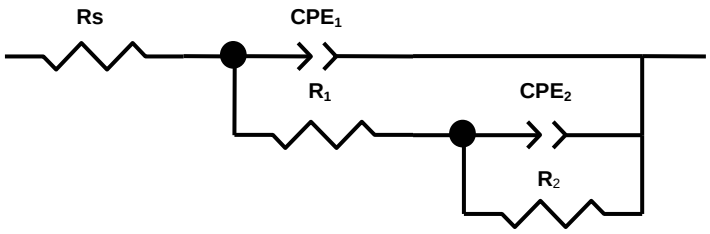

Fig. 4.7. Equivalent circuit modeling a porous coating.

It should be noted that with regard to the microstructure of the coating, different combinations of elements (such as resistor, capacitor, and Warburg diffusion) in different sequence (i.e. parallel, series) were checked. Among these different combinations, the equivalent circuits of Fig. 4.7 gave the best fitting results with the lowest error.

5 Results

The results are divided in two separate sections to present the work in a proper way. The study of the "formation process and structure of the coating" which gives basic information regarding the PEO process is presented first. After understanding the essentials of the formation process and the way different parameters influence the process, the results of the "influence of the electrolyte composition on the PEO coating" is presented. The latter study examines different compositions of solutions to find out which composition, and for which reasons, results in higher performance of the PEO coating.

5.1 Formation process and structure of the PEO coating

5.1.1 Sparking phenomenon

Essentially, formation of the PEO coating starts when the sparking phenomenon takes place on the surface. The sparks, apart from their spectacular appearance, provide the proper environment for the elements to react together to form the coating. The reactions happening in the plasma environment of each single spark are the main factor converting the surface to the oxide material. Behaviour of the sparks during the PEO process was studied because it provides a better understanding regarding the PEO process and formation study. The process was observed in different stages and the sparks were characterized. Precise observation of the events revealed that feature, size and number of the sparks change as the process is going on.

Fig. 5.1-a shows that as soon as the voltage rises, gas bubbles forms on the surface. Reaching to a certain voltage known as breakdown voltage, some tiny scattered sparks were observed on the anode surface. The sparking phenomenon was studied by considering the spark characteristics such as colour, size, life time and quantity, listed in Table 5.1. As the process proceeds, five different phases can clearly be recognized.

In the first phase, from the beginning of the sparking phenomenon to about 900 seconds, the sparks are white in colour, equal or smaller than 0.1 mm, with a density of about 55 sparks/cm^2 and with a life time shorter than 0.15 seconds (Fig. 5.1-b). In this phase of the process no audible sound is heard and the sparking process keeps going on without any sound.

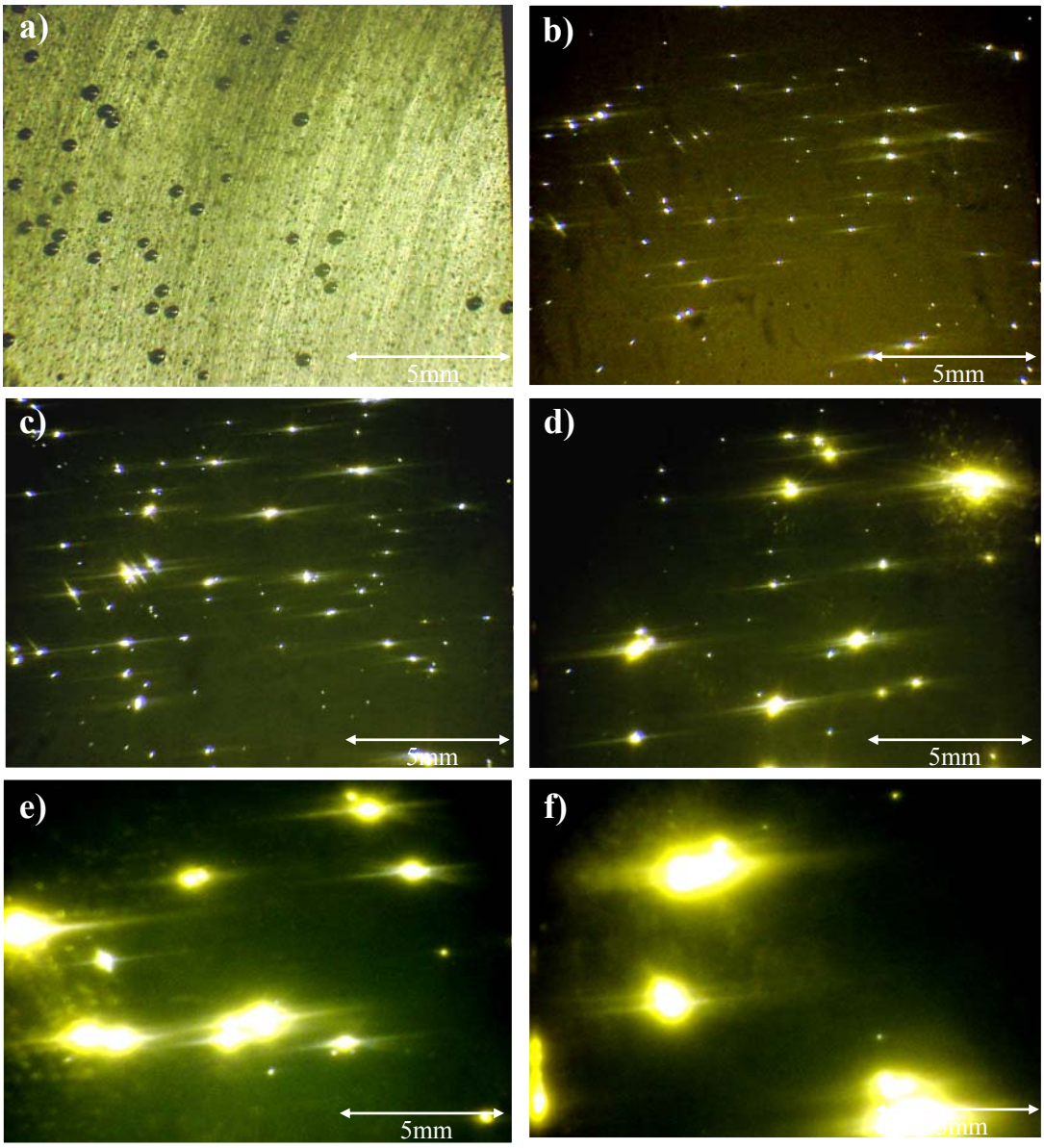

Fig. 5.1. Magnesium alloy (AM 50) under PEO treatment after about a) 100 (before sparking), b) 650, c) 1500, d) 3000, e) 5000, f)7000 seconds.

The second phase starts from 900 seconds and ends at 1800 seconds. Within this period, the sparks change to a yellow colour, a size of ~0.5 mm, and a density of

approximately 42 sparks/cm^2 but the life time of the sparks still is shorter than 0.15 seconds (Fig. 5.1-c). Unlike the previous phase, low audible sounds can be heard in this phase.

In the third phase, which ranges between 1800 and 3500 seconds, the colour of the sparks shifts to orange, with lower spark density which is approximately 20 sparks/cm^2. The sparks of sizes smaller than 1.5 mm appear on the surface and the maximum life time of the sparks reaches about 0.7 seconds (Fig. 5.1-d). In this phase of the process a clear sound can be heard as a result of the sparking process.

Table 5.1. Chang of the visual characteristics of sparks during the coating process

Character / Time(sec.)	Colour	Approximate size (mm)	Quantity (spks./cm^2)	Life time (s)	Sound
0-900	White	≤ 0.1	55 ± 7	$< 150\times10^{-3}$	inaudible
900-1800	Yellow	≤ 0.5	42 ± 5	$< 150\times10^{-3}$	quiet
1800-3500	Orange	≤ 1.5	20 ± 3	$\leq 700\times10^{-3}$	audible
3500-6000	Orange	≤ 2	7 ± 2	$\leq 1800\times10^{-3}$	noisy
6000-7200	Orange	≤ 2.5	2 ± 1	$\leq 3000\times10^{-3}$	loud

The time period of the forth phase varies between 3500 and 6000 seconds. The orange colour of the sparks becomes more recognizable and most of the events are bigger in size i.e. ~2 mm but lower in the number i.e. ~7 sparks/cm^2 (Fig. 5.1-e). Reaching to this point, the process produces more noise and although some sparks still appear and fade in a short duration of time, the life time of the sparks increases to about 1.8 seconds.

In the last phase of the coating process which starts at 6000 and ends at 7200 seconds (which is start of the burning effect) no considerable change occurs in the colour of the sparks. However the size of the sparks becomes equal or smaller than 2.5 mm and number of the sparks reduces to about 2 sparks/cm^2 with longer life time of ~ 3 seconds (Fig. 5.1-f). The noise of the process can still be heard and from time to time it reaches a loud and annoying sound.

5.1.2 Formation process on different components of the substrate

Fig. 5.2 shows the microstructure of the substrate employed in the study which is produced by the casting method. The lower magnification picture shows that the alloy contains large grains (~400 µm) and the higher magnification shows that η-Al_8Mn_5, β-$Mg_{17}Al_{12}$ and α-Mg are different phases existing in the structure of the alloy.

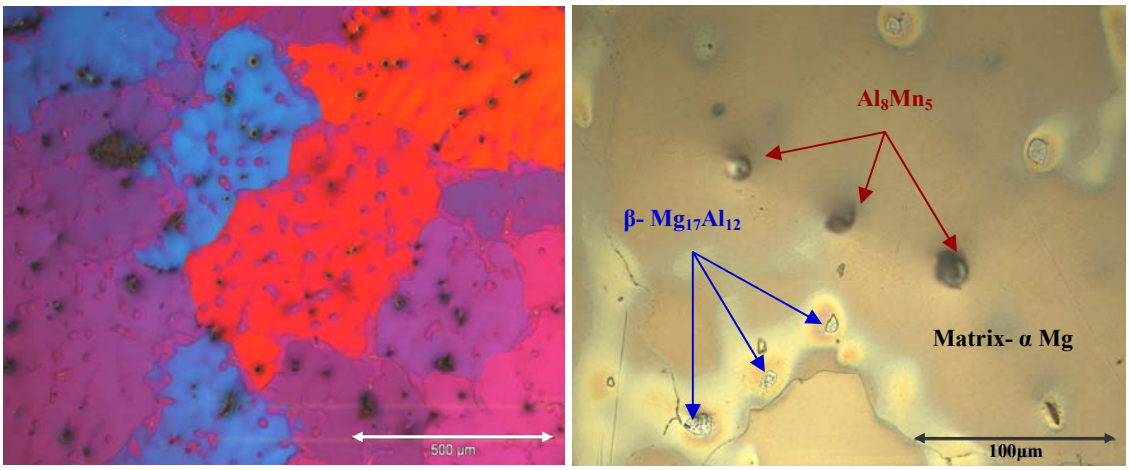

Fig. 5.2. Microstructure of AM50 alloy in L) low and R) high magnification.

Microstructure of the AM 50 magnesium alloy was also identified by SEM and EDAX. Fig. 5.3 shows typical morphology of the η-Al_8Mn_5 and β-$Mg_{17}Al_{12}$ particles embedded in the α-Mg matrix with no treatment and after 24h immersion in a coating solution (10g/l Na_2SiO_3+10g/l KOH). It is seen that the particles have an intact surface and there is no gap between the phases and matrix even after 24h immersion in coating solution. On the other hand, it is seen that the interface regions between phase and matrix are continuous and ceaseless. Table 5.2 contains the data showing the composition of the phases. As expected, the Al_8Mn_5 phases contained a high percentage of aluminium and manganese and β-phase composed mainly of magnesium and aluminium. The results also showed that the matrix region was composed of a high percentage of magnesium and little amount of aluminium.

5.1.2.1 Formation process on Al_8Mn_5 particles

Fig. 5.4 shows the coating evolution on Al_8Mn_5 phase with a typical blocky shape in different steps. The chemical composition of the particles was analysed by EDAX and the results are entered in Table 5.3

Table 5.2. Point analysis of the phases in Fig. 5.3-a,c.

Elements (at%)	**O k**	**Mg k**	**Al k**	**Si k**	**Mn k**
η-Al_8Mn_5 phase	13.62±1.2	1.46±0.6	49.45±2.4	0.22±0.08	35.25±2.2
β-phase	0.81±0.1	65.39±2.3	33.25±2.1	0.49±0.09	0
α-Mg	0.28±0.2	95.4±2.5	3.31±1.1	0	0.06±0.01

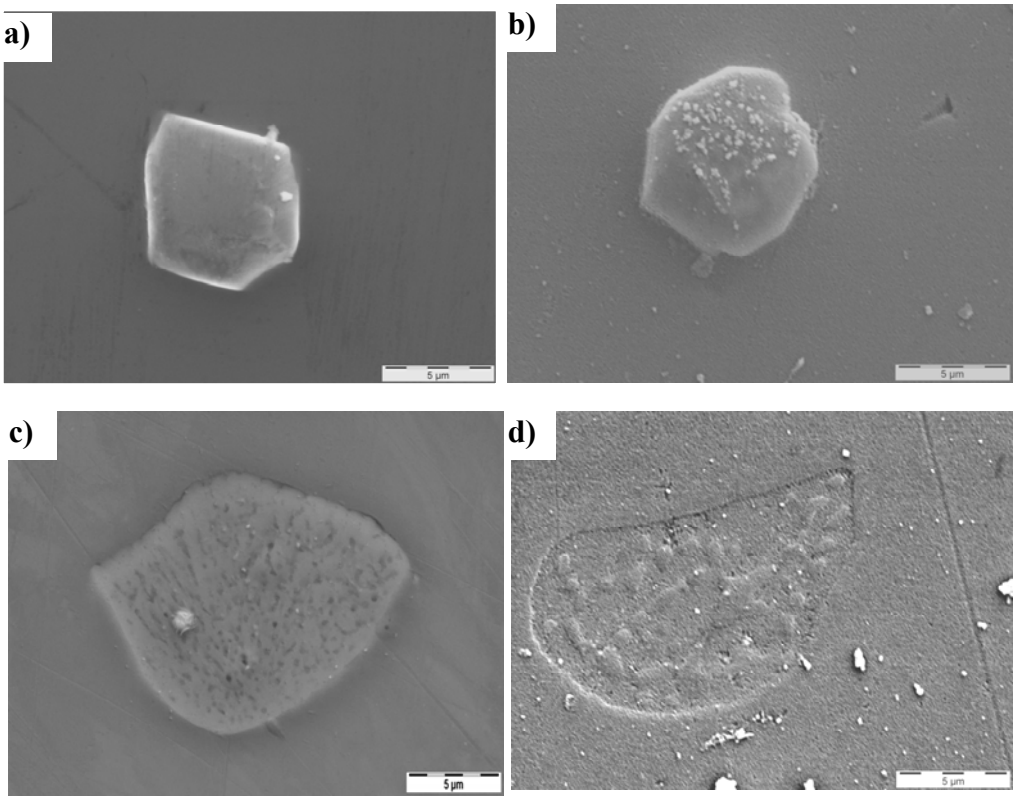

Fig. 5.3. Typical morphology of the a,b) Al_8Mn_5 and c,d) β-phase under condition of a,c) no treatment and b,d) after 24 h immersion in Na_2SiO_3+KOH solution.

In addition to their typical morphology, the high percentage of Al and Mn confirms that the detected phases are the Al_8Mn_5 particles. Fig. 5.4-a gives clear evidence that even within a short duration of the process, i.e. just after 20 seconds, obvious changes occur around the particle. The changes show that the connectivity between the matrix and particle in the matrix/phase interface region is gone and a peripheral

ring has formed around the particle. Some dendrites also are seen in the outer layer of the ring which shows the growth direction of the new products.

Table 5.3 Point analysis of Al_8Mn_5 phases in the different duration

Elements (At%)		**O k**	**Mg k**	**Al k**	**Si k**	**Mn k**
Al-Mn phase (Al_8Mn_5)	**20 sec.**	16.98±1.1	1.48±0.4	47.14±1.9	1.8±0.5	32.61±1.2
	V< V_{BD}	22.9±1.2	1.26±0.5	46.43±1.8	1.61±0.4	27.79±1.1
	V> V_{BD}	41.26±1.5	1.49±0.6	36.99±1.4	3.37±0.6	16.2±1.3
	750 sec.	43.01±1.4	1.1±0.7	36.16±1.3	4.02±1	15.03±1
	1500 sec.	46.68±1.8	0.98±0.2	32.69±1.6	5.55±1.2	13.65±0.9

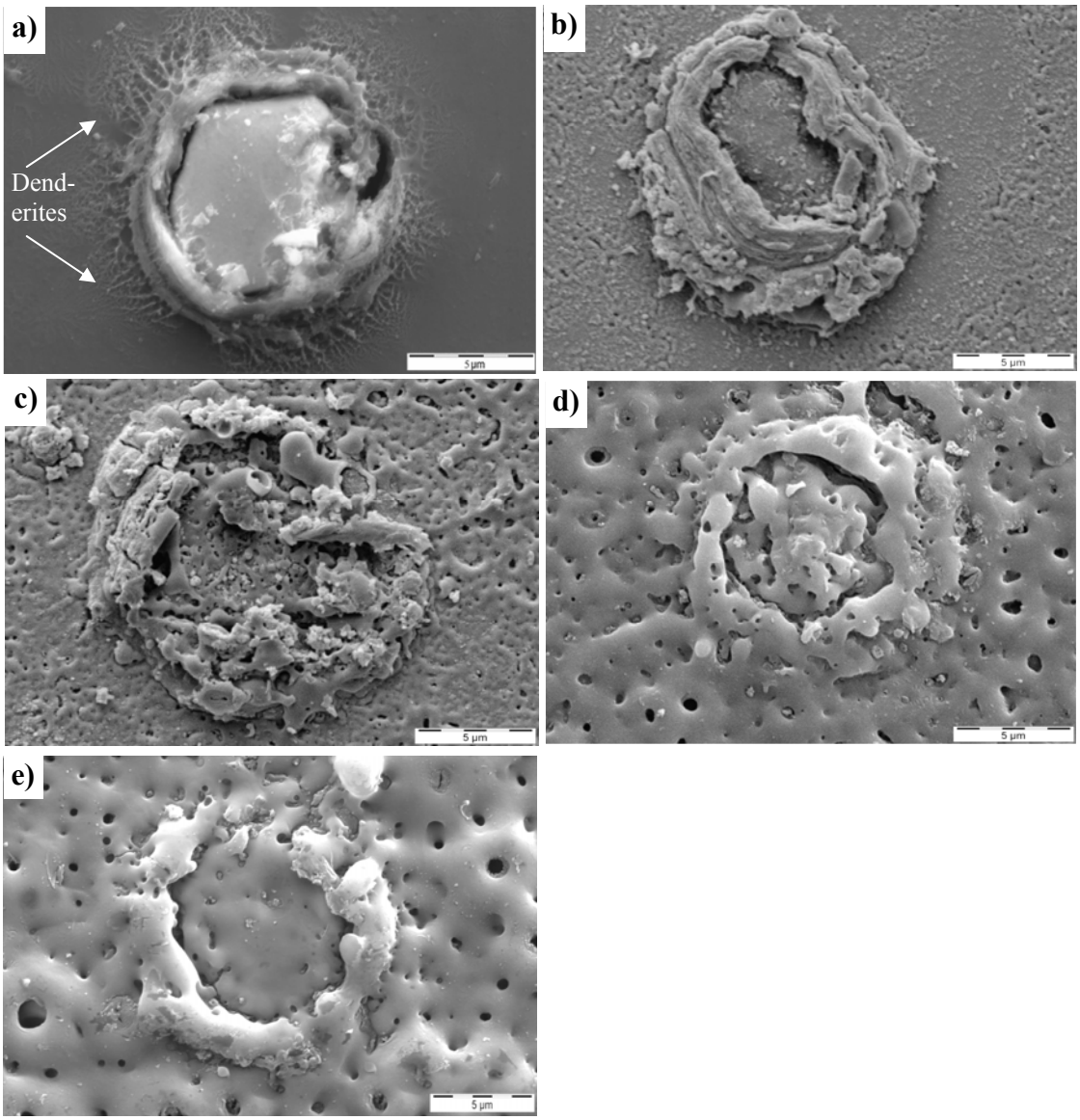

Fig. 5.4. Coating evolution on Al_8Mn_5 particle after a) 20 seconds, b) lower and c) higher than V_{BD}, d and e) 750 and 1500 seconds.

The chemical composition variation of the matrix, peripheral ring and the particle was determined by employing the EDAX experiment. The results in the Fig. 5.5 clearly show that the ring in the matrix/particle interface regions has higher Si and O compared to that of the adjacent area.

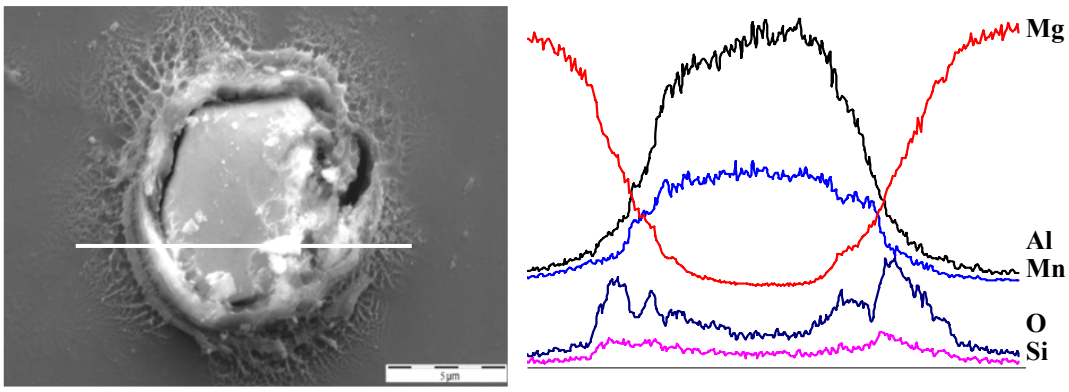

Fig.5.5. The line scan results of the Al_8Mn_5 after 20sec.

Fig. 5.4-b contains an image of the Al_8Mn_5 phase in voltage lower than V_{BD}. It shows that the peripheral ring around the particle has grown. The central area of the particle however shows no evidence of breakdown and it seems still intact.

Fig. 5.4-c shows the surface morphology of the particle after the sparking phenomena. Non-uniform surface as well as some tiny discharge tunnels on the surface of Al_8Mn_5 particle, clearly indicates that the particle involved in the coating process and PEO coating start forming on the surface of the particle. However the coating layer formed on the particle surface and on the peripheral ring are still disconnected and some cavities can be observed in the interface regions.

Fig. 5.4-d and e show the morphology of the particle after 750 and 1500 seconds. The figures show that a complete PEO coating layer has formed on the Al-Mn phase. However, the ring with the greater thickness is still distinguishable around the particle. The coating layer on the round ring shows proper continuity with that on the matrix however that on the ring and the particle does not show proper continuity.

5.1.2.2 Formation process on β phase

The formation process and chemical composition of the β particles in different durations of the process is shown in Fig.5.6 and Table 5.4 , respectively. Fig.5.6-a shows surface of the β particle after 20 seconds. The surface of the β particle and α-Mg matrix shows that different formation behaviour of the phases occurs. It shows that unlike the β particle, very thin nets forms on the α-Mg matrix areas.

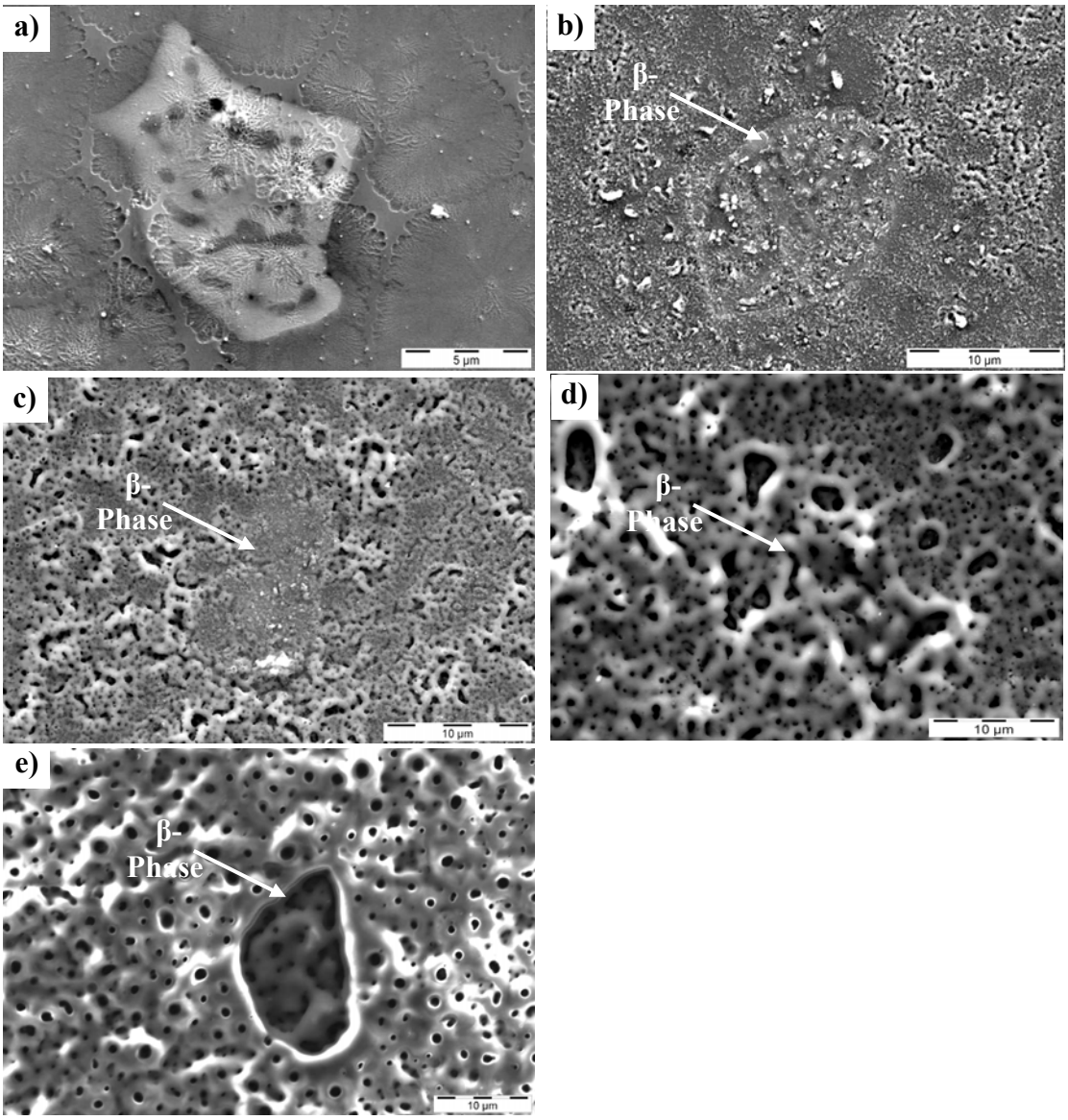

Fig. 5.6. Coating evolution on β phase after a) 20 seconds, b) lower and c) higher than V_{BD}, d and e) 750 and 1500 seconds.

Table 5.4 . Point analysis of β-phase in the different duration

Elements (At%)		**O k**	**Mg k**	**Al k**	**Si k**
β-phase ($Mg_{17}Al_{12}$)	**20 sec.**	4.08±1.2	61.28±2.5	33.03±1.7	0.41±0.1
	V< V_{BD}	8.2±1.7	61.29±1.7	29.93±2.2	0.58±0.1
	V> V_{BD}	16.18±1.8	53.62±2.1	27.54±1.8	2.65±1.3
	750 sec.	26.33±2.3	42.89±1.4	21.9±1.6	6.5±1.2
	1500 sec.	36.44±2.6	32.04±1.3	21.46±2.3	10.06±1.7

On the β particle however, a different kind of layer forms. To get more detailed information of the nature of the layer, the line scan studies were conducted for the β-particle. The results in Fig. 5.7 shows a higher amount of the silicon and oxygen on the surface of the β-phase compared to that on the matrix area. This shows that, from initial steps of the coating process a different layer forms on the β particle surface.

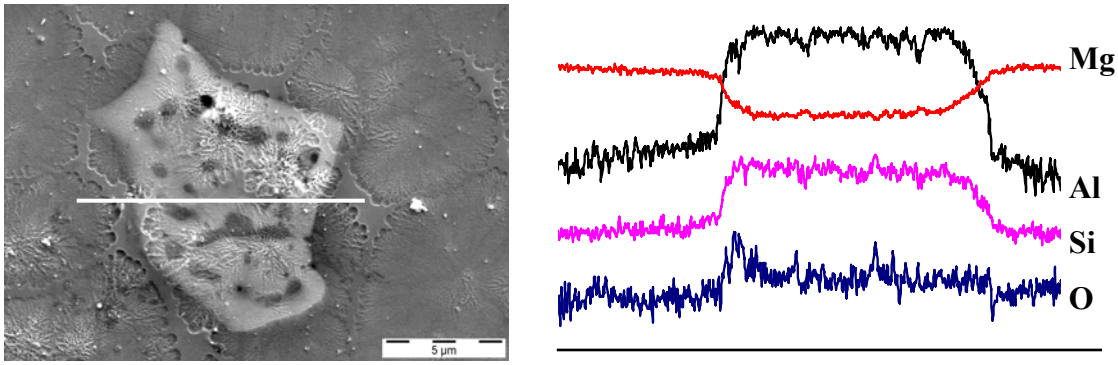

Fig. 5.7. The line scan results of the β-particle.

The surface of the β particle in Figs. 5.6-b which is related to the V<V_{BD} stage, is less distinguishable compared to the previous stage. Figs. 5.6-c, which is related to the V>V_{BD} stage, shows that the surface of the particle has been covered by a layer. The layer on the β particle does not show any evidence of holes which point to the fact that unlike the matrix area it has not still not been affected by the sparking phenomenon. As the process proceeds and voltage reaches to higher values, the required energy for the breakdown of the layer is provided. Fig. 5.6-d shows the surface of the β-phase after 750 seconds of the coating process. The picture gives clear evidence on the formation of pores on the particle surface which are noticeably distinguishably bigger compared to the adjacent matrix. The longer duration of the

process presented in Fig. 5.6-e shows that after 1500 seconds of coating process, the PEO coating on the β-phase has less thickness than the matrix area.

5.1.2.3 Formation process on α-Mg Matrix

Fig. 5.8 shows the coating evolution on the matrix in different durations of the coating process. The point analysis results are also listed in Table 5.5. The first picture shows that after just 20 seconds the formation process follows a net like deposition behaviour on the surface.

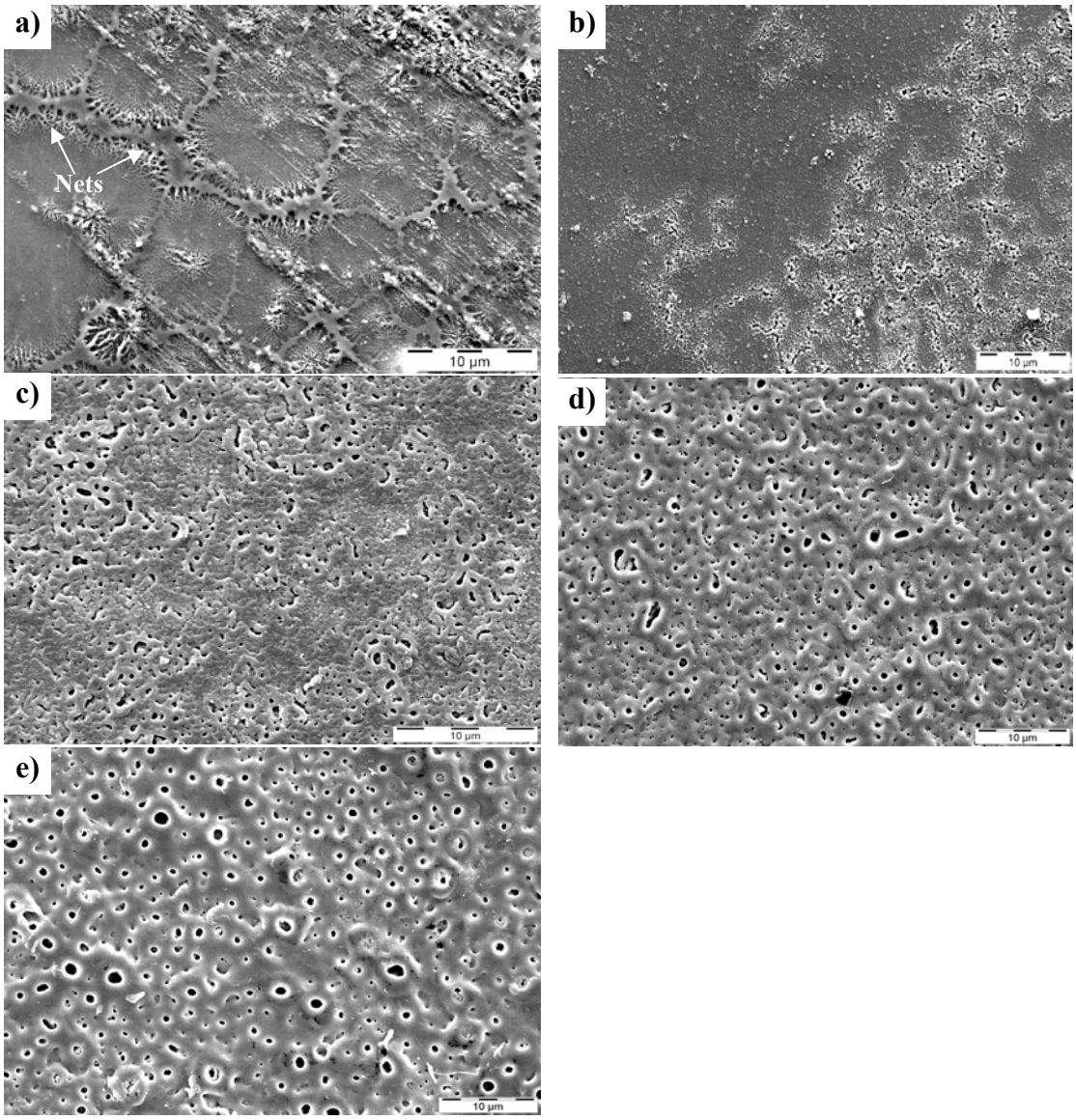

Fig. 5.8.Coating evolution on α-Mg matrix after a) 20 seconds, b) lower and c) higher than V_{BD}, d and e) 750 and 1500 seconds.

Table 5.5. Point analysis of α-Mg in different duration

Elements (At%)		O k	Mg k	Al k	Si k
α-Mg Matrix	**20 sec.**	2.17±1.2	93.97±2.4	3.45±1.7	0.31±0.2
	V< V_{BD}	8.12±0.9	86.98±1.9	3.64±0.9	1.26±0.6
	V> V_{BD}	16.68±1.5	75.65±2.1	2.27±1.4	4.23±1.5
	750 sec.	32.29±2.3	58.68±2.0	1.29±0.4	7.74±1.9
	1500 sec.	49.86±1.6	32.22±1.4	0.49±0.3	16.01±1.7

The matrix surface after 20 seconds of the process was checked by EDX mapping examination to reveal the nature of the nets. Fig. 5.9 shows the distribution of the O, Si and Mg on the matrix area. The EDX mapping shows that the formation process on the matrix area follows a net like deposition behavior. In other words, coverage of a thin uniform layer in the beginning and then the thickening of the layer is not what takes place during the PEO process. However the formation of the coating in the primary steps occurs together with the deposition of the nets and then lateral grow of the nets. As the PEO process develops an oxide layer, the higher amount of oxygen and silicon on the nets confirms that the nets are the coating which is in the beginning steps of the formation process.

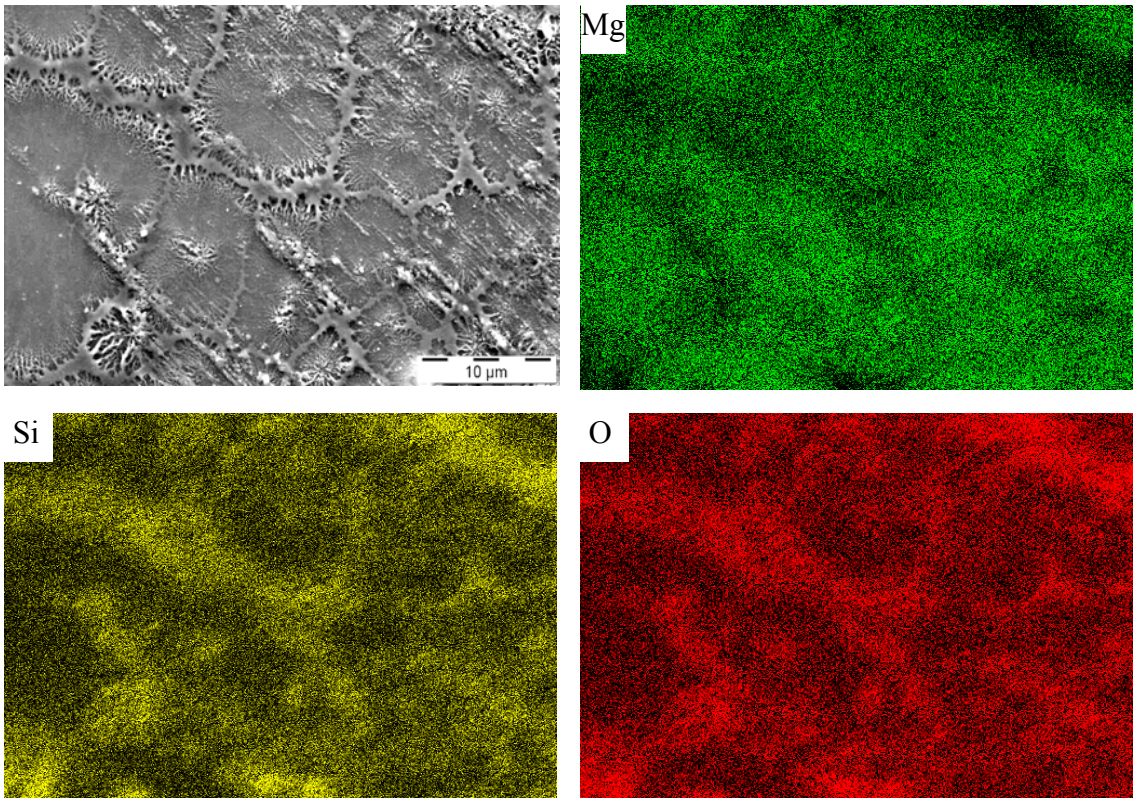

Fig. 5.9. The mapping results for α-Mg matrix after 20 seconds.

Surface of the sample was also examined by XPS to get more information about distribution of the elements involved in the formation process. Variation of atomic concentration within the cross section of the layer after 20 seconds is shown in Fig. 5.10.

The initial steps of the etching process revealed that a layer mainly consisting of O and Si has formed on the surface. It should be mentioned that detection of carbon could be related to the superficial dirt on the surface. Further etching to about 800 seconds showed that the concentration of oxygen remains almost constant at about 50% through the layer but magnesium and silicon are reversely changing. The concentration of the Mg increases but that of the Si reduces through thickness of the layer. In reaching the layer/substrate interface which lies between about 800 and 1800 seconds, the amount of oxygen starts decreasing while the magnesium keeps increasing until it reaches a steady state condition (~ 90%) after about 1800 seconds. The percentage of Si concentration also reaches very low level values close to zero. High and steady percentage of Mg as well as very low percentage of oxygen and silicon shows that after about 1800 seconds, the etching process has reached the substrate.

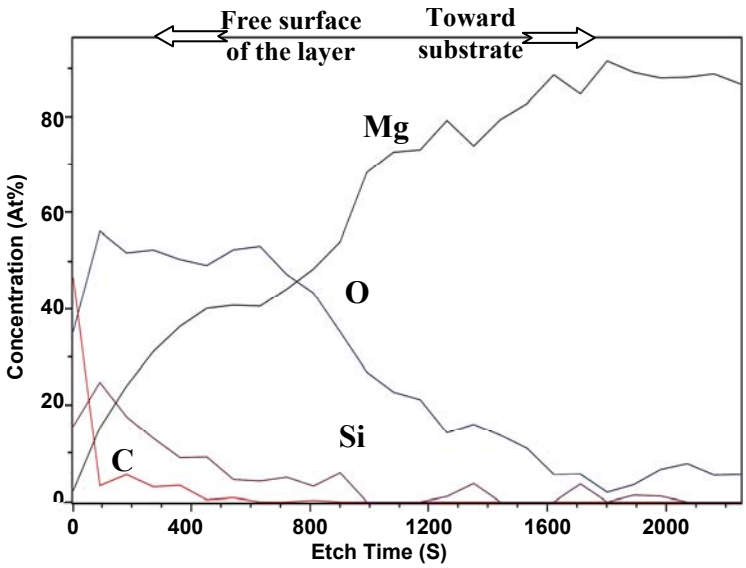

Fig. 5.10. Concentration profile of the sample after 20 seconds.

In the Fig. 5.8-b, which is related to the coating process lower than V_{BD}, two regions can be distinguished i.e. the regions affected and unaffected by the breakdown. The left side of the picture shows mainly the unaffected part of the barrier layer. This part of the picture indicates that the formation of the barrier layer is complete and the surface has been entirely covered. The right side of the picture however shows the region was affected by the breakdown and pores can clearly be seen on the surface.

Fig. 5.8-c shows the surface morphology of the sample shortly after breakdown. It can be seen that the distribution of holes is non-uniform and still some small areas are not affected by discharges. It is seen that the pores are not in the circular shape. In Fig. 5.8-d which is related to the coating after 750 seconds, it can be seen that almost whole the surface is evenly covered by the holes which are mostly circular in shape. However as well as the Fig. 5.8-c, some elongated holes still can be seen on the surface but they are comparatively lower in number. After about 1500 seconds, which is shown in Fig 5.8-e, it is seen that a longer duration of the process increases the size of the holes (≤ 2 μm), compared to those in Fig. 5.8-d which are (≤ 1.8 μm). The elongated holes disappeared and only circular holes formed on the surface.

5.1.3 Formation process in different solution concentrations

As it was explained in the second chapter, the concentration of the solution is the parameter which has a direct influence on the magnitude of the breakdown voltage and consequently on the formation process of the PEO coating. In the last section, the basic behaviour of the PEO coating in 10g/l solution was presented. The 10g/l coating was selected as a base for comparison because of higher performance of the coating.

In the next section, the formation behaviour of the coating will be presented in more dilute and more concentrated solutions i.e. 1 and 20 g/l. The influence of the concentration on the PEO process can be studied by considering the results of these three different concentrations. The results will show how the change of concentration influences the morphology, thickness and properties of the coating formed on the Al_8Mn_5 particle, β-phase and α-Mg.

5.1.3.1 Formation process on Al_8Mn_5

Fig. 5.11 shows the evolution of the coating on the Al_8Mn_5 particle prepared in 1g/l and 20g/l solutions. It is seen that from the surface morphology point of view the Al_8Mn_5 phase essentially behaves almost similar to that of the 10g/l solution. Regardless of process duration or solution concentration, formation reactions present in an Al_8Mn_5 phase are initiated by the particle/matrix interface and result in a ring around the particle. The peripheral ring around the particle remains distinguishable even after a long duration of the process. As well as the previous results, discontinuity of the coating formed on the ring with that on the particle area creates a kind of defect in the interface area which can act like a crack. The defects could facilitate absorption of the corrosive medium into the coating and subsequently have a negative effect on the corrosion performance of the coating, especially if it leads directly to the substrate.

5.1.3.2 Formation process on β- phase

Fig. 5.12 shows different stages of the layer formation on the β-phase in 1g/l and 20g/l solutions. Fig. 5.12-a shows that after 20 seconds of the process, the surface of the β phase can clearly be recognized. Fig. 5.12-Lb shows a β particle prepared as $V<V_{BD}$ in 1g/l solution. The matrix area adjacent to the particle shows that the barrier layer is still under development. The surface of the particle in higher magnification illustrated in Fig. 5.13-a, shows that a thin layer is under development over the β phase. However, the layer is so thin that the underlying particle is clearly visible. In order to check the trend of the formation process, the atomic percentage of the oxygen was analysed by EDAX test. The amount of oxygen was analysed because the PEO process essentially produces an oxide layer on the surface. The value detected for this sample was about 7.39±0.9 %.

Under similar conditions but in 10g/l solution (Fig.5.6-b), the β-phase could not be clearly observed but it was somehow distinguishable. The oxygen measured on this sample was about 8.2±1.7 %. This shows that a thin barrier layer has already covered the particle.

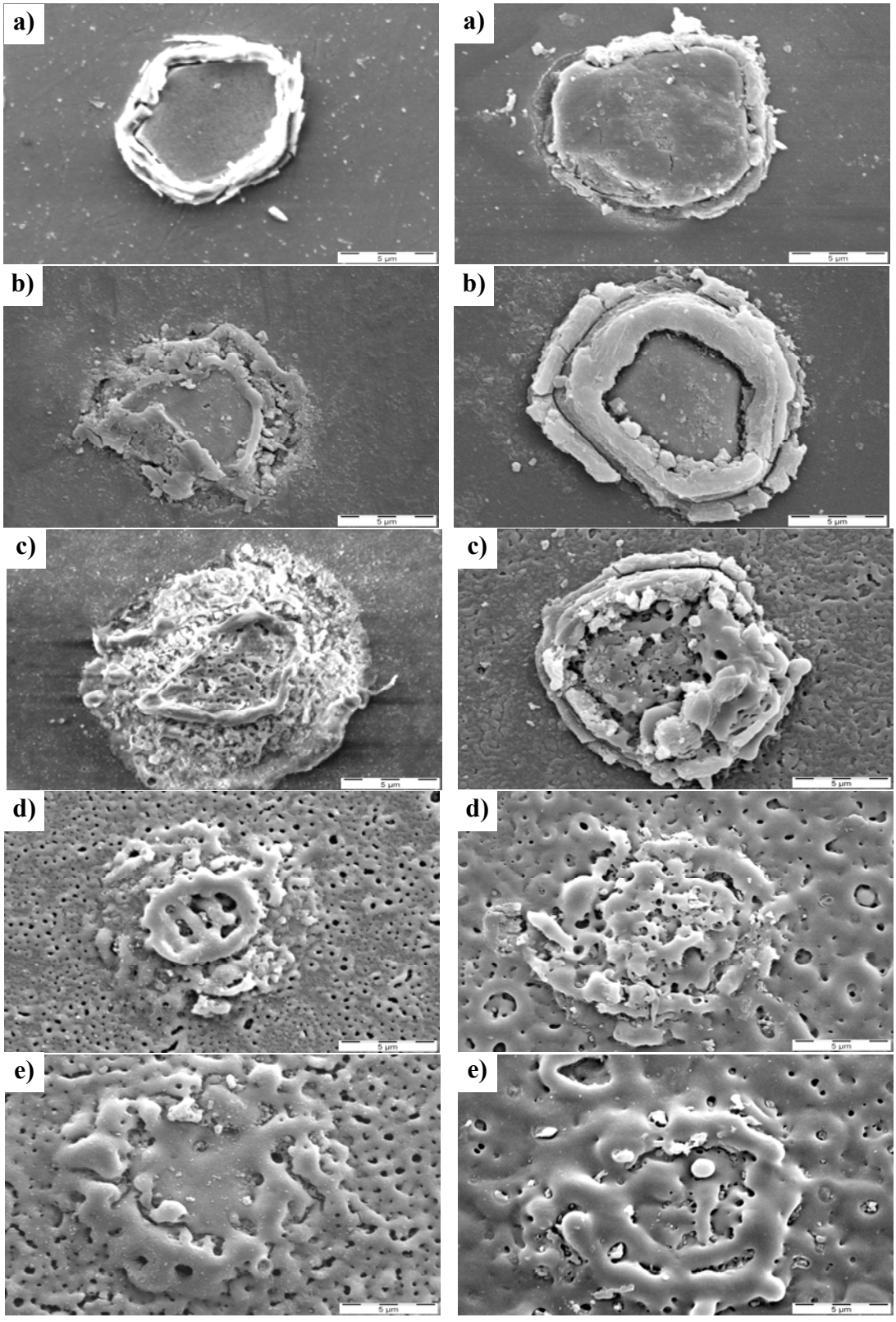

Fig. 5.11. Coating evolution on Al_8Mn_5 phase in concentration of L)1g/l and R)20g/l after a) 20 seconds, b) lower and c) higher than V_{BD}, d and e) 750 and1500 seconds.

In 20g/l solution, which is shown in Fig. 5.12-Rb, the thickness of the barrier layer is so thick that the surface of the β phase cannot be seen any more and it was detected only by EDAX tests. The oxygen measured on this sample was about 10.17±1.6 %. Increase in the value of oxygen as the concentration increases shows that in this period of coating process, higher concentration of solution facilitates the formation process and the pictures also confirm that a thicker barrier layer forms on the surface.

Fig. 5.12-Lc, related to the next step ($V>V_{BD}$), shows that even after breakdown, the surface of the β phase in 1g/l solution is still observable. The presence of some tiny holes on the β phase as well as the matrix area implies that the surface of the β phase is affected by the sparking phenomenon concurrent with the α-matrix. That of the 20g/l in Fig. 5.12-Rc shows similar behaviour as the 10g/l solution (Fig. 5.6-c), in which the barrier layer still has not been affected by the breakdown phenomenon.

Surface morphologies of the layer formed on the β phase after 750 seconds are shown in Fig 5.12-d. The results clearly show that the holes formed on the β surface in 1g/l solution are much bigger than those on the adjacent matrix area. Where the hole size on the β surface are in the range of about 1-5μm, those on the matrix are in the range of 0.1-0.4 μm. It means that more than 5 times difference exists between the size of holes on the β phase and matrix. However, the hole size difference between what forms on a β phase and on the matrix area becomes lower when solutions with higher concentration are used. It can be seen that in 10g/l solution (Fig. 5.6-d), the holes on the β phase are in range of 2-4μm while those on the matrix area are in range of 0.6-1.5μm. In this case the hole size difference between β phase and matrix is about 2-3 times which is lower than 1g/l solution. Fig. 5.12-Rd which is related to the 20g/l solution, shows that the hole size difference between the coating formed on the β phase and that on the matrix is insignificant.

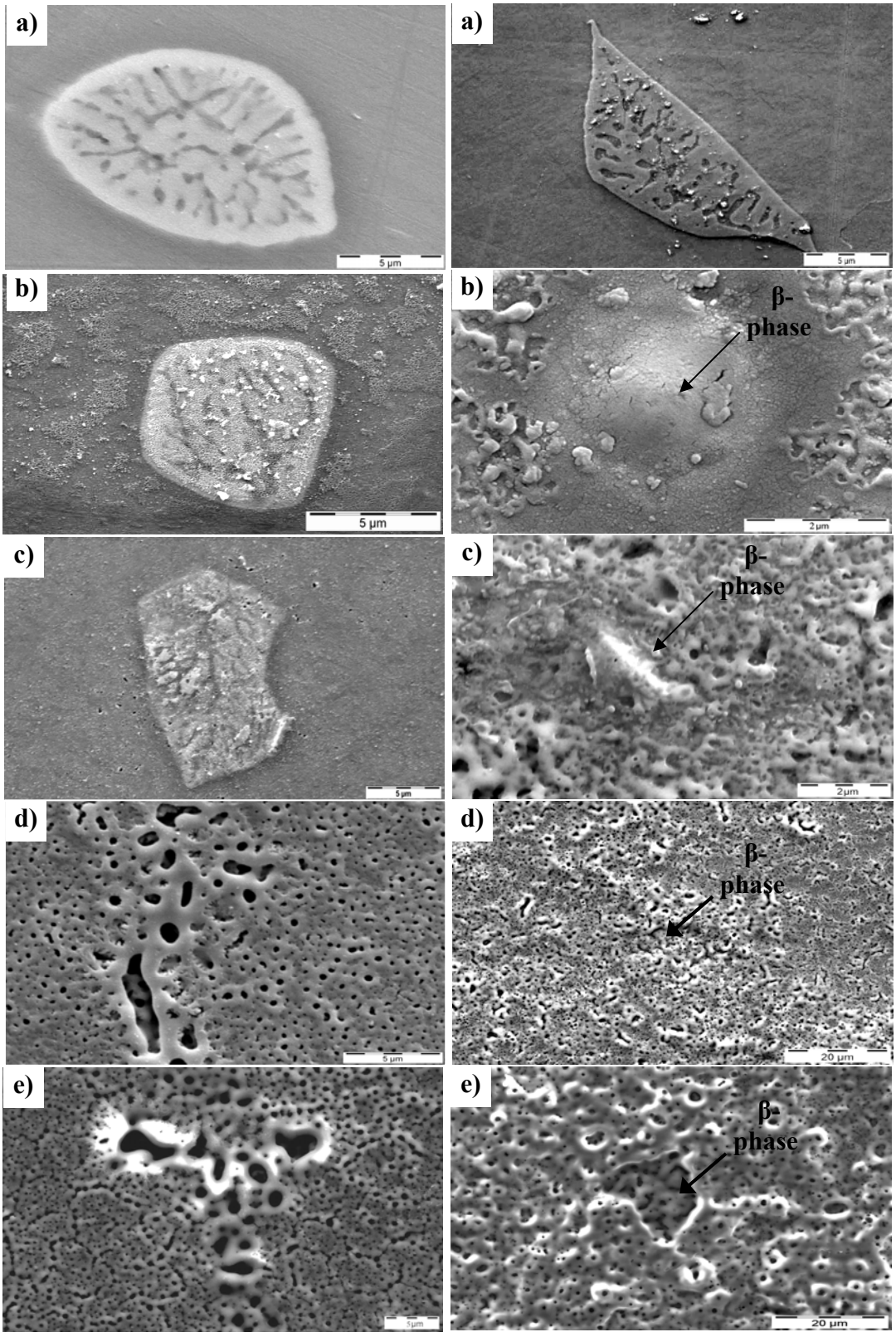

Fig. 5.12. Coating evolution on β-phase in concentration of L)1g/l and R)20g/l after a) 20 seconds, b) lower & c) higher than lower than V_{BD}, d and e) 750 and 1500 seconds.

Figs. 5.12-Le, 5.6-e and 5.12-Re show the coating layers formed on the β-phase after 1500 seconds. It can be seen that the coatings in the Figs 5.12-Re and 5.6-e follow a similar formation process which is different from that of the Fig. 5.12-Le. The Fig . 5.12-Le show that the coating in a diluted solution (1g/l) has bigger hole size compared to what forms on the surrounding matrix. However what Figs 5.12-Re and 5.6-e show is that the coating layer in 10 and 20g/l have less thickness compared to the surrounding matrix.

In order to see the difference of the coating thickness formed on the β-phase and matrix area, cross section of the coatings were examined. Fig. 5.13-b shows the cross section of the coating on the β phase. It clearly shows that the thickness of the coating on β-phase is less than what is formed on the matrix area.

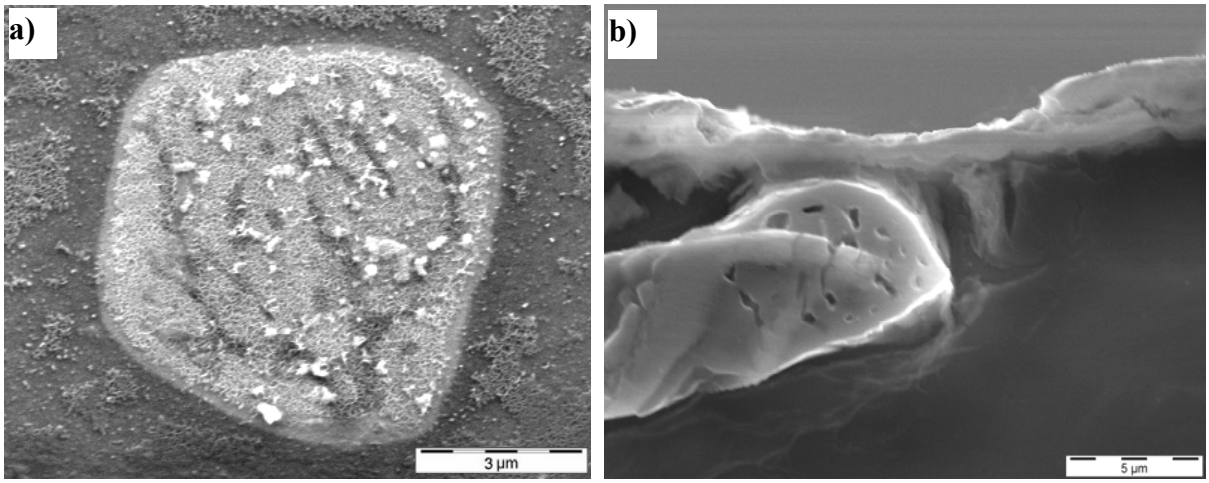

Fig. 5.13. Layer formation on β-phase a) high magnification of fig. 5.12-Lb and b)cross section of PEO coating after 1500s

5.1.3.3 Formation process on α-Mg matrix

Figs. 5.14-La, 5.8-a and 5.14-Ra show the surface morphology of the layer formed on the matrix area in1, 10, 20 g/l solutions after just 20 seconds. The obtained results show that the solution concentrations influence the development rate of the layer. It is seen that while no clear evidence of layer formation can be observed in the 1g/l solution, a net like deposition has formed in the 10g/l solution and an almost developed layer has covered the matrix area in 20 g/l solution.

Figs. 5.14-Lb, 5.8-b and 5.14-Rb show the formation process on the matrix regions in the stage when $V<V_{BD}$. Fig. 5.14-Lb which corresponds to the 1g/l solution shows that the barrier layer is under development and it still needs time to cover the whole surface. Fig. 5.8-b corresponds to the 10 g/l solution and in some parts of this image very small and tiny pores can be seen on the surface. This reveals that a barrier layer has formed on the surface and it is partly affected by the sparking phenomenon. Fig. 5.14-Rb corresponds to the 20g/l solution. This image, unlike the 10g/l solution, shows that the major part of the layer is affected by the sparks. This shows that a barrier layer has formed on the surface. However, the barrier layer in this case has been under the effect of the sparking phenomenon for the longer periods of time. This also confirms that the barrier layer forms more quickly in the 20 g/l solution compared to the 10g/l solution.

The surface morphologies of the samples after breakdown are illustrated in Figs. 5.14-Lc, 5.8-c and 5.14-Rc. The first picture, which is related to the 1 g/l solution, gives clear evidence not only of coverage of the surface by the barrier layer but also of the existence of some scatter holes on the surface. The holes are lower in number ($\sim 46\times10^3$ pore/mm^2) and smaller in size ($\leq 0.4\mu m$) compared to those on the 10 and 20 g/l samples. The figures corresponding to the 10 and 20 g/l coatings reveal that the formation of typical PEO coating has started on the matrix areas. The surface morphology of the 20 g/l coating contains 289×10^3 pore/mm^2 which are in size of about ($\leq 0.8\ \mu m$). These are finer than those of the 10 g/l coating, which are about 215×10^3 pore/mm^2 in size of ($\leq 1.2\ \mu m$).

The way a PEO coating forms on the matrix surface in different concentrations after 750 seconds is illustrated in Figs. 5.14-Ld, 5.8-d and 5.14-Rd. The results show that the size of the holes ($\leq 0.7\ \mu m$) in the coating of 1g/l solution is much lower than those on the 10 and 20 g/l coatings which are ($\leq 1.8\ \mu m$). On the other hand, although the size of the holes on the 10 and 20 g/l samples are comparable, the holes formed on the surface of the 20g/l coating show more irregular shapes than those of the 10g/l coating.

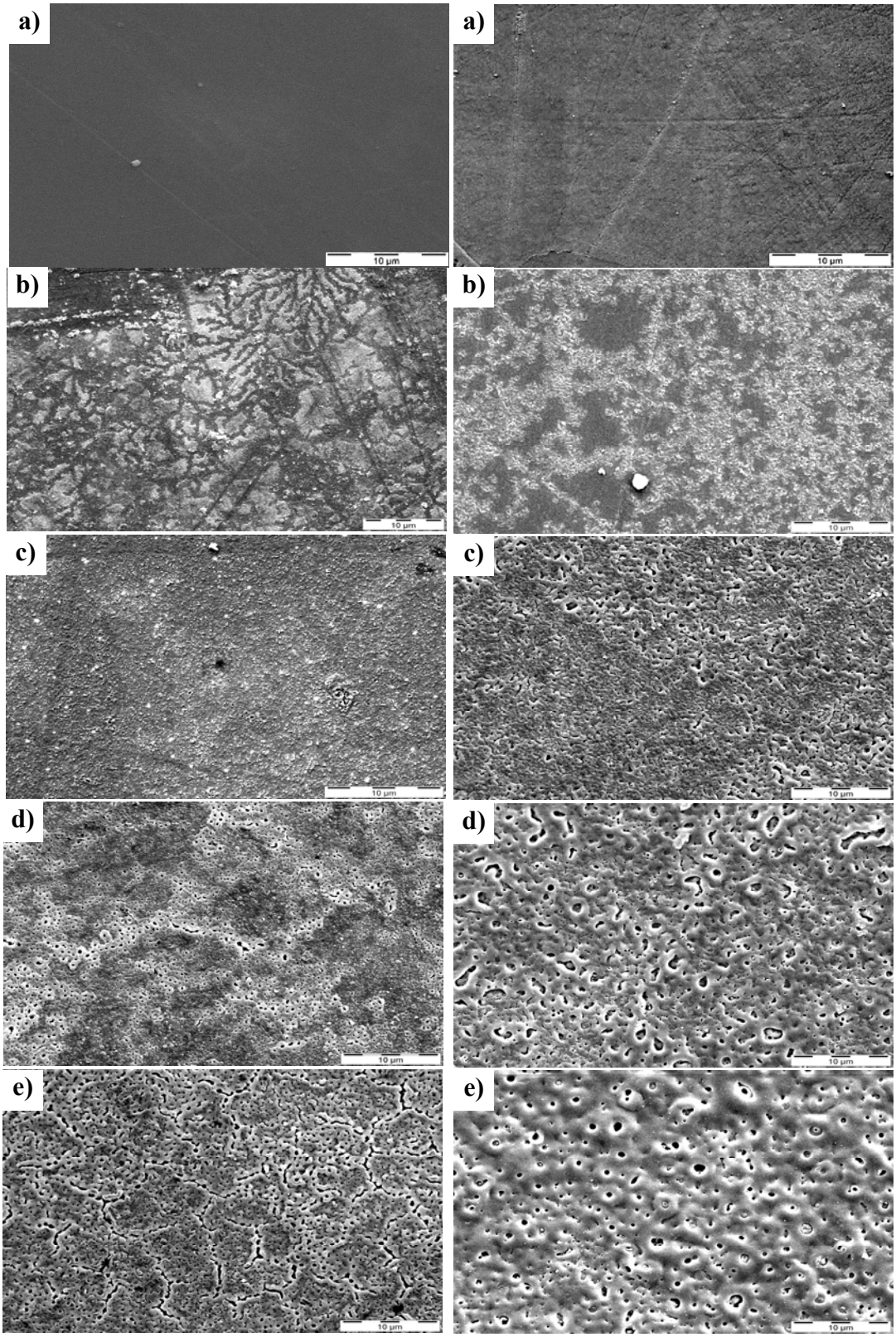

Fig. 5.14. Coating evolution on matrix in concentration of L)1g/l and R)20g/l after a) 20 seconds, b) lower and c) higher than V_{BD}, d and e) 750 and 1500 seconds.

Figs. 5.14-Le, 5.8-e and 5.14-Re show the surface morphology of the coatings prepared within 1500 seconds in different concentrations. As well as in the previous step, the structure of the 1g/l coating is finer than those of 10 and 20 g/l coatings. However what makes the morphology of the 1g/l coating more distinctive compared to those of the 10 or 20g/l samples is the joining of the adjacent holes which subsequently creates the elongated structure of the holes on the surface. The individual and circular holes on the 10 or 20g/l samples follow typical morphology of the PEO coating. Despite many similarities, more precise observation reveals that the 20 g/l coating maintains the trend of having a finer structure compared to that of the 10 g/l coating. It is seen that both coatings contain a wide range of pore sizes between 0.2-2 μm, but the number of holes in the 10g/l coating with a size in the range of 1.5-2 μm is approximately 3-4 times greater than in the 20 g/l coating.

5.1.3.4 Involvement of oxygen during the formation process

The percentage of oxygen was measured by EDAX point analysis experiments. Fig. 5.15 shows variation of oxygen in the coating formed on Al_8Mn_5, β-phase and α-Mg phases. Drawing the curves versus voltage makes it possible to check the breakdown voltage position which plays an important role in this study. Except for the data located on the vertical axis and related to the untreated sample, each curve is made out of five points. The first, fourth and fifth points are related to the samples prepared after 20, 750 and 1500 seconds and the second and third points correspond to the samples before and after breakdown voltage. The results indicate that from the composition point of view, the PEO coating is a non homogeneous coating and the chemical composition of the coating varies from one point to another.

The results of voltage zero, i.e. untreated samples, suggest that unlike the β or matrix phase, an oxide layer exists on the Al_8Mn_5 particles even before the beginning of the process. By the beginning of the process, the oxygen percentage on the Al_8Mn_5 particle approximately follows a common trend in 1, 10 and 20 g/l solutions. The curves initially show slow increase until the breakdown point and then it experiences a significant shift. Involvement of more oxygen after the breakdown point confirms that the formation mechanism of the coating layer has changed.

The curves show that independent of the process duration or solution concentration, more oxygen was detected on the Al_8Mn_5 particles compared to on the β-phase or matrix regions. The amount of oxygen in the coating formed on the Al_8Mn_5 particles shows a sharp increase as the breakdown phenomenon takes place. After breakdown point, the amount of oxygen in the coating remains almost constant and it does not show great variation. The curves corresponding to the β-phase show that the oxygen amount in the coatings prepared in 1 and 20 g/l solutions are higher than that of the α-Mg. However, the 10 g/l solution curves show that the amount of oxygen in the coating formed on the α-Mg is higher than that of the β-phase.

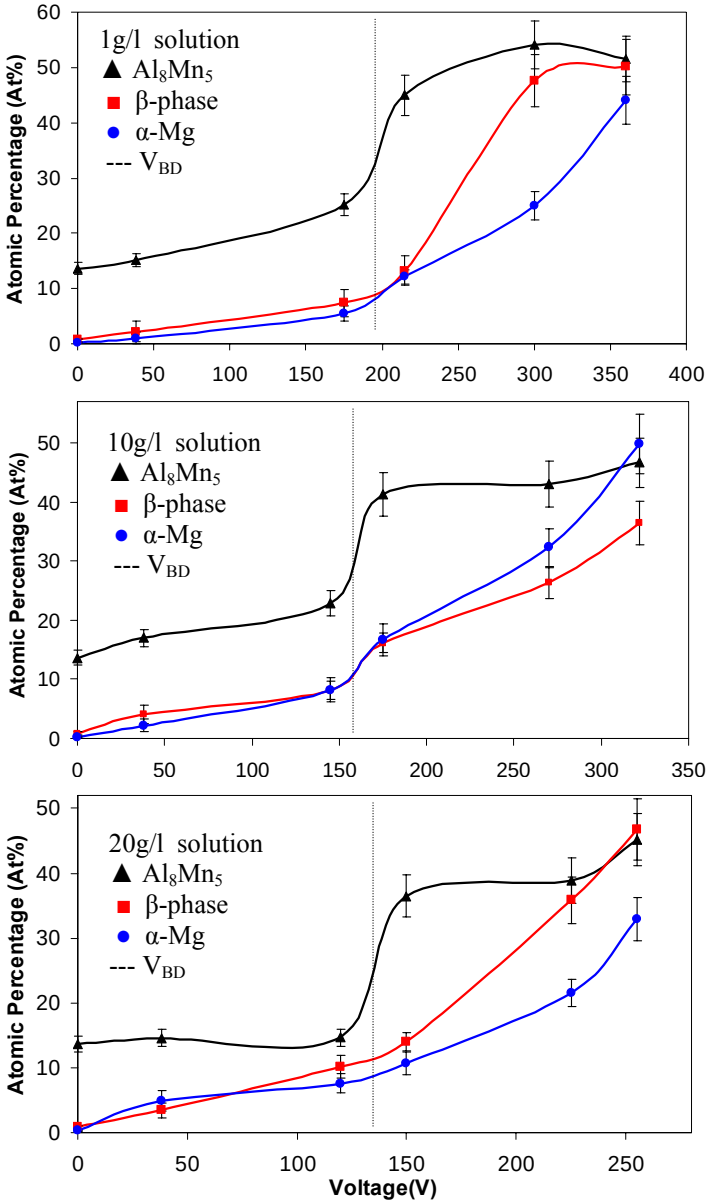

Fig. 5.15. Oxygen percentage of the coating formed in 1, 10 and 20g/l solutions.

5.1.4 Structure of the coatings

5.1.4.1 Cross section of the coatings

Figs. 5.16 shows cross sections of the samples treated for 1500sec in 1, 10, 20 g/l solutions, which are about 1.5, 3.1, 1.7 μm thick, respectively. Apart from different thickness of the coatings, the pores and defects can be seen in the structure of the coatings.

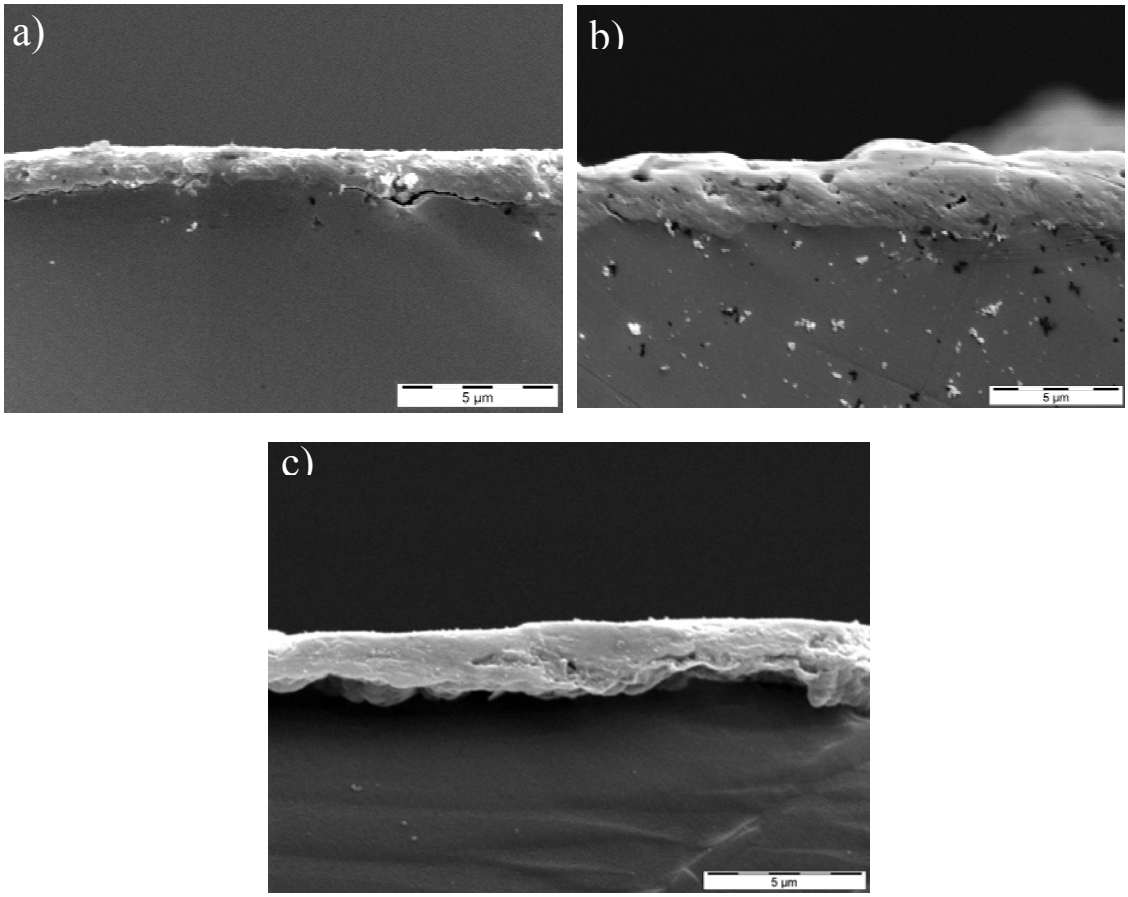

Fig. 5.16.Cross section of the a)1g/l b)10g/l c)20g/l coatings after 1500 s treatment.

5.1.4.2 Phase evaluation of the coatings

To determine the phases existing in the structure of the 1, 10, 20 g/l coatings, the samples were examined by the XRD method. The JCPS files were used to index the XRD patterns. The XRD patterns in Fig. 5.17 show that the coatings are mainly made of Mg_2SiO_4 and MgO. It is believed that the Mg peaks originate from the

substrate. Such an observation was also made by others who examined PEO coatings and attributed the presence of magnesium peaks to the penetration of the X-rays through the PEO coating into the substrate [91]. The results of the XPS study in the next section also confirms that no pure magnesium exists in the PEO coating.

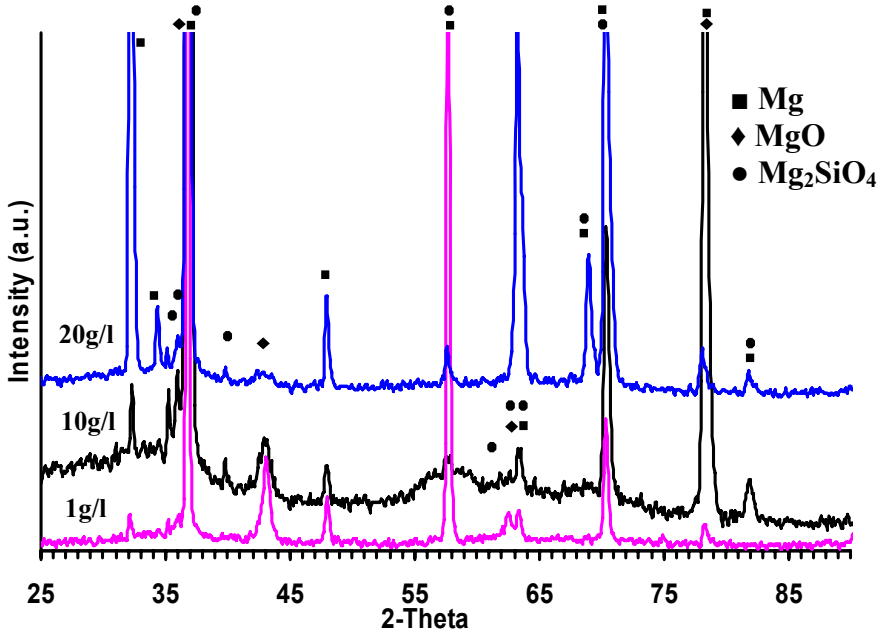

Fig. 5.17. XRD pattern of PEO coatings prepared in different concentrations.

5.1.4.3 Phase distribution in cross section of the coatings

To get a better understanding of the structure of the PEO coatings, the structure of the passive layer were determined by XPS. To determine the phase distribution of the passive film, the layer formed within 20 seconds was analysed layer by layer from the free surface of the film toward the substrate. Fig 5.18 shows the peaks of O 1s obtained in different depths of the layer analysed. These peaks were respectively presented in Fig 5.19 in 3D format to show the distribution of the phases in the coating.

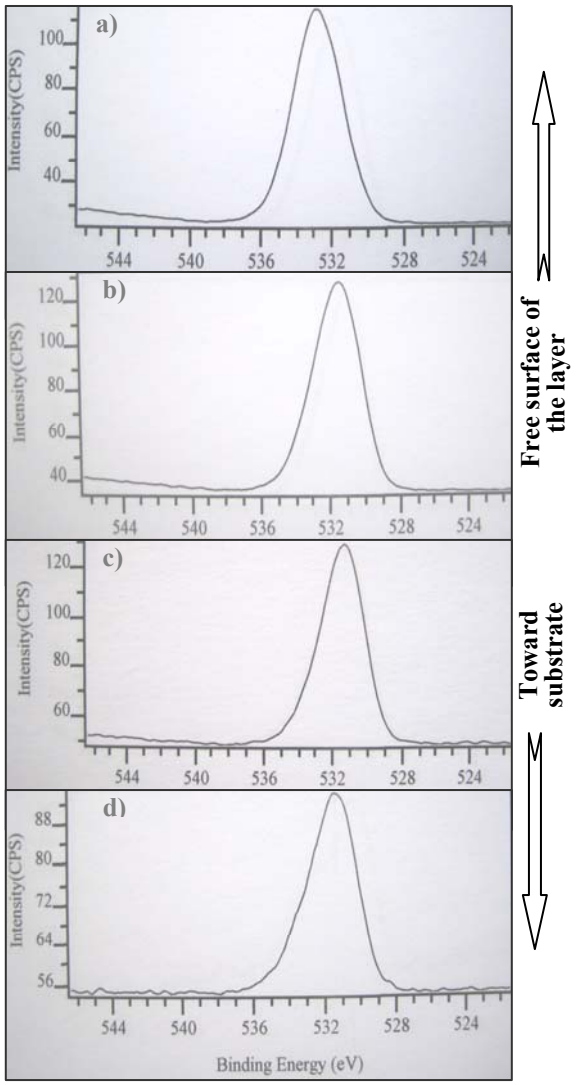

Fig. 5.18 O1s spectra in different etching time namely after a) 270s, b) 810s c)990s, 1170s for sample treated just 20sec.

The results presented in the Fig 5.19 show the spectra of the passive layer after 20 seconds of the PEO process. It shows that the spectra coming from the most outer layer have binding energy of 533eV (O 1s) and 155 eV (Si 2S). As the etching process continues, the peaks with binding energies of 51.5eV (Mg 2p), 532ev (O 1s) appear but silicate peaks disappear. The (O 1s) spectra also disappear as the process reaches a longer time of etching. In this stage just the peaks of 50eV (Mg 2p) can be seen in the detected spectra.

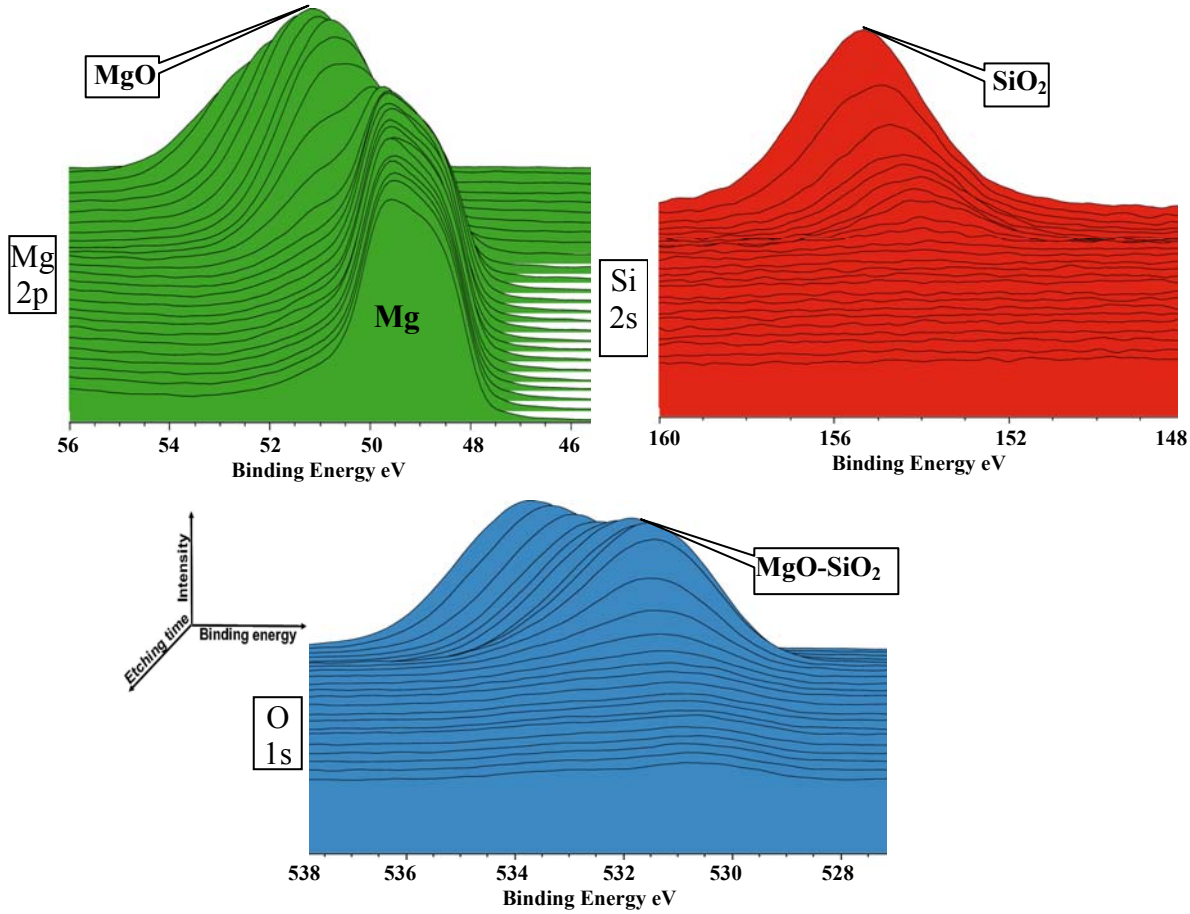

Fig. 5.19. XPS patterns of the coating prepared for 20 sec. in 10g/l solution.

Fig. 5.20 shows the phases distribution of the coatings prepared in 1, 10 and 20 g/l solutions after 1500 seconds of the PEO process. The spectra in the first row which are related to the Mg 2p show three different peaks with binding energies of 48, 50 and 51.5 eV. The 48eV spectra emerge during the initial stages of the etching process (outer layer of the coating). As the etching process proceeds, the intensity of the 48 eV peaks get lower but the 51.5 eV peaks emerge. The peaks with binding energy of 50eV are the spectra appearing at the end of the etching process (close to the substrate).

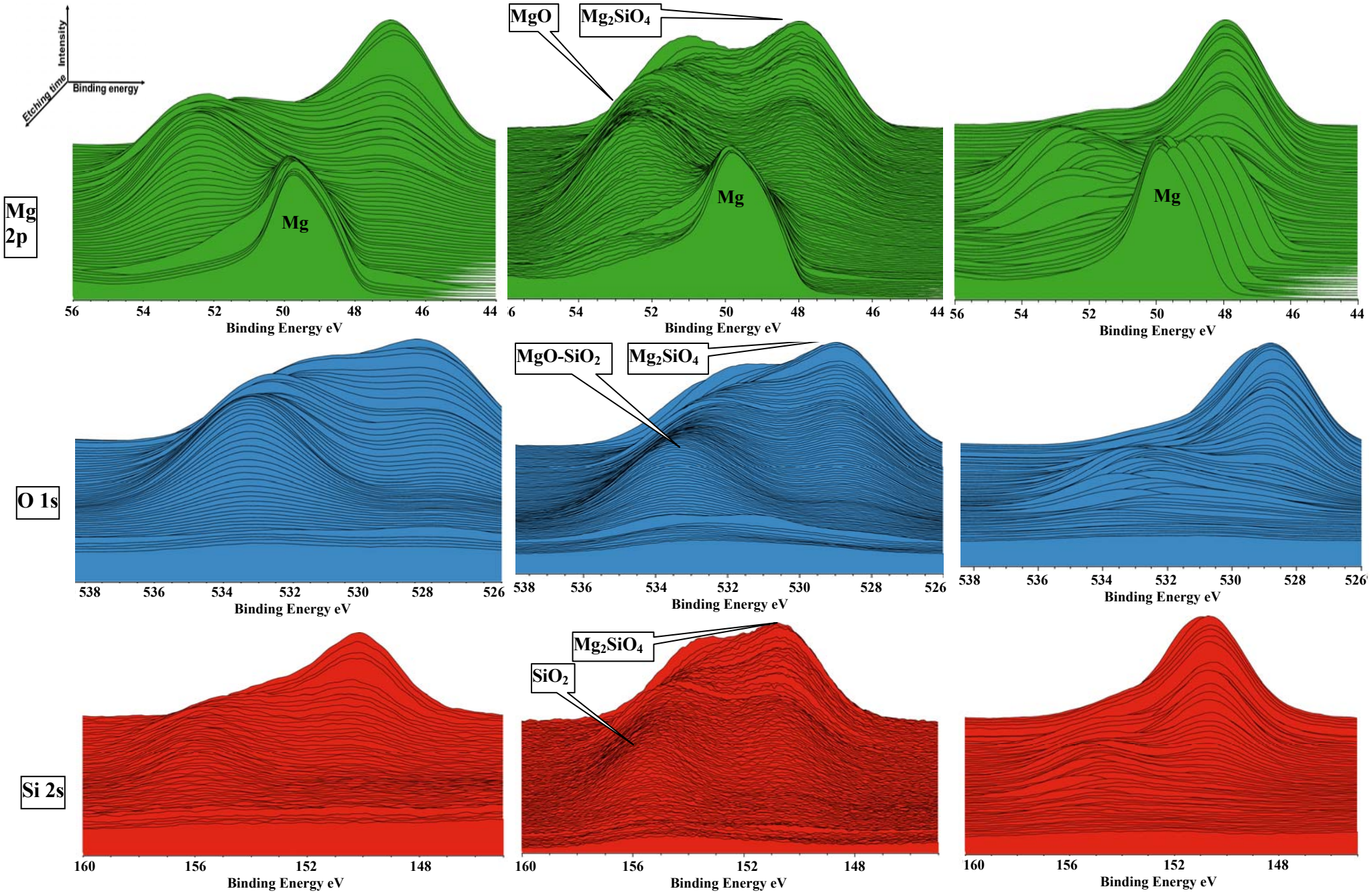

Fig. 5.20. XPS patterns of the coatings prepared in different concentrations in 1500 seconds. Right) 1g/l Middle) 10g/l Left) 20 g/l

The O1s spectra standing in the second row show two different peaks with binding energies of 528.5 and 532.5 eV. The 528.5 eV(O 1s) is the spectra which emerge during the initial steps of the etching process (outer layer of the coating). As the etching process proceeds, the 528.5eV (O 1s) spectra gradually reach a lower intensity and disappear but the 532.5 spectra emerge. The latter spectra appear concurrent with that of the 51.5eV (Mg 2p) and 155eV (Si 2s) and reach a lower intensity and finally disappear as the etching process approaches the substrate.

The third row of the figures belongs to the Si 2s spectra which contains two peaks with binding energies of 150.5 eV and 155eV. The 150.5eV (Si 2s) is the spectra appearing during the initial steps of the etching process. The spectra of the 48eV (Mg 2p) and 528.5eV (O 1s) also appear concurrently with the latter spectra. Proceeding in etching process leads to appearance of the 155eV (Si 2s) spectra which shows concurrency with those of 51.5eV (Mg 2p) and 532.5eV (O 1s).

5.1.4.4 Corrosion evaluation of the coatings

Fig 5.21 shows the corrosion resistance of the coatings prepared in diluted (1g/l), intermediate (10g/l) and concentrated (20g/l) solutions in 1500s of the PEO process. The impedance and corrosion rate value of the coatings is $(2.5\pm0.6)\times10^{5}$, $(1.5\pm0.8)\times10^{6}$, $(7.9\pm0.5)\times10^{5}$ $\Omega\cdot cm^{2}$ and $(5.6\pm0.5)\times10^{-2}$, $(5.7\pm0.6)\times10^{-4}$ and $(3.5\pm0.1)\times10^{-2}$ mm/year, respectively.

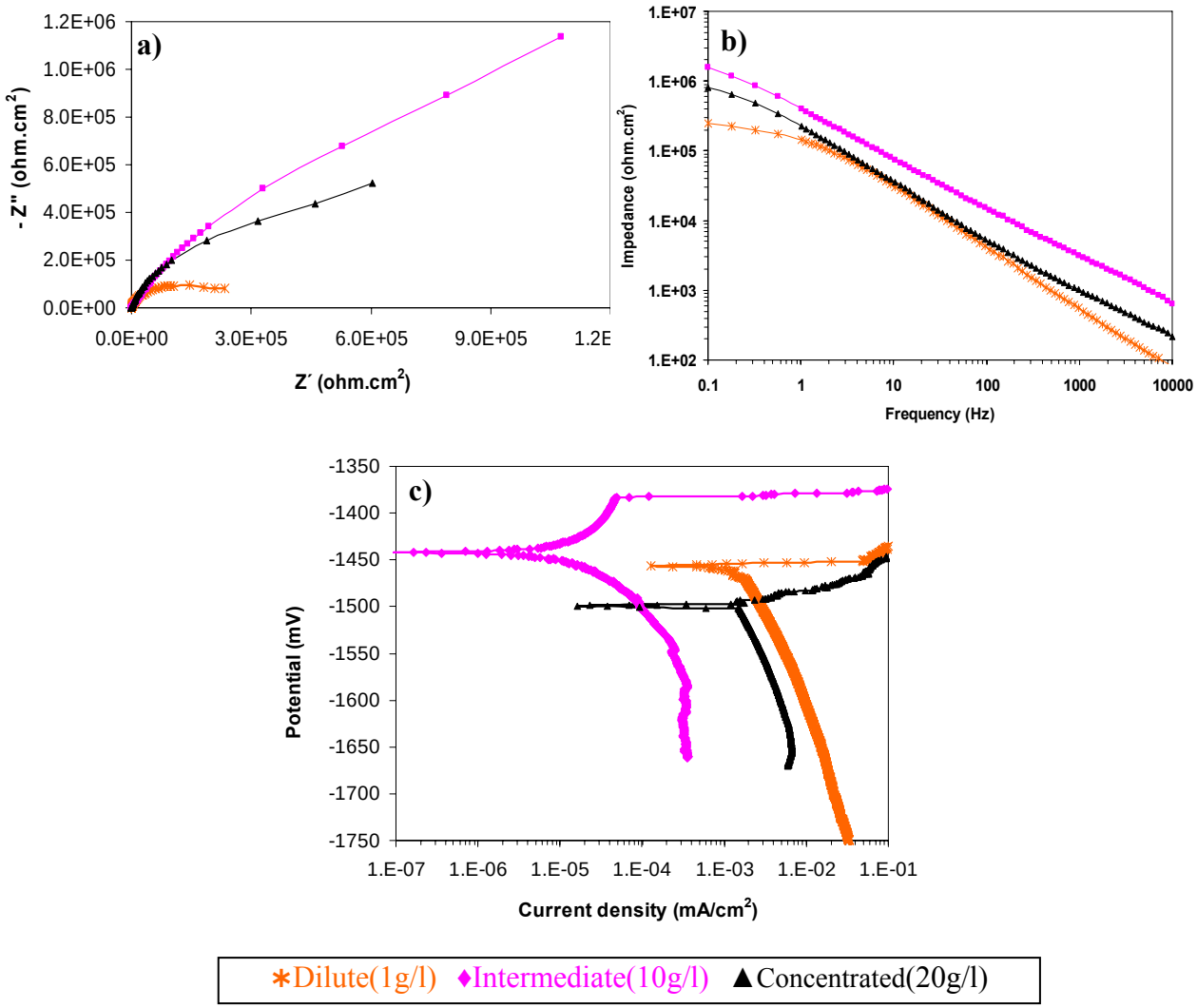

Fig. 5.21. Corrosion resistance of the coatings prepared in dilute, intermediate and concentrated solutions a) Nyquist, b) Impedance and c) Polarization curves

5.2 Influence of the electrolyte composition on stability of the passive layer and corrosion resistance of the PEO coating

The AM50 magnesium alloy was treated in solutions with different compositions to study and evaluate the stability of the passive layer as well as the corrosion resistance of the corresponding PEO coatings.

5.2.1 Passive layer study

It is known that a passive layer forms on the surface of some metals when they get exposed to an aqueous environment. The chemical composition and physical characteristics of the layer depends on the substrate as well as the composition of the solution. As the formation of a passive layer during the initial steps of the coating formation plays an important role in the PEO process, behaviour of the layers in different salt solutions were studied by immersion and anodic polarization methods. Table 5.6 classifies the solutions and presents the data regarding the properties such as pH and conductivity of the salt solutions.

Table 5.6. properties of 10 g/l of salt solutions

Solutions / **property**	Na_2SiO_3	K_2SiO_3	Na_3PO_4	$Na_5P_3O_{10}$	$Na_2H_2P_2O_7$	K_3PO_4	$K_4P_2O_7$	$NaAlO_2$
pH	12.6	11.56	12.12	9.42	4.33	12.21	10.02	12.23
conductivity (mS/cm)	18.6	1.39	11.77	6.40	5.53	11.93	7.44	8.8

5.2.1.1 Immersion method

Fig. 5.22 shows the impedance data. These data were employed for evaluation of the passive layers which form on the metal surface in different salt solutions. Based on the results, the layers which are formed in the Na_2SiO_3, Na_3PO_4 and K_3PO_4 solutions show higher value in their own group. Resistance of the layers is $(1.6\pm0.1)\times10^4$, $(5.2\pm0.4)\times10^3$ and $(5.1\pm0.3)\times10^3$ $\Omega\cdot cm^2$ respectively. In the case of the $NaAlO_2$ solution the layer has a value in the magnitude of about 850 ± 70 $\Omega\cdot cm^2$. It is seen that the highest resistivity belongs to the layer formed in the Na_2SiO_3 solution. This

shows that sodium silicate has a greater ability to produce a more stable passive layer on the metal surface.

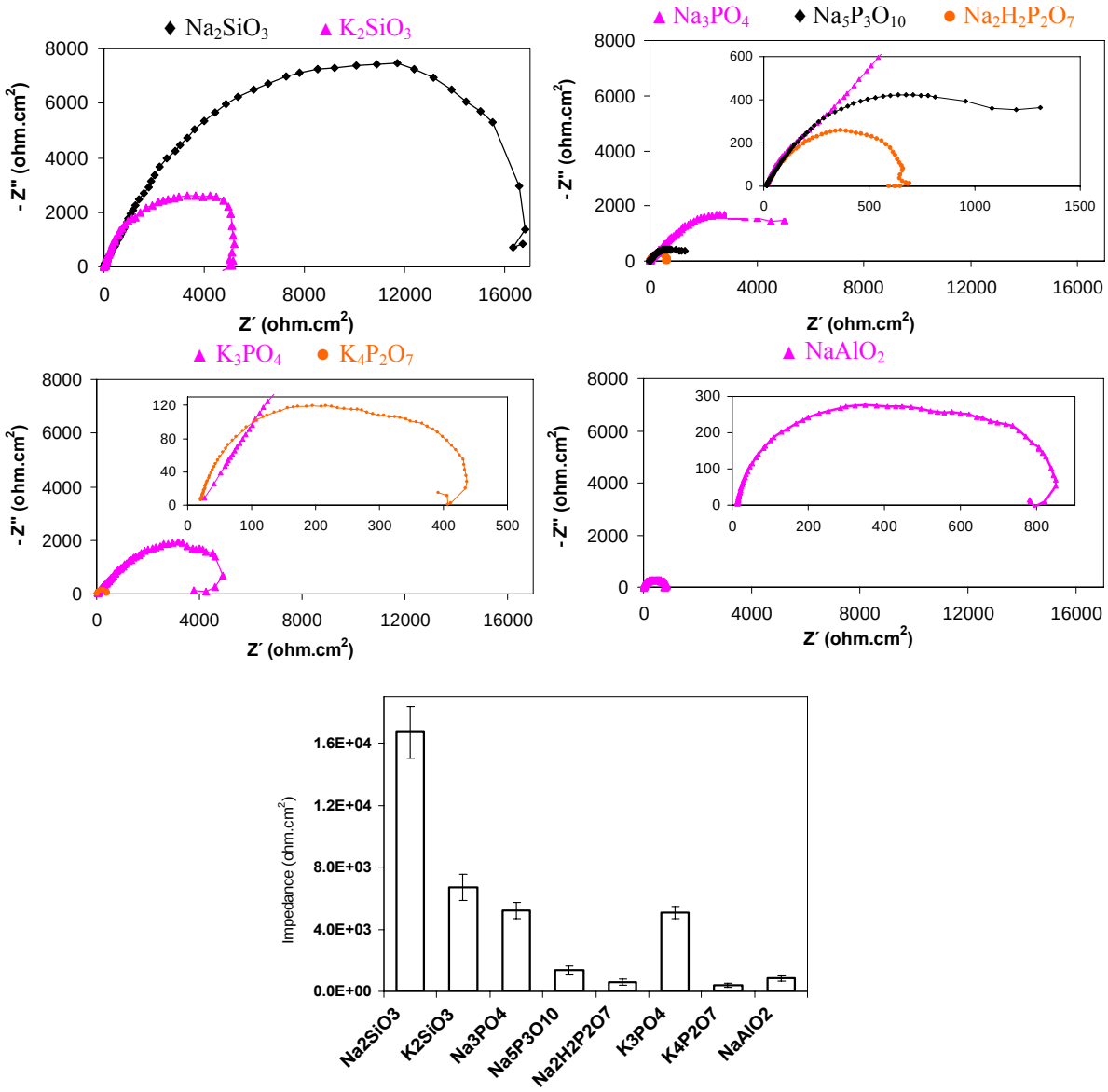

Fig. 5.22. Corrosion evaluation (with 3.5% NaCl as test solution) of passive layers formed on the substrate after immersion in the salt solutions.

5.2.1.2 Anodic polarization method

The polarization results presented in the Fig. 5.23 and Table 5.7 show that the Na_2SiO_3 with $(3\pm0.2)\times10^{-4}$ mA/cm^2 has a lower passive current than that of the K_2SiO_3, the value of which is about $(5\pm0.4)\times10^{-4}$ mA/cm^2. The passive currents of

the Na_3PO_4, $Na_5P_3O_{10}$, $Na_2H_2P_2O_7$ solutions are about $(4\pm0.4)\times10^{-3}$, (1.8 ± 0.1) and (6.7 ± 0.5) mA/cm^2, respectively. In the next group, the K_3PO_4 solution shows unusual passive behaviour. The passive current which initially has a value of 3×10^{-2} mA/cm^2 reduces and reaches about 8.5×10^{-3} mA/cm^2 at the end of the scan process. This kind of behaviour in the K_3PO_4 solution could be originated from the stability of the passive layer which becomes more stable as the potential reaches more positive values. The curves shows that another solution in this group, namely $K_4P_2O_7$, has the average passive current of about $(3.5\pm0.4)\times10^{-1}$mA/cm^2.

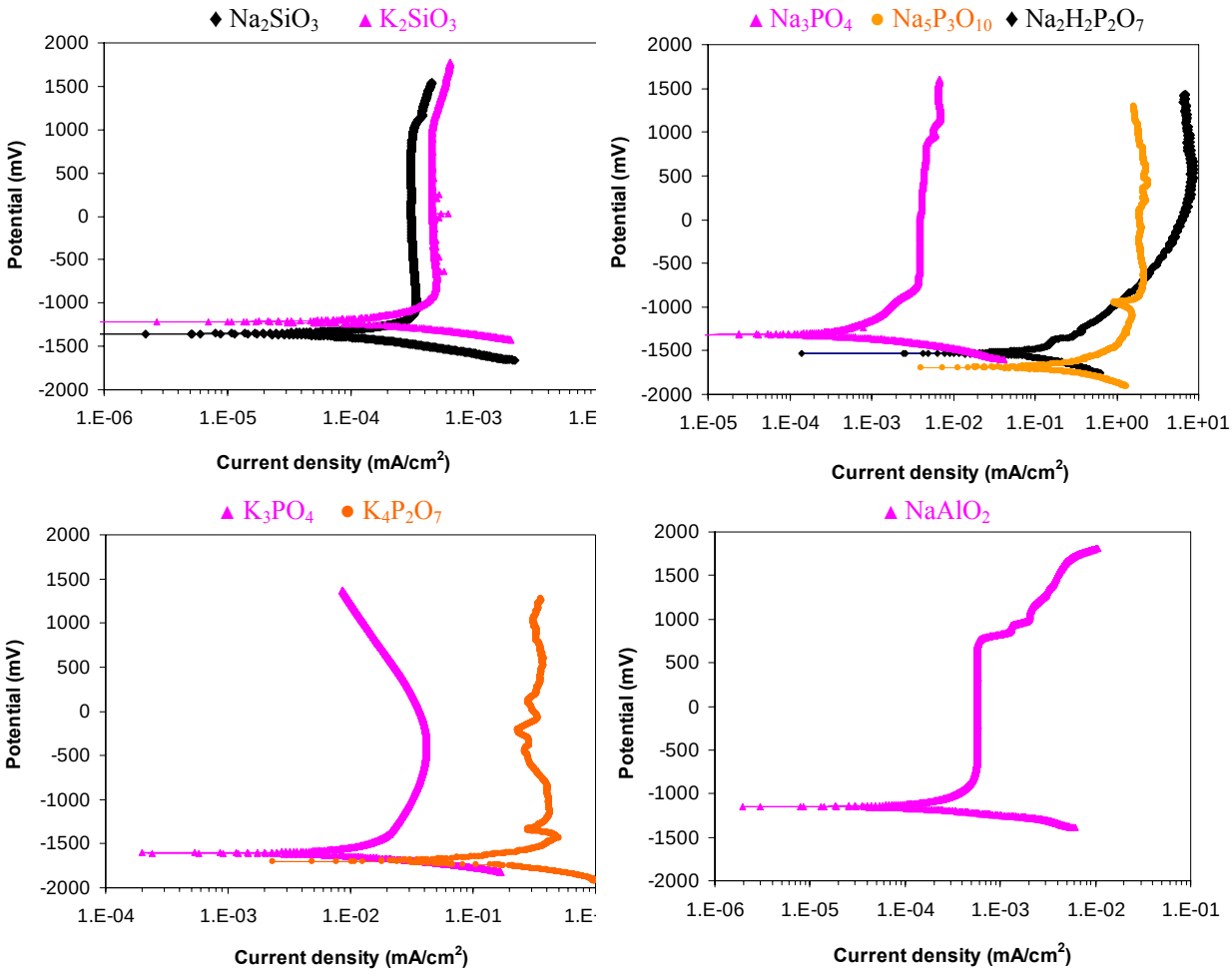

Fig. 5.23. Anodic polarization on the substrate by salt solutions.

Table 5.7. Passive current of the experiments shown in Fig.5.23

Solutions / property	Na_2SiO_3	K_2SiO_3	Na_3PO_4	$Na_5P_3O_{10}$	$Na_2H_2P_2O_7$	K_3PO_4	$K_4P_2O_7$	$NaAlO_2$
Passive current (mA/cm^2)	$(3\pm0.2)\times10^{-4}$	$(5\pm0.4)\times10^{-4}$	$(4\pm0.4)\times10^{-3}$	(1.8 ± 0.1)	(6.7 ± 0.5)	$(8.5\pm0.6)\times10^{-3}$	$(3.5\pm0.4)\times10^{-1}$	$(1\pm0.3)\times10^{-1}$

Sodium aluminate solution also exhibits specific behaviour compared to the others. The low value of the passive current in the initial steps of the anodic scan suggests the formation of a stable passive layer in this solution, but it endures only up to the potential of 1000 mV. Beyond 1000 mV, a kind of breakdown occurs in the passive layer and consequently the current starts increasing dramatically. Therefore in a small range of the voltage, the passive current changes from $\sim5\times10^{-4}$ mA/cm^2 to nearly 1×10^{-1} mA/cm^2. The anodic polarization of the $NaAlO_2$ shows good agreement with the impedance data.

The passive study of each group showed that the Na_2SiO_3, Na_3PO_4 and K_3PO_4 have higher impedance values and lower current density in their own group. The data indicates that the passive layer formed on these solutions is more stable compared to the others in each group. On the other hand the low value of impedance data and breakdown in the polarization test of the aluminate solution showed that the passive layer formed in this solution is not stable.

5.2.2 Corrosion resistance study

5.2.2.1 Corrosion resistance of the substrate

In view of the fact that AM50 magnesium alloy is the substrate employed in the study, the corrosion resistance of the bare metal was measured to determine the natural corrosion resistance of the alloy. Fig. 5.24. shows the result of the corrosion evaluation of the alloy by impedance and polarization methods. The measurements show that the impedance and corrosion rate of the alloy are about $10^3\pm100$ $\Omega\cdot cm^2$ and $(2.4 \pm 0.2)\times10^{-1}$ mm/year, respectively.

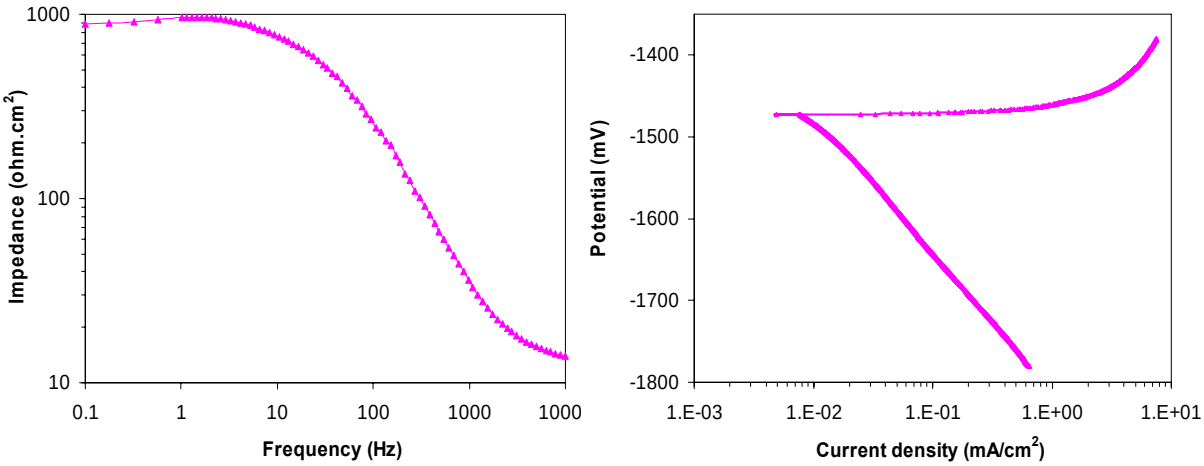

Fig. 5.24. Corrosion evaluation of AM50 magnesium alloy in 3.5% NaCl solution; L) Impedance and R) Polarization curve.

5.2.2.2 Elements in plasma environment

Depending on the solution composition, different elements are involved in the plasma environment during the PEO process. Prior to performing the PEO process, optical emission spectroscopy (OES) was employed to reveal which kind of elements are involved in the plasma environment when different salt solutions, with and without hydroxide, are used.

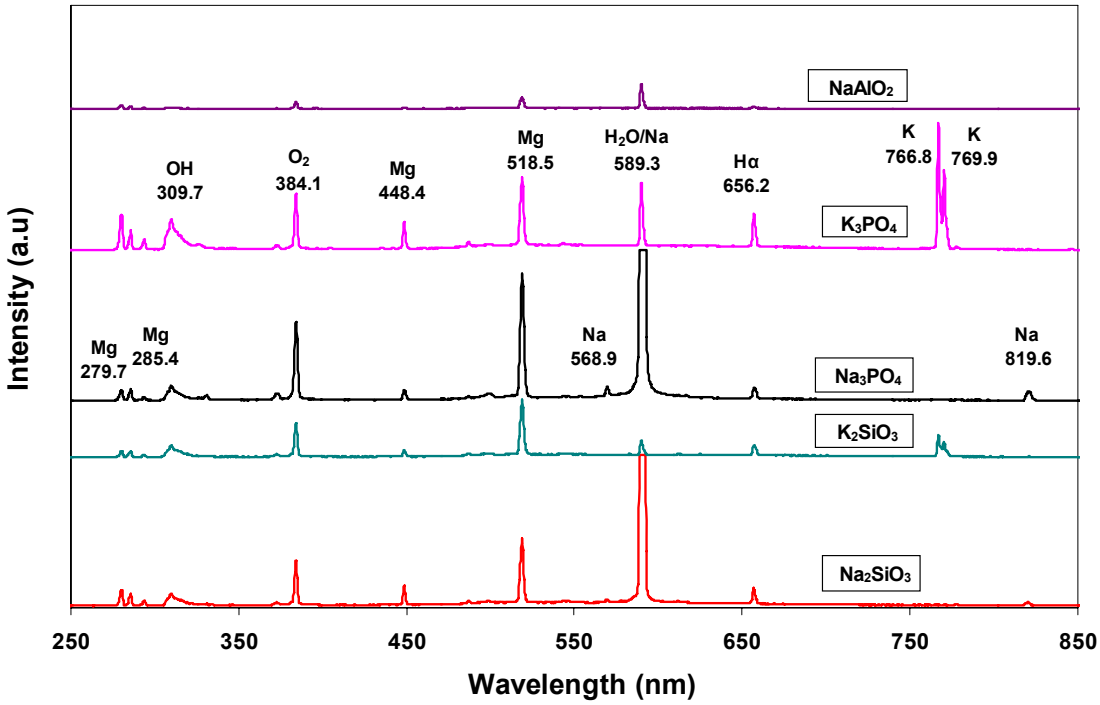

Fig. 5.25. Optical emission spectroscopy of the PEO process by different salt solutions.

Fig.5.25 shows the radiation patterns of each salt solution, namely Na_2SiO_3, K_2SiO_3, Na_3PO_4, K_3PO_4 and $NaAlO_2$. To study the behaviour of the coating solution, KOH were added to the salts solutions. The related patterns in Fig 5.26 show that, depending on the chemical composition of the solutions, different elements such as K (766.8, 769.9 nm), Na (819.6, 589.3, 568.9 nm), Hα (656.2 nm), O_2 (384.1nm), Mg (518.5, 448.4, 285.4, 279.7 nm) and OH (309.7nm) participate in the plasma environment.

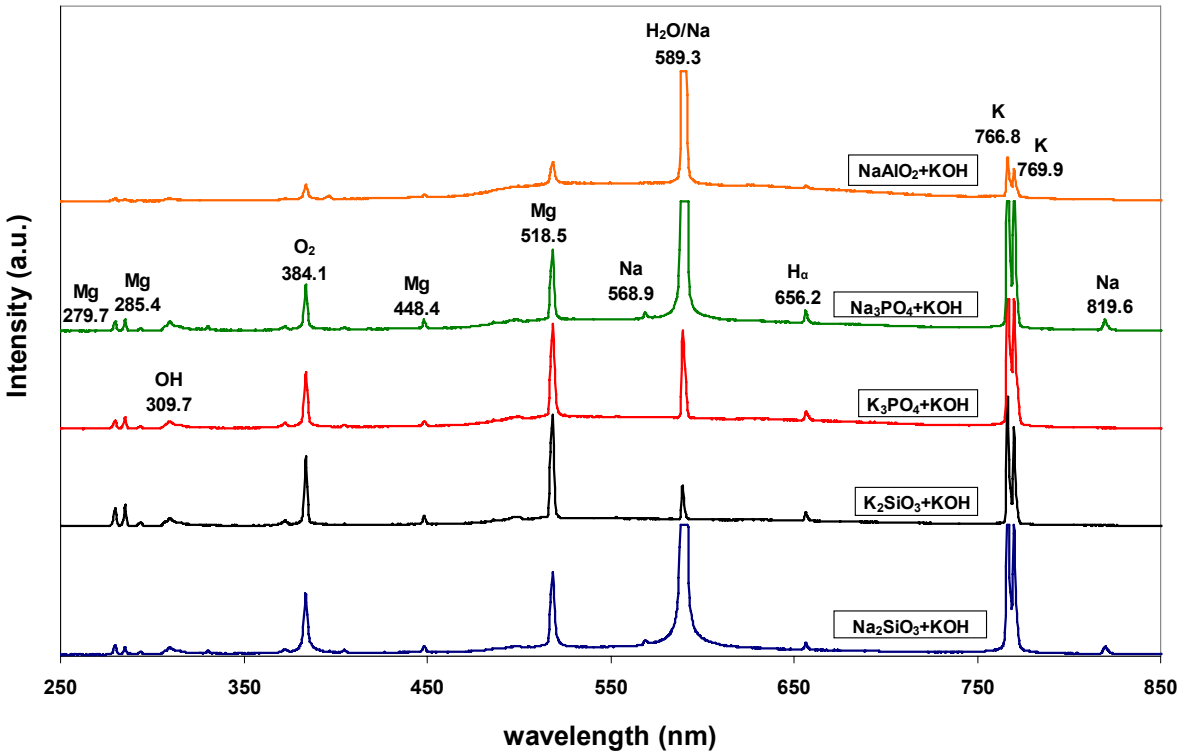

Fig. 5.26. Optical emission spectroscopy of the PEO process by different solutions

5.2.2.3 Corrosion resistance of the PEO Coatings

The solutions listed in Table 5.8 were used to prepare the PEO coating on the substrate. The solutions were classified into four groups based on the chemical composition of the salts. The data on conductivity, pH, breakdown voltage, final voltage, coating thickness and open pore density of solutions were taken and are presented in Table 5.8. One point which needs to be explained in Table 5.8 is the higher breakdown voltage of the $NaAO_2$+KOH solution compared to the solutions with lower conductivity. This could be explained based on the equation 2.5 which

gives the relation between breakdown voltage and conductivity. It is seen that as well as conductivity, two constant values, namely a_B and b_B, also influence the breakdown voltage. The a_B and b_B depend on the type of the substrate and electrolyte composition, respectively. So based on this equation, comparison of the breakdown voltage of the solutions with different composition is not applicable and could be misleading.

Table 5.8. Measured value of the solution in 10g/l and corresponding coating.

Name / Value	Na_2SiO_3 +KOH	K_2SiO_3 +KOH	Na_3PO_4 +KOH	$Na_5P_2O_7$ +KOH	$Na_2H_2P_2O_7$ +KOH	K_3PO_4 +KOH	$K_4P_2O_7$ +KOH	$NaAlO_2$ +KOH
pH	12.96	12.93	13.01	13	12.87	13.05	12.99	13
conductivity (mS/cm)	44.5	31.2	40.01	30.6	21.1	39.8	37	38.84
V_{BD} (V)	160	202	166	225	252	166	207	213
V_f (V)	376	415	367	384	360	357	369	244
Thickness(µm)	8.3	7.4	4.7	4.3	4.0	4.9	4.0	1.3
Open pores density (pores/mm^2)	13	48	17	25	19	28.5	28	33

5.2.2.3.1 Silicate coatings

Na_2SiO_3+KOH and K_2SiO_3+KOH electrolytes were employed to prepare the coatings of the first group. The breakdown voltage and conductivity of the sodium and potassium silicate are 160, 202V and 44.5, 31.2 mS/cm, respectively. The data imply that sodium silicate requires lower potential compared to the potassium silicate to achieve the sparking phenomenon. An overall view of the data in Table 5.8 also shows that higher conductivity of solutions results in lower breakdown potential. This shows good agreement with the theory which indicates that there is direct relationship between breakdown voltage and the electrolyte resistance [52].

Fig. 5.27 shows the surface morphology and cross section of the coatings. The surface morphology of both coatings is porous. The size of the pores varies from approximately 0.5 to 8 µm in both cases, but they have dissimilar structures. The

surface morphology of the Na_2SiO_3+KOH coating is more uniform and most of the pores have an average size of about 4.5 μm. The measurements showed that the surface morphology of the coating has about 4080 hole/mm^2 with diameter more than 3μm. However, the K_2SiO_3+KOH coating contains either very big or very fine pores. The average size of the pores is about 3 μm and the coating has about 660 hole/mm^2, with a diameter of more than 6μm. Cross sections of the coatings also show different structures. The results show that the cross section of the K_2SiO_3 coating contains more defect-like pores and cracks compared to that of the Na_2SiO_3 coating.

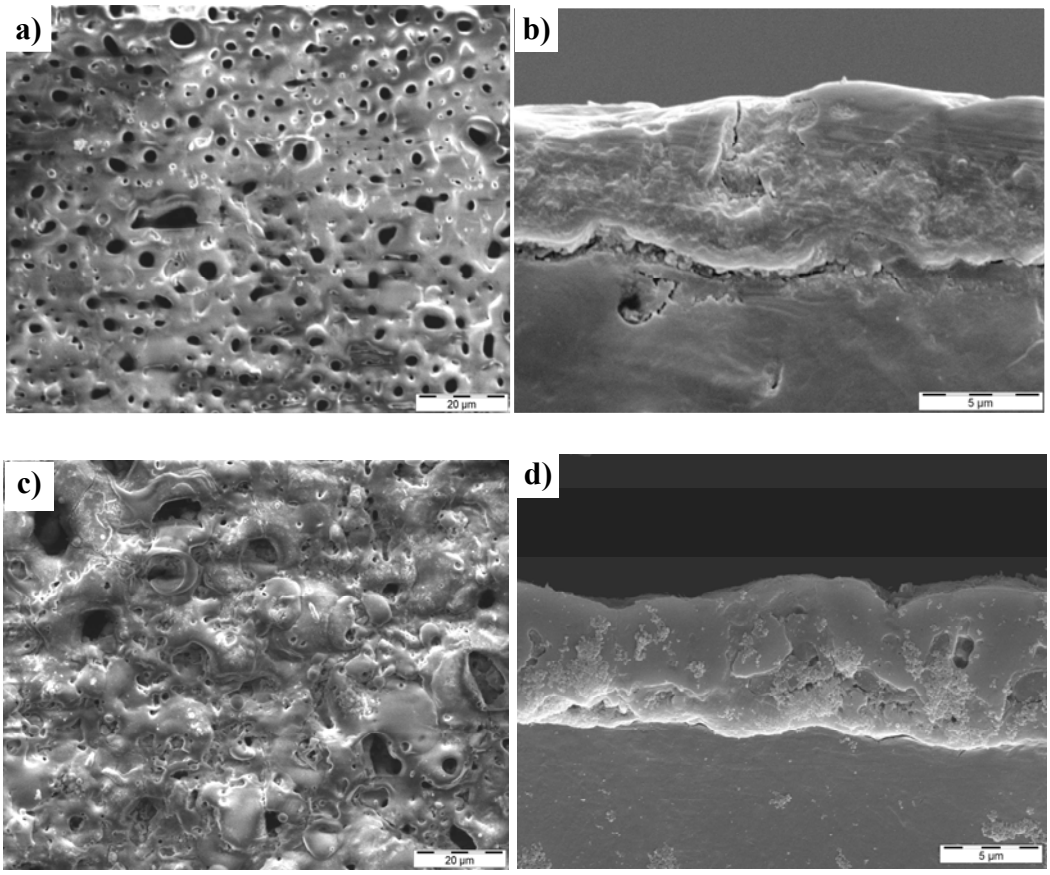

Fig. 5.27. Surface morphology and cross section of the a,b) Na_2SiO_3, c,d) K_2SiO_3 coatings

The electrochemical spectroscopy data in Fig. 5.28 show that the impedance value of the Na_2SiO_3+KOH coating reaches about $(2\pm0.4)\times10^6$ $\Omega \cdot cm^2$ while that of the

K_2SiO_3+KOH coating is lower around $(2.3\pm0.2)\times10^5$ $\Omega \cdot cm^2$. Polarization data also show the same trend of corrosion resistance for both coatings. The corrosion rate of Na_2SiO_3+KOH and K_2SiO_3+KOH coating are $(8.4\pm0.8)\times10^{-4}$ and $(2.5\pm0.2)\times10^{-3}$ mm/year respectively. It is seen that both methods suggest higher corrosion resistance for the sodium silicate coating compared to that of the potassium silicate coating. According to the XRD patterns illustrated in Fig. 5.28-d, MgO and Mg_2SiO_4 are the major phases existing in both coatings. In addition to the major phases, the patterns also consist of the Mg peaks, which are believed to reflect the substrate information [91].

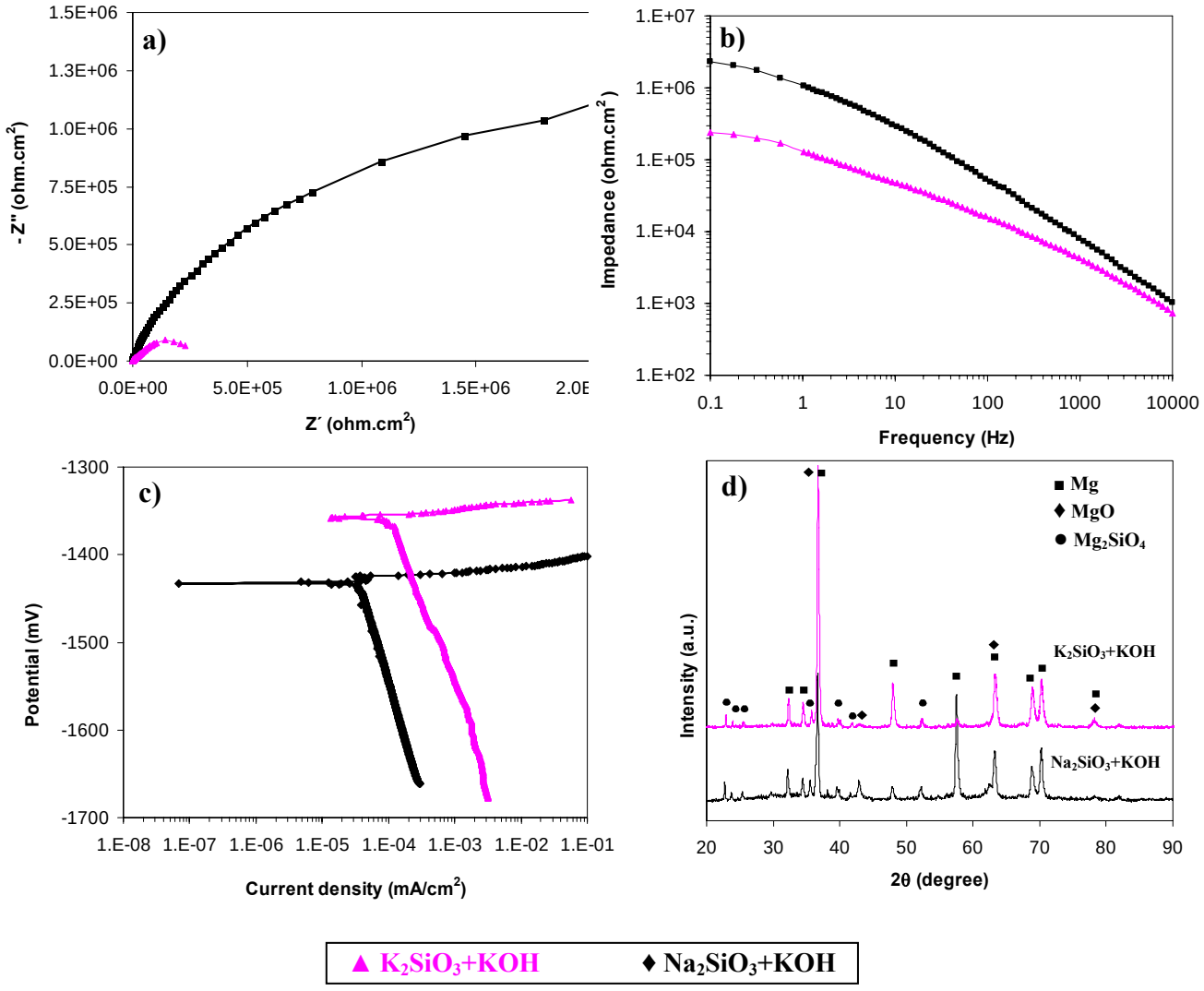

Fig. 5.28. Characterization of the coatings prepared by Na_2SiO_3+KOH and K_2SiO_3 + KOH, a) Nyquist b) Impedance, c) Polarization curves and d) XRD pattern.

5.2.2.3.2 Sodium–phosphate coatings

Na_3PO_4+KOH, $Na_5P_3O_{10}$+KOH and $Na_2H_2P_2O_7$+KOH solutions were used to prepare the coatings of the second group. The breakdown voltages of the coatings and conductivity of the solutions are 166, 225, 252 V and 40.01, 30.06, 21.1 mS/cm respectively.

Fig. 5.29 shows the surface morphology of the coatings. The surface of the coatings show that the size and number of the pores is noticeably reduced compared to that of the silicate coatings. The coatings prepared by $Na_2H_2P_2O_7$+KOH, Na_3PO_4+KOH and $Na_5P_3O_{10}$+KOH solutions respectively have about 2500, 3580 and 2920 hole/mm^2 with a size of more than 2μm. However another kind of defect, namely cracks, could be commonly observed on the surface morphology of the coatings. The cross section results show that the coating produced by $Na_2H_2P_2O_7$+KOH solution has an uneven structure which contains several defects. The structure of the Na_3PO_4 and $Na_5P_3O_{10}$ coatings is more established with a more uniform structure. The cross section of both coatings contains pores however they are separated and do not go through the substrate.

In addition, two electrochemical methods were employed to evaluate the corrosion resistance of the coatings. The corrosion evaluation results are presented in Fig. 5.30. Based on the data, the Na_3PO_4+KOH and $Na_2H_2P_2O_7$+KOH solutions result in the highest and the lowest corrosion resistance, respectively, of the coatings in the group. The coating prepared by $Na_5P_3O_{10}$+KOH has an intermediate value. The impedance values of the Na_3PO_4+KOH, $Na_5P_3O_{10}$+KOH and $Na_2H_2P_2O_7$+KOH coatings are $(2.56\pm0.2)\times10^5$, $(1.1\pm0.1)\times10^5$ and $(1.9\pm0.2)\times10^4$ $\Omega\cdot cm^2$, respectively. The polarization test results also suggest the same order for corrosion resistance of the coatings where the corrosion rates of the coatings are $(5.7\pm0.5)\times10^{-3}$, $(2.12\pm0.2)\times10^{-2}$ and $(9.34\pm0.1)\times10^{-1}$ mm/year, respectively.

The XRD patterns presented in Fig.5.30-d indicates that the coatings are composed of MgO and $Mg_3(PO_4)_2$. The results apparently show that changes in the stoicheiometry of the compounds or different type of the anions had an effect on the

peak intensities but it has no influence on the type of the phases forming in the structure of the coatings. It is seen that Na_3PO_4 has the highest and the $Na_2H_2P_2O_7$ has the lowest intensity of the MgO peak.

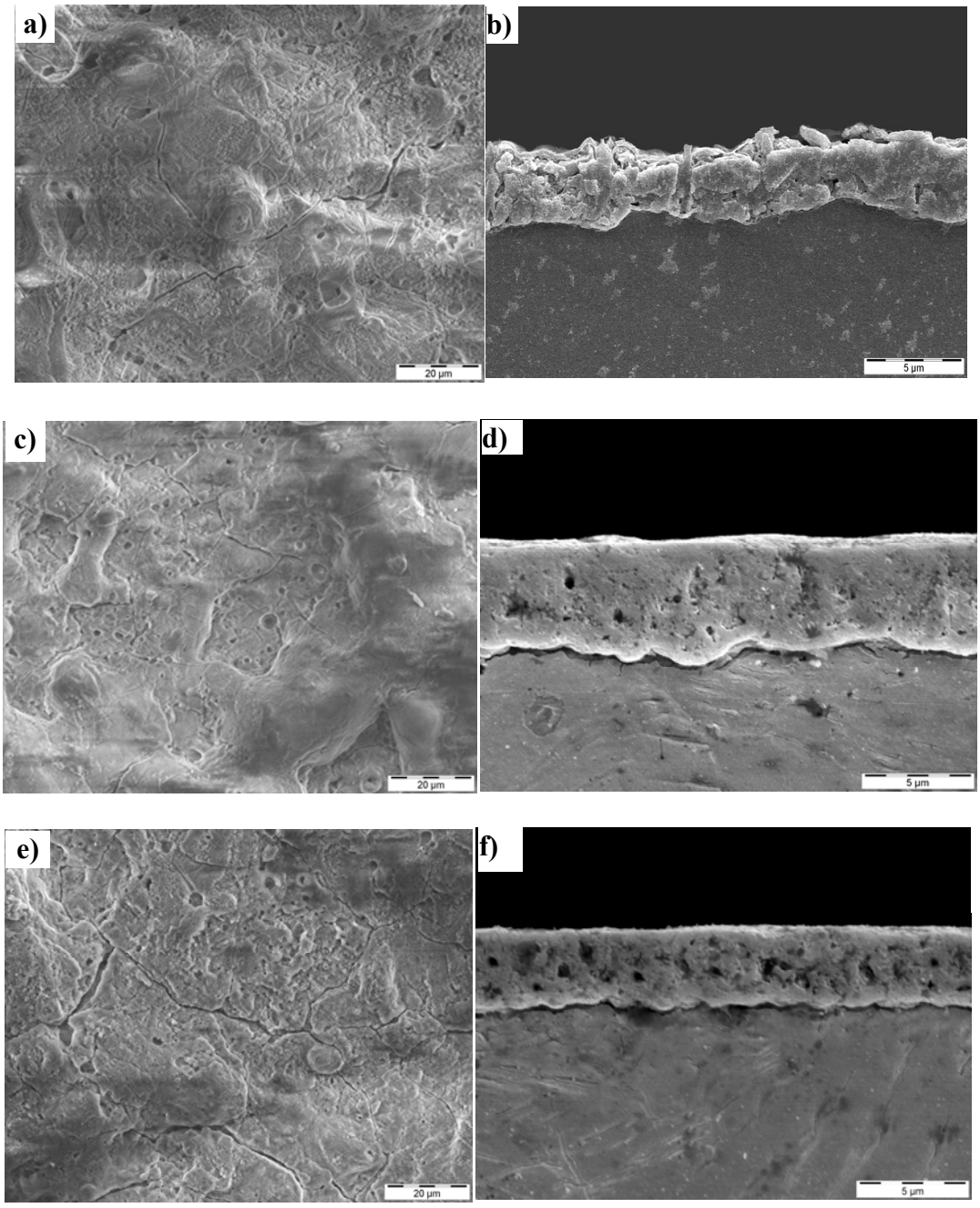

Fig. 5.29 Surface morphology and cross section of the a,b) $Na_2H_2P_2O_7$, c,d) Na_3PO_4, g) $Na_5P_3O_{10}$ coatings

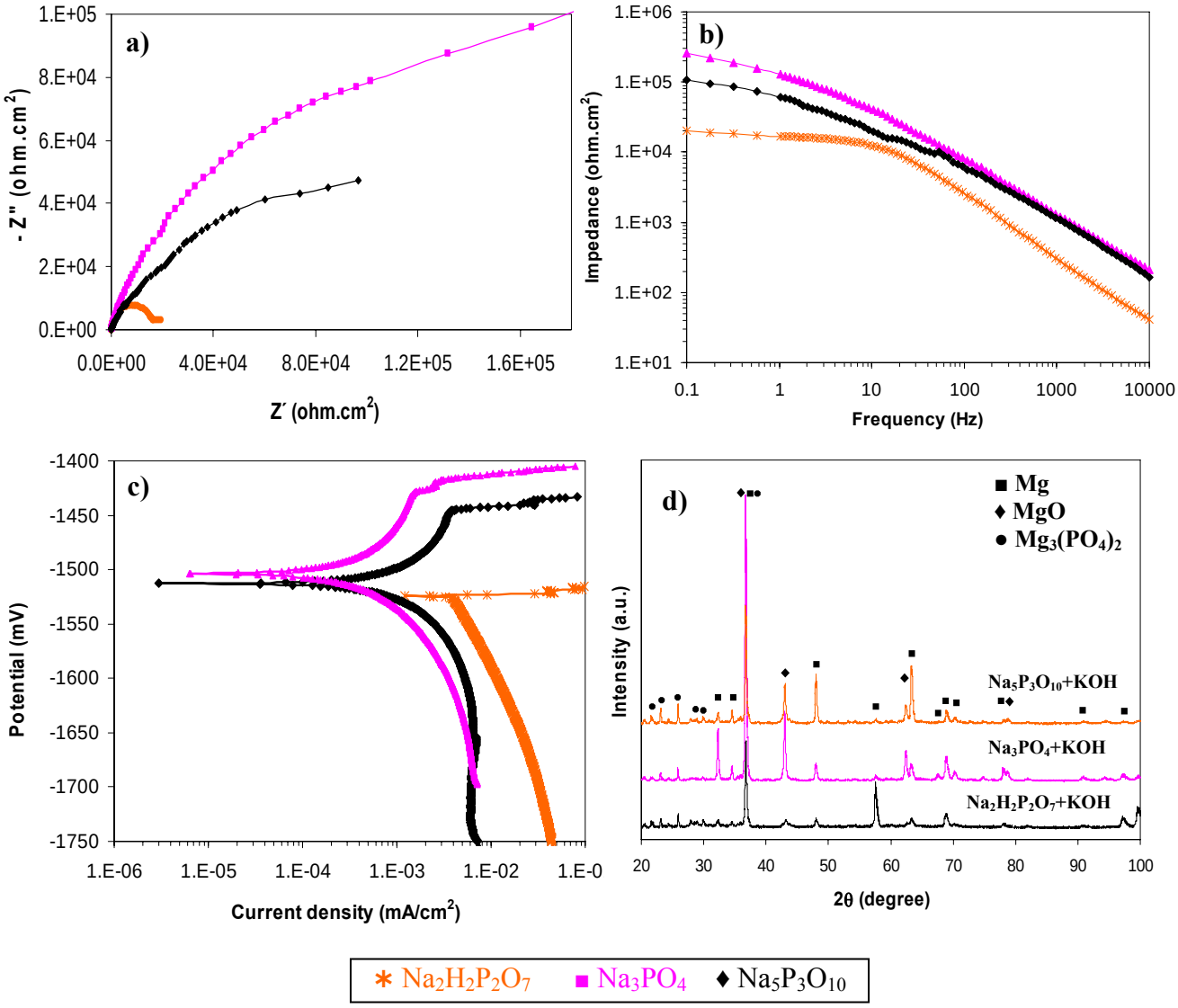

Fig. 5.30. Characterization of the coatings by $Na_2H_2P_2O_7$+KOH, Na_3PO_4+ KOH and $Na_5P_3O_{10}$+KOH, a) Nyquist, b) Impedance, c) polarization curves and d) XRD patterns.

5.2.2.3.3 Potassium–phosphate coatings

Two electrolytes based on the potassium phosphates namely K_3PO_4+KOH and $K_4P_2O_7$ +KOH were used to prepare the coatings of the third group. The breakdown voltage and conductivity of the coating solutions are 166, 207 V and 39.8, 37 mS/cm, respectively.

The surface morphology of the coatings illustrated in Fig. 5.31 shows the porous structure of the coatings. A wide range of pore sizes from, ~0.5 to 8 µm, can be seen in the surface morphology of both coatings. But the average size of the pores is in the range of 4 - 4.5 µm. The pores of the K_3PO_4+KOH coating are less in number but bigger in diameter compared to those of the $K_4P_2O_7$ +KOH. The measurements showed that the former has about 2085 holes/mm^2 with a diameter between 4-8µm while the latter has about 4150 holes/mm^2 with diameters between 3-6µm. It is seen that the surface morphology of the coatings are dissimilar in terms of number and size of the holes but in general they have more common characteristics in comparison with the coatings of the other groups. The figures related to the cross section of the coatings show cracks and individual pores in the structure of the K_3PO_4+KOH coating. The pores in the structure of the $K_4P_2O_7$+KOH coating however, are interconnected and they are distributed throughout almost the whole structure of the coating even very close to the coating /substrate interface.

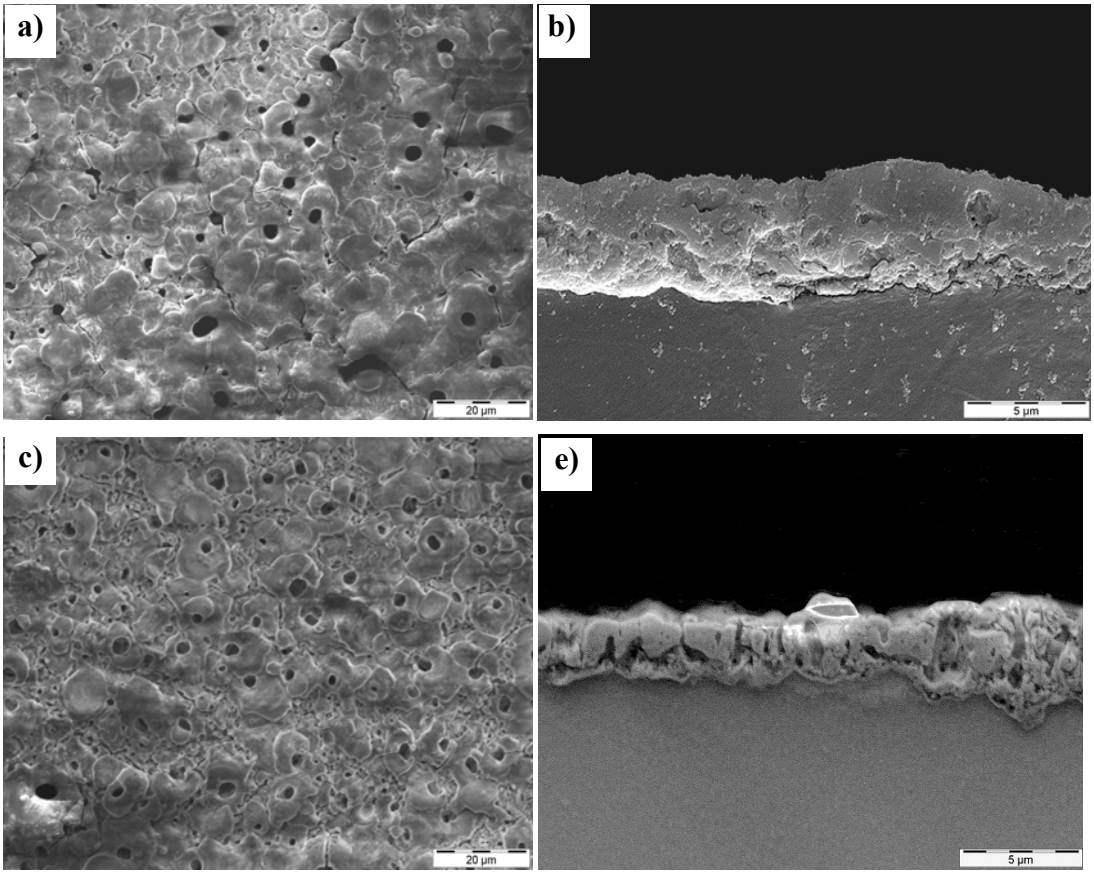

Fig. 5.31 Surface morphology and cross section of the a,b) K_3PO_4 and c,d) $K_4P_2O_7$ coatings

Nyquist and impedance curves in Fig. 5.32-a,b clearly show that the K_3PO_4+KOH coating with an impedance value of $(2.27\pm0.2)\times10^5$ $\Omega\cdot cm^2$ has a higher resistance to corrosion than the $K_4P_2O_7$+KOH coating with its impedance which reaches only $(4.1\pm0.4)\times10^3$ $\Omega\cdot cm^2$. Similarly, polarization test data with respective corrosion rates of $(2.99\pm0.2)\times10^{-3}$ and $(4.41\pm0.4)\times10^{-1}$ mm/year show the same tendency. The type of the coating phases were evaluated by XRD method. The patterns in Fig. 5.32-d show that the potassium phosphate coatings are mostly composed of MgO.

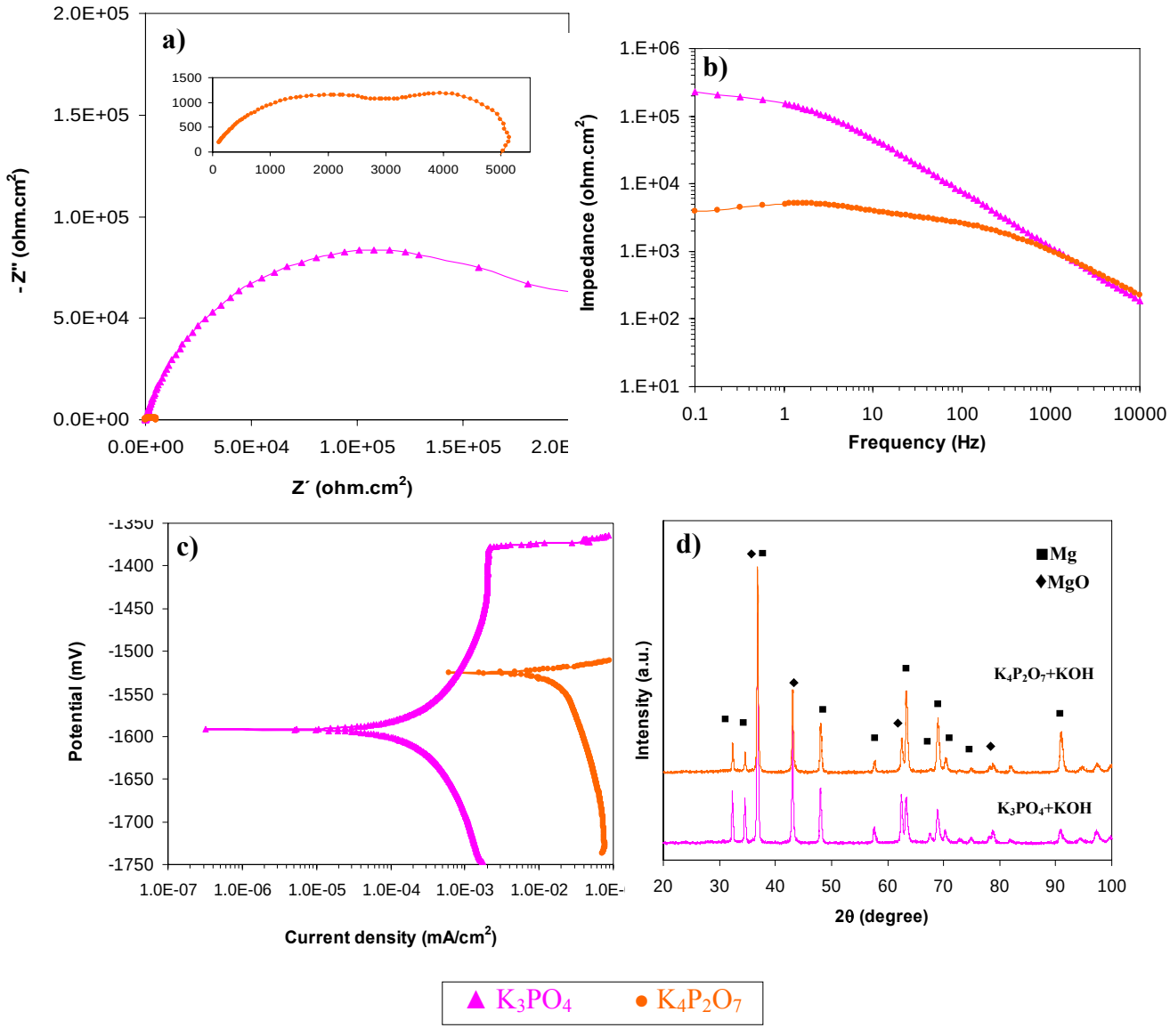

Fig. 5.32. Characterization of the coatings prepared by K_3PO_4+KOH and $K_4P_2O_7$ +KOH, a) Nyquist, b) Impedance and c) Polarization,

5.2.2.3.4 Aluminate coating

The measurements of the breakdown voltage and conductivity of the sodium aluminate solution resulted in the 213 V and 38.8 mS/cm respectively. The surface morphology of the coating presented in Fig. 5.33 shows a different type of morphology compared to the previous coatings. Some parts of the coating seem thicker than the adjacent area. The surface morphology of the coating is mainly covered by tiny pores with a diameter below 1 μm and a density of about 70000 hole /mm^2. The cross section of the coating also shows the formation of an uneven layer on the surface of the substrate. The formation of a thin non-uniform coating which is just about 1 μm thick points to the unfavourable effect of the aluminate anions on the growth process of the coating.

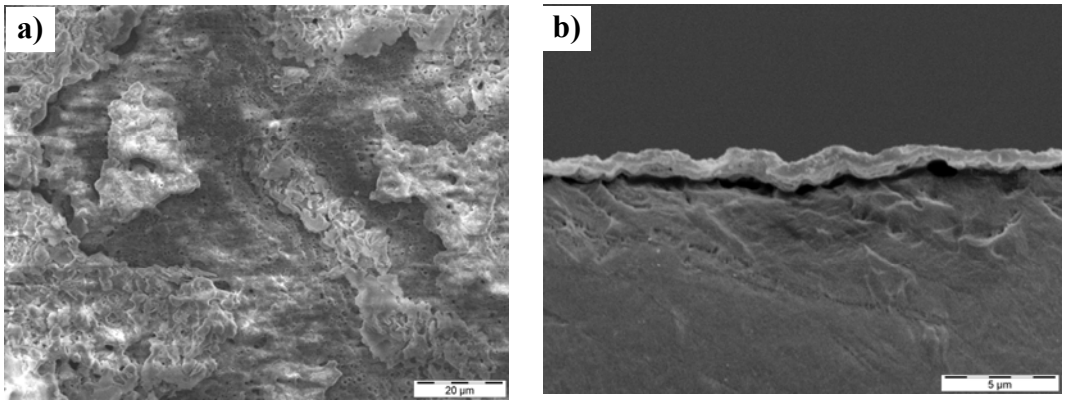

Fig. 5.33. Surface morphology and cross section of the $NaAlO_2$ coating

The results of both corrosion evaluation methods presented in Fig. 5.34 show that impedance and corrosion resistance of the coating are 2.5×10^3 $\Omega\cdot cm^2$ and 1.16 mm/year, respectively. The results of both methods accord with one another and give enough evidence that the applied coating has relatively poor corrosion resistance. Results of the phase determination in Fig. 5.34-d show that aluminium participates in the coating process and two phases of magnesium oxide (MgO) and magnesium aluminate ($MgAl_2O_4$) were detected in the coating structure.

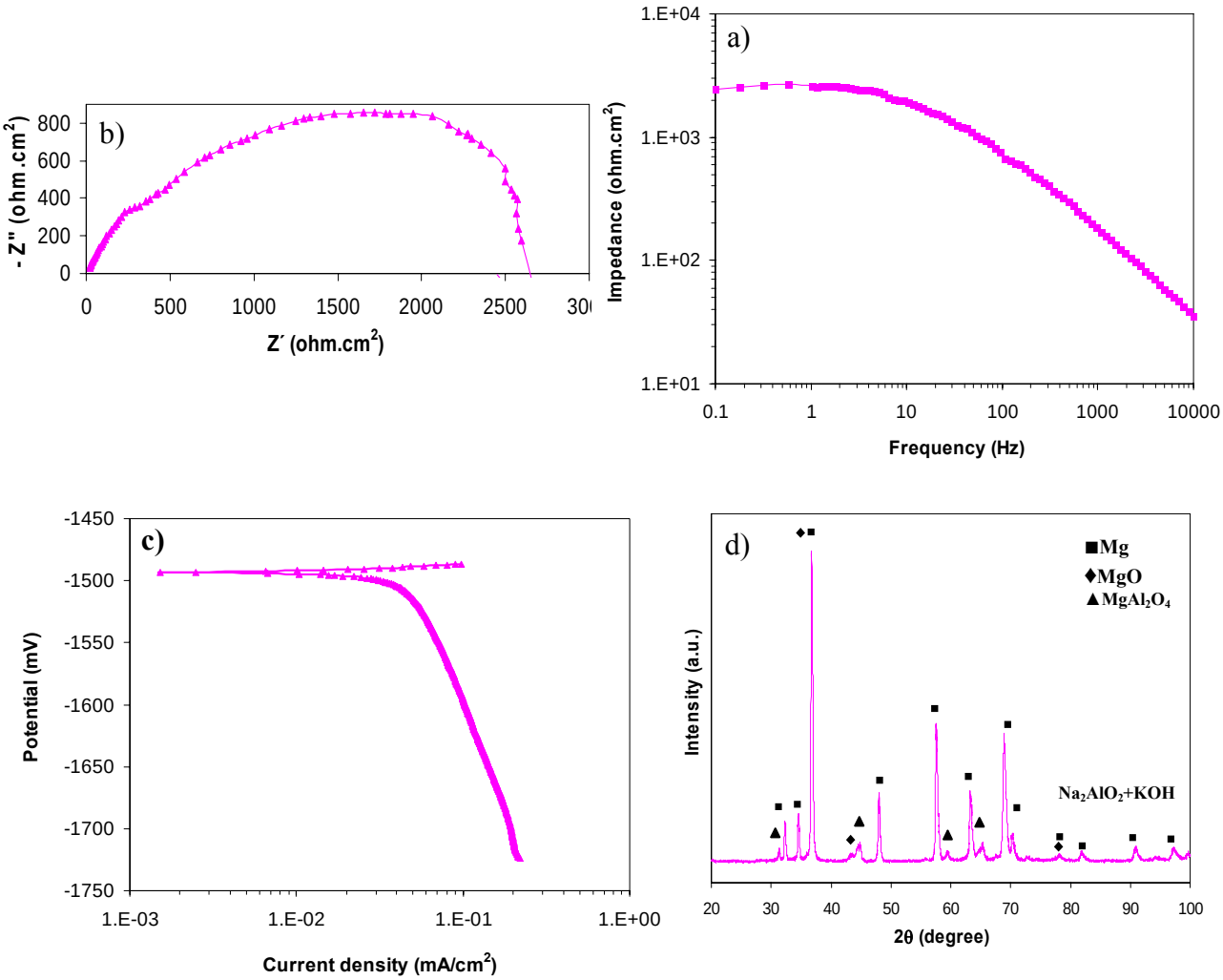

Fig. 5.34. Characterization of the coatings prepared by $NaAlO_2$, a) Nyquist b) Impedance, c) Polarization curves and d) XRD pattern.

5.2.2.4 Corrosion resistance and passivation of the hydroxides

Corrosion evaluation of the PEO coatings showed that sodium silicate as a salt solution has ability to produce a higher corrosion resistant PEO coating. To produce a successful PEO coating and to get proper properties of the PEO coating, proper hydroxide solution is what should also be added to the salt solution. The results of the current section reveal how different compositions of the hydroxide solution influence the corrosion resistance of the PEO coating.

The KOH, NaOH, $Al(OH)_3$ and $Mg(OH)_2$ are four different hydroxides added to the sodium silicate solution to prepare the PEO coatings. Basic properties of the hydroxide solutions alone and with addition of sodium silicate are listed in Table 5.9. and 5.10, respectively

Table 5.9. Properties of hydroxide solutions

Solutions / property	KOH	NaOH	$Al(OH)_3$	$Mg(OH)_2$
pH	13.1	13.3	8.7	10.5
conductivity (mS/cm)	33.6	47.2	0.01	0.1

Fig. 5.35 -a,b,d shows the corrosion evaluation results of the hydroxide coatings based on the impedance and polarization test methods. The evaluation methods indicate that the KOH solution has a higher impedance and lower corrosion rate compared to the other solutions. The corrosion rate and impedance data of the KOH, NaOH, $Al(OH)_3$ and $Mg(OH)_2$ are listed in Table 5.11. The results of both methods suggest that the KOH is the hydroxide solution which can produce a coating with higher corrosion resistance. Fig. 5.35-c illustrates the XRD patterns of the hydroxide coatings. It can be seen that the MgO exists in all coatings. However an additional phase, i.e. Mg_2SiO_4, contributes in the coating structure when KOH solution was used

Table 5.10. Measured value of the coating solution.

Name / Value	Na_2SiO_3 +KOH	Na_2SiO_3 +NaOH	Na_2SiO_3 +$Al(OH)_3$	Na_2SiO_3 +$Mg(OH)_2$
pH	12.96	13.1	12.6	12.54
conductivity (mS/cm)	44.5	55.9	15.7	16.2
V_{BD} (V)	160	150	243	255
V_f (V)	376	270	442	442
Thickness(µm)	8.3	3.7	6.8	7.1

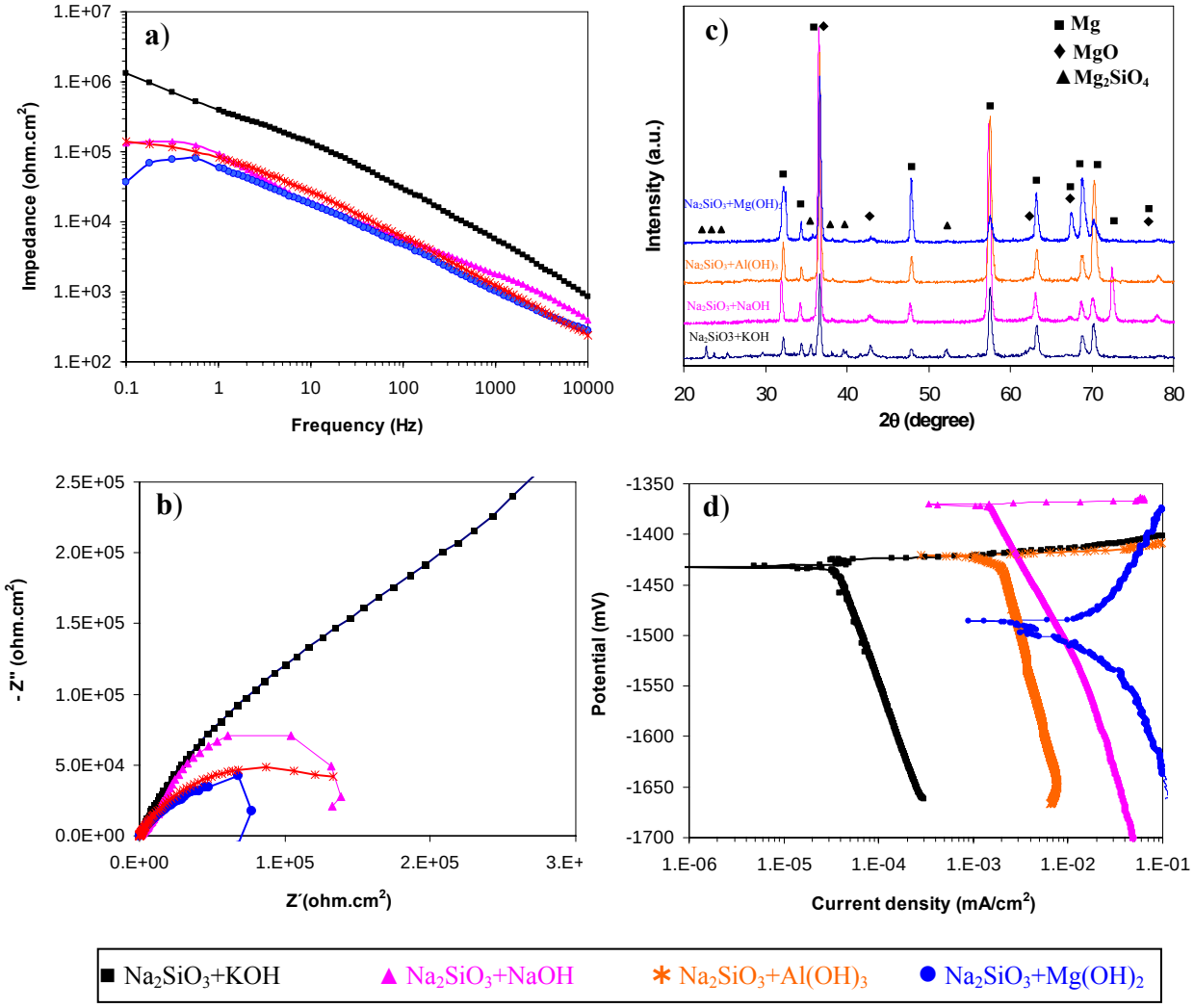

Fig. 5. 35. Properties of the coatings prepared by different hydroxides a) Impedance and b) Nyquist curve, c) XRD pattern, d) Polarization curves.

Table 5.11. Corrosion resistance data of the coatings.

Name / Value	Na_2SiO_3 +KOH	Na_2SiO_3 +NaOH	Na_2SiO_3 +$Al(OH)_3$	Na_2SiO_3 +$Mg(OH)_2$
Corrosion rate (mm/year)	$(8.4\pm0.8)\times10^{-4}$	$(3.6\pm0.3)\times10^{-2}$	$(4.2\pm0.3)\times10^{-2}$	$(5.8\pm0.5)\times10^{-1}$
Impedance ($\Omega\cdot cm^2$)	$(2\pm0.2)\times10^{6}$	$(1.4\pm0.2)\times10^{5}$	$(1.3\pm0.3)\times10^{5}$	$(3.7\pm0.4)\times10^{4}$

In order to check the relation of the corrosion resistance of the PEO coating with stability of the passive layers in hydroxide solutions, the stability of the passive layer was also evaluated. The results shown in the Fig. 5.36 evidently point to the fact that the passive current of KOH is about 5×10^{-4} mA/cm^2, which is the lowest value compared to the other hydroxides. The average value for the NaOH, $Al(OH)_3$, $Mg(OH)_2$ solutions is about 3×10^{-3}, 2×10^{-2} and 3×10^{-1} mA/cm^2 respectively. It can be seen that the polarization curve of the $Mg(OH)_2$ shows different behaviour compared to the other solutions. In the primary stage of the potential scan i.e. between OCP and -700V, the polarization curve has an average passive current of around 5×10^{-3} mA/cm^2. However by getting to potentials around -700 mV, a sudden increase of the current to ~3×10^{-1} mA/cm^2 occurs and is maintained until the end of the scan process without considerable change.

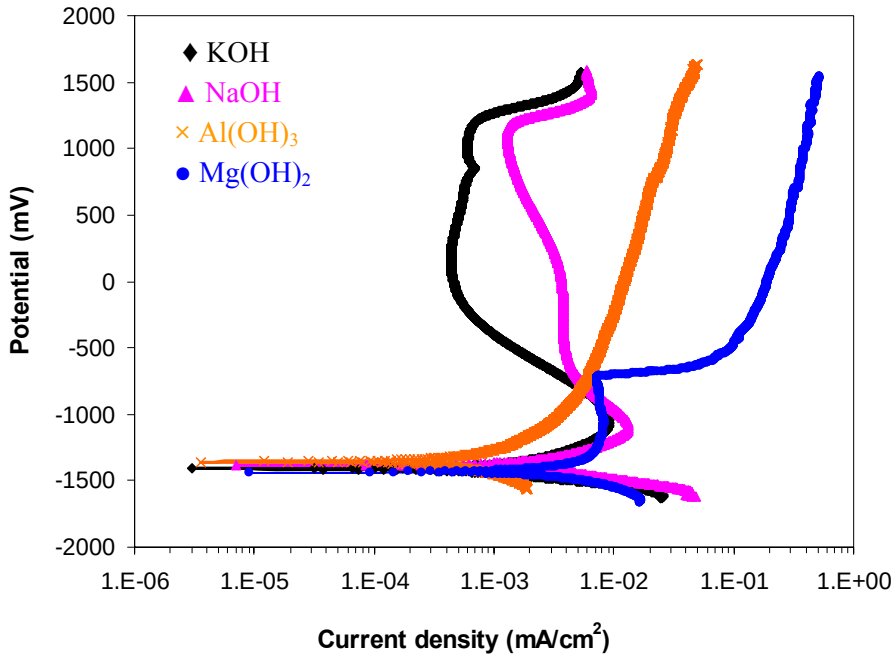

Fig. 5.36. Anodic polarization on the substrate by hydroxide solutions.

5.2.3 Role of passive layer in corrosion resistance

So far the stability of the passive layers formed in salts and hydroxides solutions was determined separately. Similar studies were done to determine how stable the passive layer in the coating solution is. In order to get the results, the coating solutions which had produced better corrosion resistance in each group were used. The bare substrate was anodically polarized in Na_2SiO_3+KOH, Na_3PO_4+KOH, K_3PO_4+KOH, $NaAlO_2$+KOH solutions which is shown in the Fig. 5.37. It is seen that the passive currents of the Na_2SiO_3+KOH and $NaAlO_2$+KOH are about $(3.5\pm0.4)\times10^{-4}$ and $(1.1\pm0.2)\times10^{-3}$, mA/cm^2 which are the lowest and highest value, respectively. That of the Na_3PO_4+KOH and K_3PO_4+KOH, which shows similar value, is about $(6.5\pm0.5)\times10^{-4}$ mA/cm^2. Based on the results the sodium silicate produces the highest and sodium aluminate results in the lowest stability of the passive layers and those in the Na_3PO_4+KOH and K_3PO_4+KOH solutions show moderate stability. It can be seen that this is the same trend which was followed by the corrosion resistance of the associated coatings.

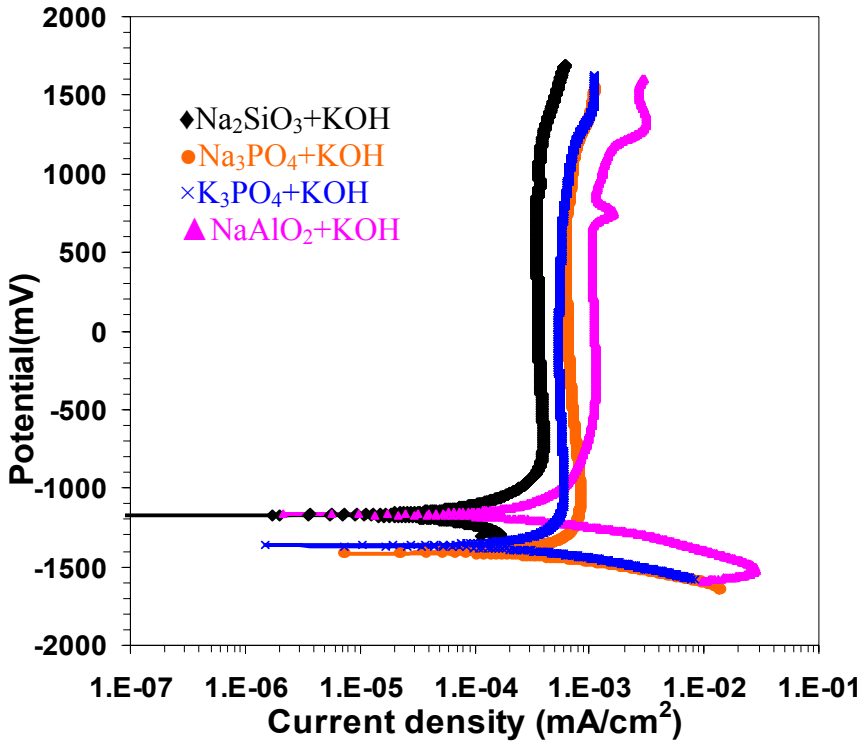

Fig. 5.37 Anodic polarization of the substrate by coating solutions

5.2.4 Corrosion process of the PEO coating

Corrosion evaluation of the PEO coating showed that the combination of sodium silicate and potassium hydroxide produced a PEO coating showing proper corrosion resistance. The coating prepared by this solution was used to study the corrosion process of the PEO coating.

5.2.4.1 Corrosion pattern

Fig. 5.38 shows the corrosion behaviour of the coating while it was immersed in the 3.5%NaCl solution. The corrosion behaviour was observed by taking continuous photos. It is seen that small bubbles appear on the surface after a short period of time and they get bigger as time passes. After 5 hours, the bubbles get bigger and are continually liberated from some local points which shows the corrosion reaction starting to take place. The results show that it is after about 10 hour when the first signs of corrosion products appear on the surface.

5.2.4.2 Corrosion progress

The curve fitting method and morphology of the coating were employed to study the corrosion behaviour of the coating step by step. The best fit was obtained by using an equivalent circuit, shown in Fig. 3.7. Combination of the elements in the circuit suggests that the coating consists of an outer and an inner layer. The outer layer has direct contact with the electrolyte while the inner layer lies directly on the metal surface beneath the outer layer. The surface morphology and cross section of the coating shown in Fig. 5.39 indicate that the outer layer of the coating is very porous and contains big holes.

Fig. 5.40 shows the curve fitted to the impedance data after 30 min of the immersion process. The exact value of the circuit components and errors are listed in Table 5.12. The low amount of errors indicates that the curves are properly fitted to the experimental data.

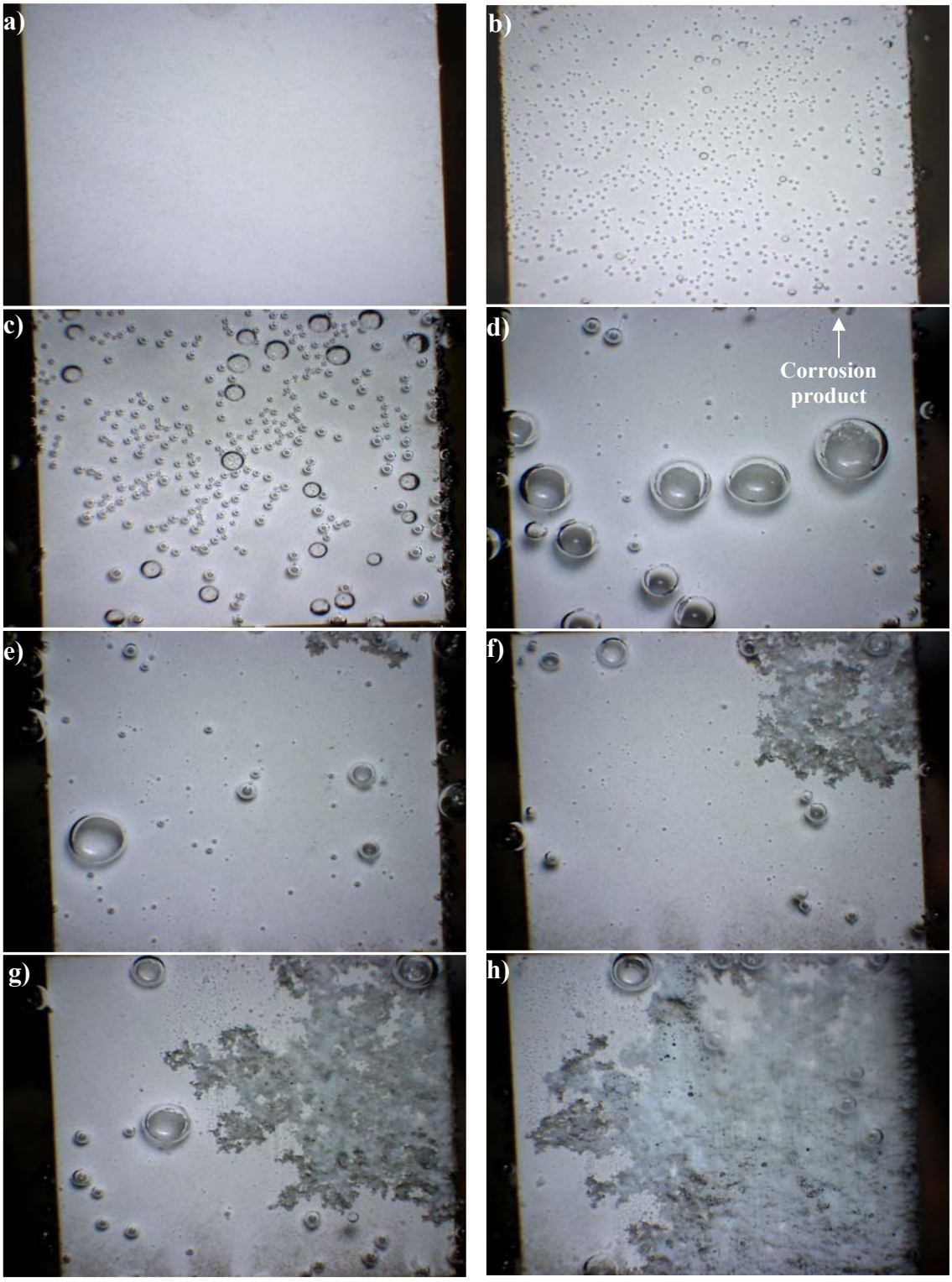

Fig. 5.38. Corroding behaviour of the PEO coating in 3.5% NaCl after immersion time of about a)0 b)1 c) 5 d)10 e)20 f)30 g)40 h)50 hours.

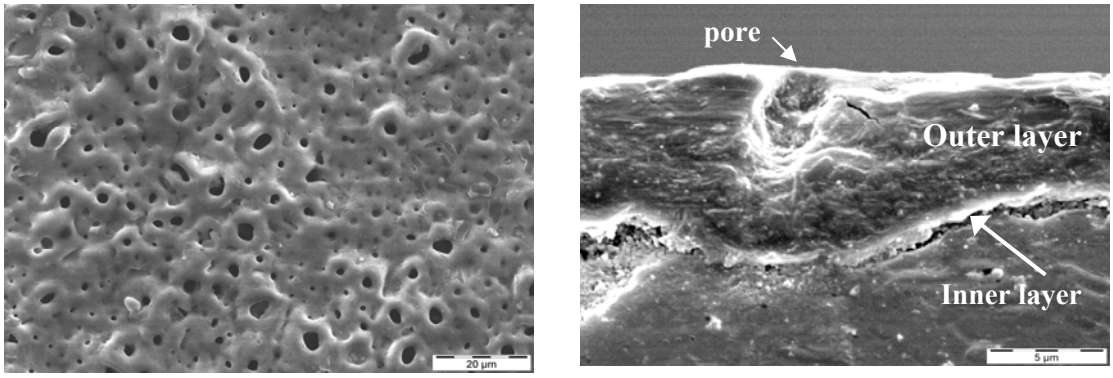

Fig. 5.39. Surface morphology and cross section of the coating prepared by selected solution.

The first impedance data were collected after 30 min immersion time, which is required to reach a stable condition. For the first impedance data the magnitude of the R_1 and R_2 are 3.2×10^4 and 5.6×10^6 ohm·cm^2, respectively. The data clearly imply that the resistance of the outer layer is very low and total resistance of the coating is mainly maintained by the inner layer. Such a high resistivity can be attributed to a dense and compact layer providing a strong barrier against corrosive species to reach to the substrate.

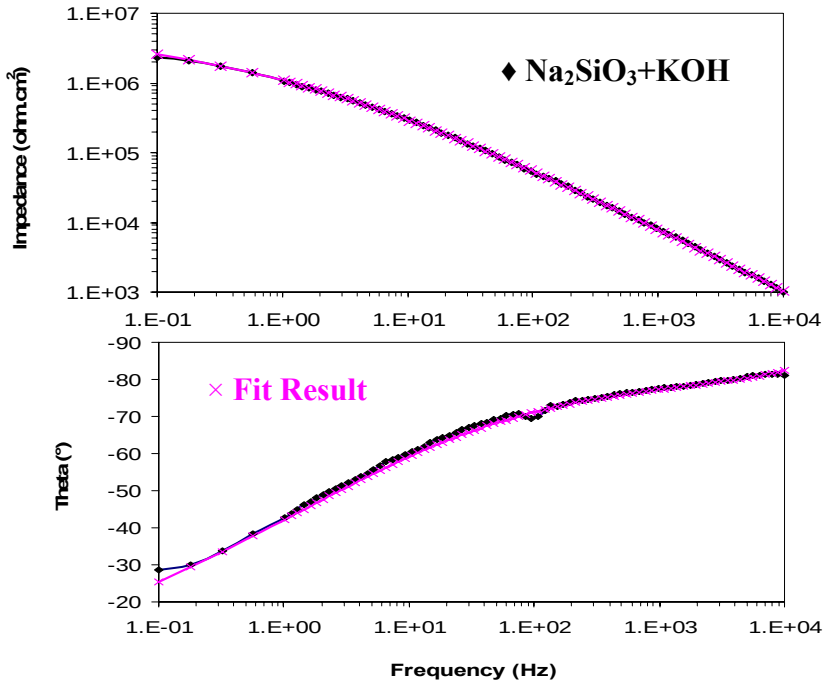

Fig. 5.40 Fit result to the impedance data of the Na_2SiO_3 + KOH coating after 30 min of immersion time

Table 5.12. Data of the equivalent circuit in different immersion time

Immersion time (hour)	CPE1-P	CPE1-T	R_1 ($\Omega \cdot cm^2$)	CPE2-P	CPE2-T	R_2 ($\Omega \cdot cm^2$)	Chi-Squared	Weighted Sum of Squares
0.5	0.89	5.19E-08	3.21E4	0.42	2.70E-07	5.64E6	9.9E-04	0.160
1.5	0.85	7.67E-08	1.23E4	0.44	3.84E-07	3.83E6	4.2E-03	0.692
2.5	0.34	5.39E-07	3.79E2	0.82	1.24E-07	5.50E6	5.1E-04	0.083
3.5	0.82	1.27E-07	3.40E2	0.40	5.99E-07	2.79E6	7.8E-04	0.121
4.5	0.77	2.39E-07	1.89E5	0.85	6.31E-07	1.85E5	4.2E-04	0.068
5.5	0.83	2.13E-07	1.64E5	0.67	1.20E-06	1.79E5	4.6E-03	0.741
6.5	0.83	2.48E-07	1.09E5	0.82	1.60E-06	1.25E5	8.3E-04	0.133
7.5	0.82	2.74E-07	5.68E4	0.76	3.37E-06	4.67E4	3.9E-04	0.063
8.5	0.82	2.93E-07	1.08E5	0.65	3.32E-06	1.40E5	5.7E-04	0.092
9.5	0.82	2.97E-07	9.19E4	0.44	3.55E-06	2.33E5	5.6E-04	0.090
10.5	0.82	3.41E-07	7.91E4	0.66	4.59E-06	8.91E4	5.2E-04	0.084

The descending trend of R_1 and R_2 data in Table 5.12 shows that the coating resistance deteriorates according to immersion time. The impedance plots in Fig. 5.41 also show a reducing trend in the impedance values as immersion time gets longer. The general deterioration of the coating can be understood by considering the impedance data, however the way the inner and outer layer behave during the immersion process can only be studied by analyzing the circuit data which are plotted in Fig. 5.42.

Fig 5.43 shows the corroded area of the coating tested in 3.5% NaCl solution. It is seen that the major damage is concentrated in the corroded area surrounded by the coating. The surface morphology of the coating has changed locally and severe damage together with deep cracks appears on the surface.

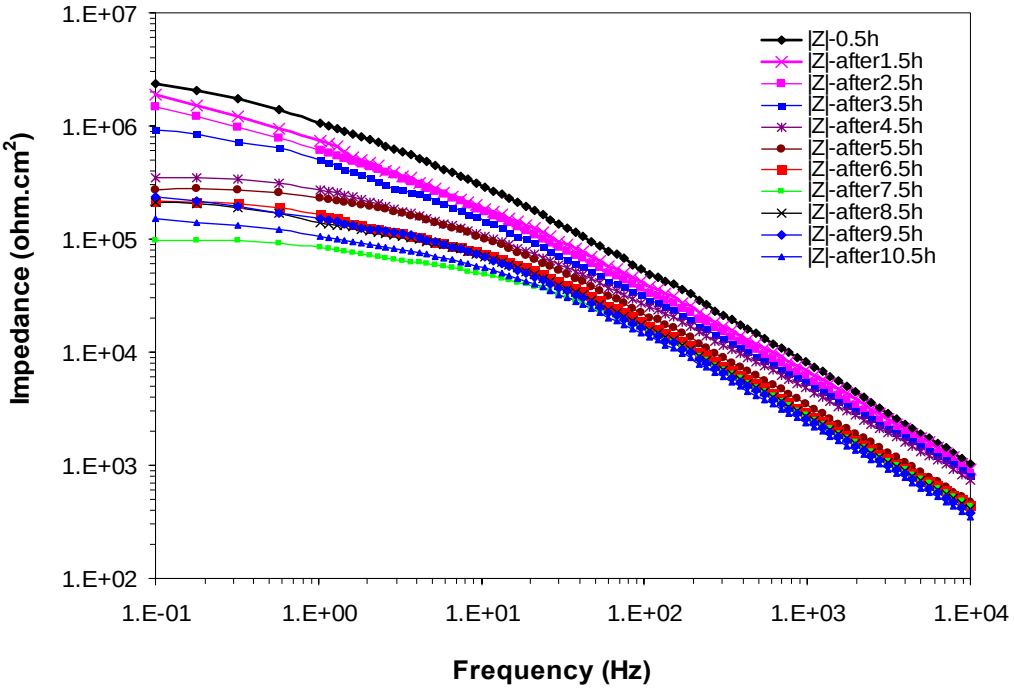

Fig. 5.41. Impedance plots of PEO coating in different times of immersion.

It was explained that the amount of R_1 and R_2 follows an increasing and decreasing trend during the immersion in the test solution. This kind of behaviour suggests fluctuating corrosion behaviour for a PEO coating when it is in a contact with a corrosive environment. In order to check the coating behaviour in long immersion times, the PEO coating was examined by impedance tests within 60 hours.

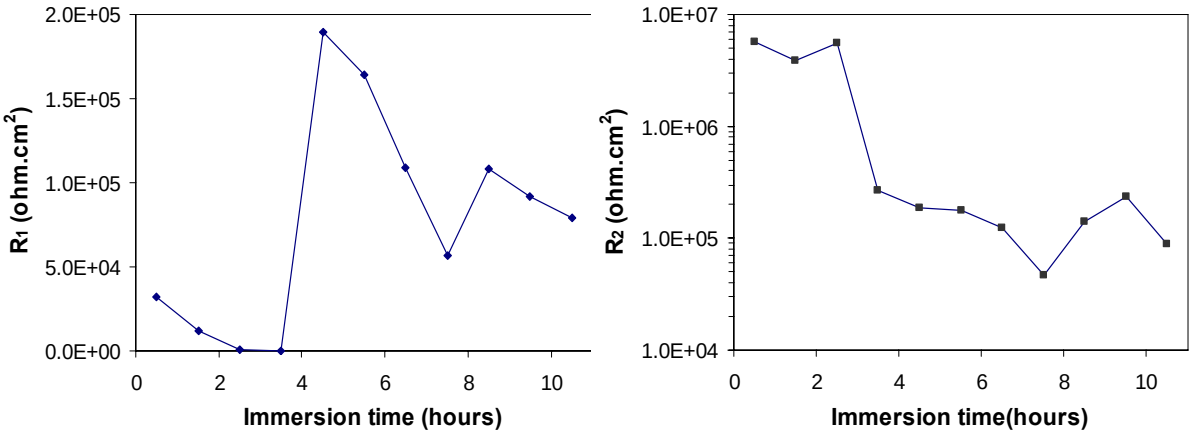

Fig. 5.42. Resistance of different layers of the PEO coating in different immersion time L) R_1 and R) R_2.

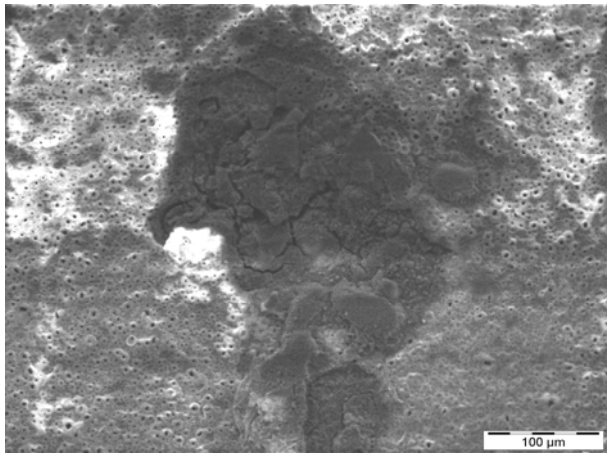

Fig. 5.43. Corroded area of the Na_2SiO_3+KOH coating in 3.5% NaCl solution.

The impedance data shown in Fig. 5.44, as well as the previous results, indicate that the corrosion of the coating takes place in a fluctuating manner. However, it can clearly be seen that in spite of sequential increases and decreases of resistivity the overall resistance of the coating deteriorates and decreases in value. Resistance of the coating after about 45 hours reaches very low values close to ~10^3 $\Omega \cdot cm^2$. In this moment the coating is almost gone and the measured data are more or less equal to the impedance value of the bare metal.

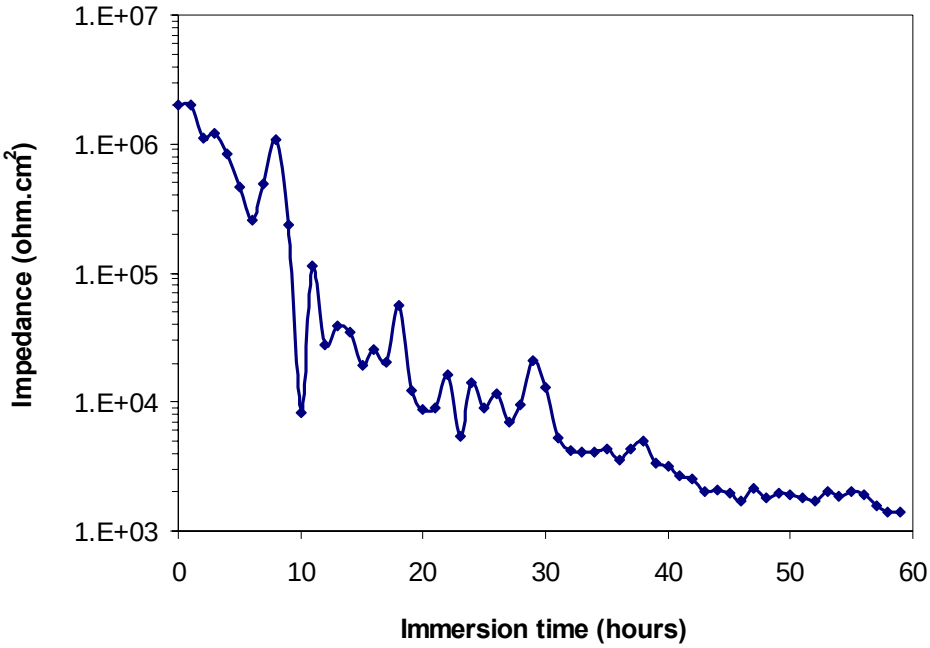

Fig. 5.44. Impedance variations of the PEO coating in a long immersion time.

5.3 The role of thickness in the corrosion resistance of the PEO coating

This chapter studies the influence of thickness on the corrosion resistance of the coating. PEO coatings were prepared under different condition of current density, time and solution concentration. These conditions resulted coatings in different thicknesses. The corrosion resistance of the coatings were evaluated and influence of the thickness on the corrosion resistance of the coating was studied. In addition to the above experiments, the behaviour of the PEO process in a constant voltage process was also studied. Prior considering the other parameters, the results corresponding to the constant voltage process will be presented to provide better understanding of the process.

5.3.1 Constant voltage treatments

Variation of the current density versus time was studied in different constant voltage processes of 120, 150, 180, 225, 270, 330, 375 V. The selected voltages provide proper condition for study of the behaviour of the PEO process in different stages because the breakdown voltage (V_{BD}) and burning voltage (V_{BU}) of the process are about 160 and 375V, respectively.

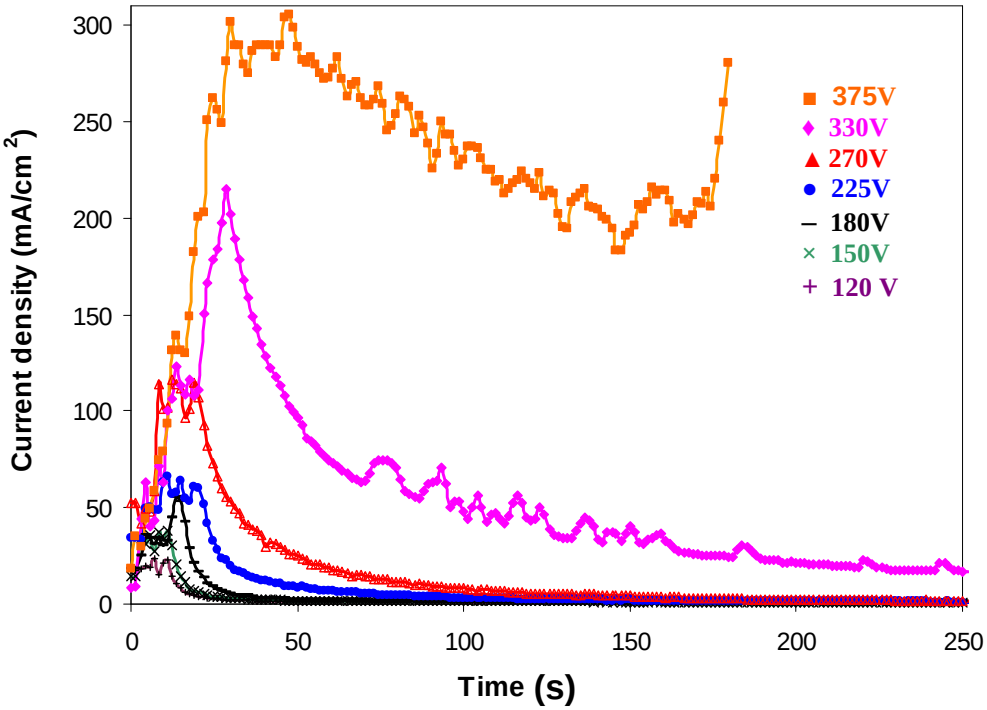

Fig. 5.45. Variation of current density with time in constant voltages.

Fig. 5.45, shows that almost all curves are following a common trend. They have an initial sharp increase, reach a maximum, have a sharp decrease and finally reach a steady state condition. The maximum magnitude of each curve is about 23, 37, 55, 65, 115, 215, 300 mA/cm^2. These data show a direct dependence on the magnitude of voltage. It means that the higher voltages have higher maximum value. The results indicate that by applying higher voltage, longer duration of the process is required for reaching to the steady state condition. The steady state region continues without any noticeable changes in all voltages except that of the 375 V. In this case, the process never reaches the steady state region because after about 180 seconds the coating experiences the burning effect in which the current increases sharply.

The growth behaviour of the PEO coatings was studied by measuring the thickness and considering the weight gain of the coating in different constant potentials. The results can be considered in Fig. 5.46. The negative values of the weight gain clearly indicate that prior to the $V_{BD,}$ metal is mostly dissolving. The thickness measurement also shows zero values for the coatings treated by the potentials below breakdown voltage. As the process reaches the breakdown voltage and beyond, the negative value of the weight gain and thickness changes to the positive values which indicate that coating layer is forming on the metal surface.

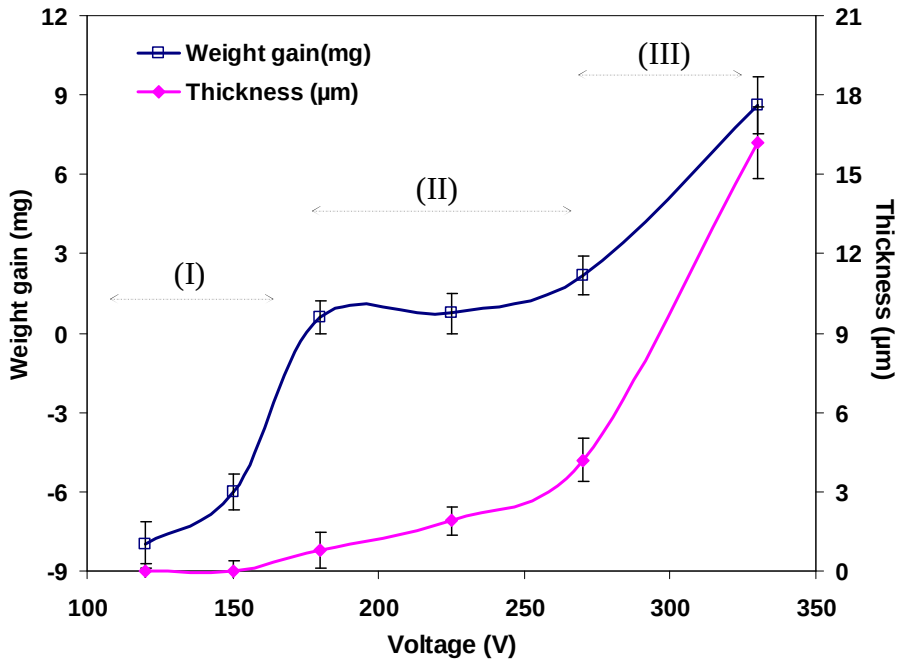

Fig. 5.46. Variation of thickness and weight gain with voltage.

5.3.2 Influence of the current densities on thickness and corrosion resistance

Fig. 5.47 shows the relation between the voltage and time in different constant current densities, namely 3.6, 9.06, 18.1, 36.2 and 72.5 mA/cm^2. As can be seen, increase in current density leads to the higher increase rate of the voltage. In the curves, two stages can be considered for the process. In the initial stage of the process the samples experience an intensive increase rate of the voltage compared to the second stage. To evaluate the increase rates of voltage, the ratios of voltage: time were calculated after 50 seconds of the process. This period of time were selected because all of the curves are in the initial stage. The calculations show that the application of current densities from 3.6 to 72.5 mA/cm^2 results in the ratios of 0.85, 1.7, 2.5, 3.4 and 4.5 V/s, respectively.

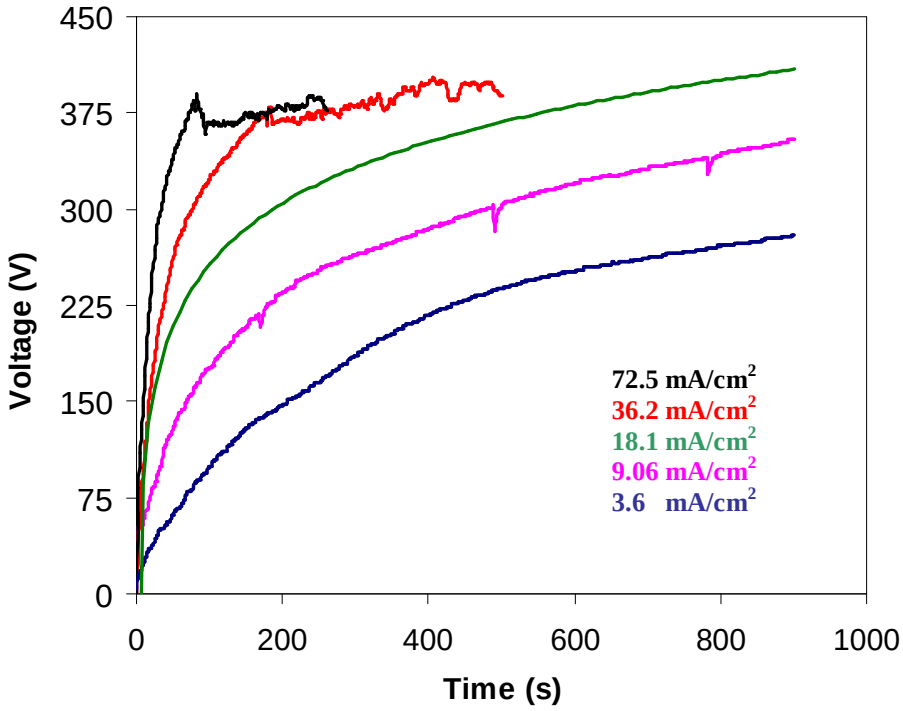

Fig. 5.47. Variation of voltage with time in constant current processes.

In the second stage of the process, the increase rate of the voltage decreases. However, the decrease in the higher current density curves is more intensive compared to the lower ones. In the higher current density curves, i.e. 36.2 and 72.5 mA/cm^2, the increase rate of the voltage is so high that it reaches 375 V (burning voltage) in a short time, then moves forward almost parallel with the horizontal axis and then burning of the coating starts. The second stage of the curves in the lower

current densities follow an ascending trend and they require more time to reach the burning voltage.

The thicknesses and weight gains corresponding to the processes of Fig. 5.47 are listed in Table 5.13. The first three data which did not reach the burning effect show that the coatings get thicker and gain more weight as higher current densities are applied. However, there is a limit for the thickening of the PEO coating by means of raising the current. The data show that application of the higher currents does not lead to coatings thicker than about 16±1 µm. The two last data indicate that although current has been increased, no considerable increase in thickness and weight gain occurs anymore. The last data, 72.5 mA/cm, show that the specimen even starts losing weight.

The corrosion resistance of the coatings was evaluated by impedance and polarization test methods. The corrosion data as well as thickness of the coatings are listed in Table5.13. The results show that the coatings with middle thickness, i.e. 5.3 and 13.3 µm, show relatively higher corrosion resistance. On the other hand, usage of very low, i.e. 3.6 mA/cm^2, and very high currents densities, i.e. 36.2 or 72.5 mA/cm^2, produces the coatings whose corrosion resistance are not good enough to provide effective protection. The weaknesses of the coatings originate from insufficient thickness of the coating prepared by 3.6 mA/cm^2 and the burning damages for those of prepared by 36.2 and 72.5 mA/cm^2.

Table 5.13. Thickness and corrosion resistance data of coatings in Fig. 5.47

Parameters / Current Density(mA/cm^2)	weight gain (mg)	Thickness (µm)	Impedance (Ω·cm^2)	Corrosion rate (mm/year)
3.6	0.8±0.1	1.5±0.1	1.5×10^{5}	2×10^{-3}
9.06	3.9±0.3	5.3±0.4	1.0×10^{6}	4×10^{-4}
18.1	10.1±1	13.3±0.9	1.05×10^{6}	2×10^{-4}
36.2	12.3±1.1	16.1±1.0	3.1×10^{5}	5×10^{-3}
72.5	11.6±1.1	17.1±1.0	4.1×10^{5}	4×10^{-3}

5.3.3 Influence of process duration on thickness and corrosion resistance

To study the growth behaviour of the coatings in different durations of the process, two series of the coatings were prepared by use of 9.06 and 18.1 mA/cm^2 current densities in different periods of time, namely 225, 900, 1800, 3600, 7200 seconds. It should be noted that by 18.1 mA/cm^2, the process was stopped after 6200 seconds because of the burning effect. As a result, 10 coated samples were produced and subsequently thickness and corrosion resistance of the coatings were evaluated. The coating periods shorter than 225 sec. or longer than 6200 sec. were not taken into consideration because they result in either very thin coating or a burning effect, respectively. Both latter effects had a negative influence on the corrosion performance of the coating.

Fig. 5.48 illustrates the relationship between thickness and the duration of the process. The results of both series clearly show that as the process proceeds, the coating gets thicker. The growth rates of the coating listed in Table 5.14 convey that the higher current densities result in the higher growth rates. However, in both cases the rate of growth reaches a maximum after about 900 seconds and subsequently it declines until the end of the process.

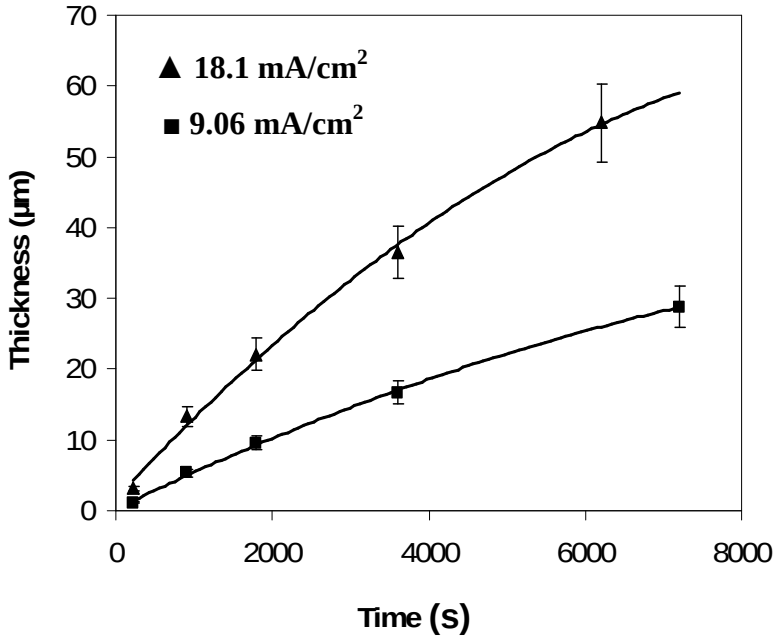

Fig. 5.48. Variation of thickness with time of the process.

As well as thickness, the weight gain of the coatings was examined. Fig. 5.49 shows that a good consistency exists between the thickness and weight gain data. The results show that the samples gain weight concurrent with the thickening of the coatings.

Table 5.14. Thickness and corrosion resistance data of coatings in different process time

Parameters / Current Density (mA/cm^2)	Time (s)	Thickness (µm)	Growth rate (µm/min)	Impedance ($\Omega \cdot cm^2$)	Corr. Rate (mm/year)
9.06	225	1.1	0.29	9.0×10^{4}	3×10^{-3}
	900	5.3	0.35	1.0×10^{6}	4×10^{-4}
	1800	9.6	0.32	1.02×10^{6}	4.8×10^{-4}
	3600	16.7	0.28	6.0×10^{5}	8×10^{-4}
	7200	28.8	0.24	1.3×10^{5}	2.2×10^{-3}
18.1	225	3.2	0.85	0.97×10^{6}	5×10^{-4}
	900	13.3	0.88	1.05×10^{6}	2×10^{-4}
	1800	22.1	0.74	5.0×10^{5}	9×10^{-4}
	3600	36.5	0.61	1.9×10^{5}	2.5×10^{-3}
	6200	54.8	0.53	2.1×10^{5}	2×10^{-3}

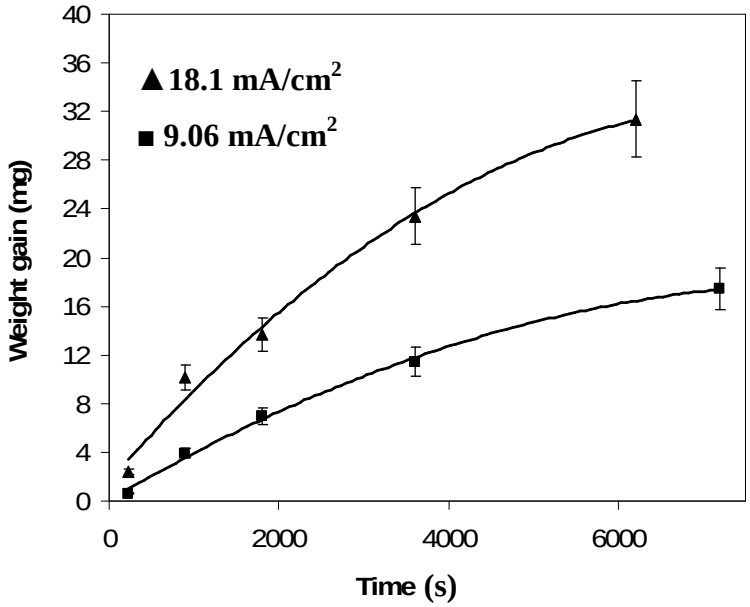

Fig. 5.49. Relation between weight gain and time for two current densities.

To check the influence of the thickness on the protectability of the coatings, the corrosion resistance of the samples was evaluated by impedance and polarization test methods. The corresponding data which are inserted in Table 5.14 and plotted in Fig. 5.50 show that the maximum corrosion resistances belong to the coatings with intermediate thicknesses namely between 3 - 13 µm. The impedance and corrosion rate of the coatings in this range of thicknesses are about 10^6 $\Omega \cdot cm^2$ and 10^{-4} mm/year, respectively. The coatings thinner than ~3µm or thicker than ~13µm deteriorate the corrosion performance of the coatings.

5.3.4 Influence of solution concentration on thickness and corrosion resistance

As well as time and current, change in the concentration of the coating solution results in different thicknesses which subsequently lead to different performances of the coating. The PEO coatings were prepared by 1, 5, 10 and 20 g/l of Na_2SiO_3 plus 10g/l KOH. It should be noted that from the beginning steps of the coating process in 20 g/l solution, the sparks were relatively bigger in size, fewer in numbers, slower in mobility and orange in colour compared to the other concentrations. The data listed in Table 5.15 show that thickness of the 1, 5, 10 and 20 g/l coatings are about 1.5, 6, 10 and 33.5 µm respectively

Table 5.15. Effect of concentration on thickness and corrosion properties of the coating prepared under common condition

Parameters / Electrolyte	Thickness (µm)	Impedance ($\Omega \cdot cm^2$)	Corrosion rate (mm/year)
1 g/l	1.5±0.3	1.8×10^5	1×10^{-3}
5 g/l	5.7±0.6	0.97×10^6	8×10^{-4}
10 g/l	8.3±1.2	1×10^6	7×10^{-4}
20 g/l	33.5±3	1×10^5	3×10^{-3}

As well as the results obtained from current and time studies, the data of Table 5.15 shows that a higher corrosion resistance of the coating occurs in the middle range of thickness. All thicknesses achieved under different conditions, namely changes in current density, time and concentration, are plotted in Fig. 5.50. The results show

that the application of high current density in a short period of coating process approximately results in equal thickness as low current density in longer period of time. So, despite the works which have been done to suggest an optimum time and current for higher performance of the PEO coating [6], the final thickness of the coating as a parameter determining the final corrosion properties of the PEO coating should be taken into consideration.

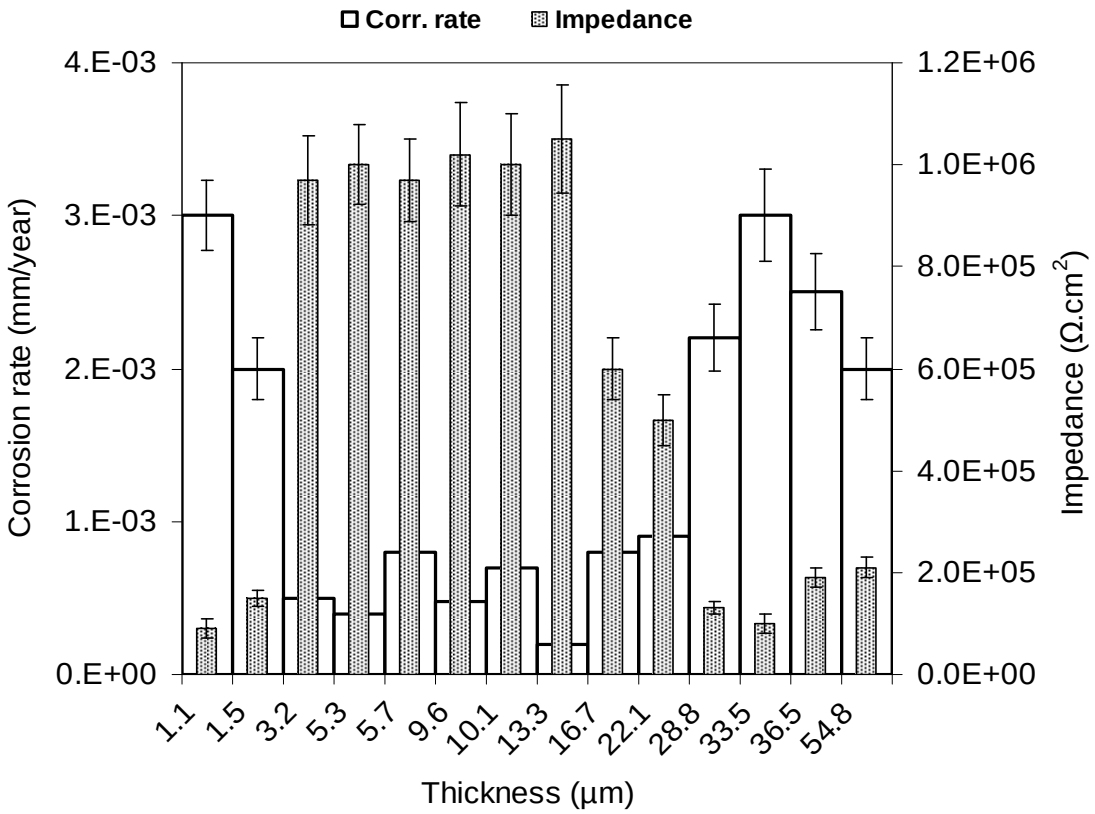

Fig. 5.50. Corrosion resistance of the PEO coatings in different thickness

6 Discussion

6.1 Formation process and structure of the PEO coating

6.1.1 Sparking phenomenon

The results showed that in the initial step of the PEO process gas bubbles is form on the surface before the sparking phenomenon comes to the effect. The formation of gas bubbles as soon as the voltage rises provides clear evidence that anodic reactions start taking place on the surface. The applied potential gives rise to a current flow through the sample which subsequently makes the anions (such as OH) move toward the anode and get oxidized based on the equation 2.2. As a result of the reactions, liberation of oxygen starts happening on the surface which can be observed in the form of gas bubbles in Fig. 5.1-a.

In the next step, the sparking phenomenon took place on the surface, which is the consequence of breakdown. To reach the breakdown in a constant current process, the voltage should be continuously increased. This could be attributed to the layer formation on the surface acting as a barrier against the passing current. As the barrier layer gradually develops, its resistance is raised and it resists the passing current more effectively. The voltage should be increased to supply enough potential for breaking down the resistance of the layer. The sparks appear on the surface and the PEO coating starts to form. An increase in the voltage is still required to maintain a constant current. However, the process reaches the point at which, unlike in the previous steps, the drop in the current rarely happens and an increase in voltage is rarely required. This happens because the potential energy is almost equal to the resistance of the PEO coating. In other word, the coating resistance and potential energy are close to together and the voltage variation reaches a steady state condition.

It was shown that progress in the PEO process resulted in bigger size, lower quantity and longer life time of the sparks. Correspondingly, it is reported that the surface of the coating gets coarser and rougher as the process proceeds and a thicker coating forms on the surface [12,58,92,95]. Essentially, thicker coatings show higher

resistance and subsequently the current requires higher energy to pass through the layer. Under this condition, the current concentrates on the weak points of the coating to find a way to pass through. The sparks become fewer in number but bigger in size. In fact, decreases in the number of sparks and increases in their size is the way by which the sparking process produces more powerful sparks to break down the layer resistance. [92].

6.1.2 Formation process on Al_8Mn_5 particles

6.1.2.1 Formation process over short duration of treatment

The results showed that, regardless of solution concentration, even after just 20 seconds of the PEO process new products in the form of a peripheral ring appear around the Al_8Mn_5 particle. Fig.5.5 showed that new phases formed around the Al_8Mn_5 particle. This clearly points to the fact that some interactions have occurred between the matrix and the particle which could be explained by considering the free corrosion potential of the Al_8Mn_5 and the matrix.

It is reported that the phases existing in the microstructure of the Mg alloys have different free corrosion potential [27,70,111]. Evaluation of the free corrosion potential of each phase has shown that there is a noticeable potential difference between different phases and α-Mg. The nobility of the phases decreases in the following order: Al-Mn phase > $Mg_{17}Al_{12}$ (β-phase) > α -Mg [27,70]. Jonsson et al. showed that the initiation of a rapid corrosion reaction during the corrosion process could be because of the micro galvanic corrosion cells between different components of the microstructure [112]. So the formation of new products around the Al_8Mn_5 particle takes place because of the high potential difference between the particle and matrix. The line scan results in Fig.5.5 pointed to a higher contribution of Si and O in the peripheral ring. This indicates that the initial step of the coating formation has begun and what has formed is not a simple corrosion product.

6.1.2.2 Formation process close to the breakdown voltage

In the next step when the process proceeds and reaches to the $V<V_{BD}$ condition, still the ring around the particle can be seen. However no reaction takes place on the central area of the particle and it looks unchanged (Figs. 5.4-b, 5.11-b). This could be because of a protective layer which has formed on the surface area of the particle and prevents the Al-Mn phase from participating in the coating reactions. It is reported that in an alkaline medium, the surface of manganese is spontaneously covered by an oxide layer [113]. Similar works which have considered the behaviour of aluminium alloys in silicate solution during the PEO process have reported that a passive layer of aluminium oxide rapidly forms on the metal surface during the first stages of the process [19,114]. Therefore the protective layer on the Al-Mn phase might be composed of each or both of the manganese oxide and/or aluminium oxide. The corresponding data in Table 5.3 also points to the relatively high percentage of oxygen on the Al_8Mn_5 surface which is in agreement with the formation of an oxide layer on the surface of the particle. The layer is so stable that the potential applied at this level is not sufficient to breakdown its resistance. Application of higher voltage in the next stage ($V>V_{BD}$ condition) showed that the resistance of the protective layer is broken down by higher potential and PEO coating starts to form on the particle surface concurrent with that on the matrix area (Figs. 5.4-c,5.11-c).

6.1.2.3 Formation process over long duration of treatment

The formation process of the PEO coating on Al_8Mn_5 particle in long duration namely 750 and 1500 seconds showed that the peripheral ring with a greater thickness is still distinguishable. Moreover, the Figs. 5.4-d,e and 5.11-d,e showed that the discontinuity between the ring and the particle which had formed during the initial steps of the formation process could keep existing even after long period of the process.

It was shown that the ring around the particle is the place from which the formation reactions start. A thicker PEO coating on the ring could be attributed to the early formation process which had started from the peripheral ring around the Al-Mn phase. This layer gets thicker as the process goes on. The tiny dendrites around the

peripheral ring in the initials steps of the process point to the growth direction of the layer (Fig. 5.4-a). It can be seen that the layer grows in the opposite direction of the particle towards the matrix. This could be because of higher dissolution rate of the matrix which provides higher concentration of the constructive elements, such as Mg^{2+}, for the formation process. So the gap between the ring and particle has no chance to be filled during the formation process even after a long period of the process. This results in different compositions of the coating layers forming on the Al_8Mn_5 and matrix. Tables 5.3 and 5.5 show that the coating on the Al_8Mn_5 particle is composed of higher Al and Mn with lower Mg, which is dissimilar to the coating formed on the matrix area. The non-homogeneous coating with gaps in between can act like a defect in the PEO coating.

6.1.3 Formation process on β phase

6.1.3.1 Formation process over short time

The formation process on the β particle was shown in Figs. 5.6 and 5.12. It was previously explained that between β-phase and α-Mg there is a potential difference [27,70,111]. However the potential difference between β-phase and α-Mg is not as high as the Al-Mn phase and α-Mg. So an intensive interaction between the β-phase and α-Mg doesn't occurs. It should be born in mind that unlike Al-Mn phases which contain very low amounts of magnesium, the β-phase is mainly composed of magnesium. The point analysis results in Table 5.2 also showed that a β-phase consists of more than 65% Mg while the Mg value of an Al-Mn phase is just lower than 1.5%. Therefore, very high potential difference and development of reaction products similar to what occurred for Al-Mn particle should not be expected.

The results showed that within the first 20 s of the PEO process, a layer forms on the surface of a β particle. The line scan studies (Fig 5.7) pointed to the higher amount of the silicon and oxygen on the β particle compared to that on the matrix area. This shows that from the initial steps of the coating process a different layer forms on the β particle surface compared to on the matrix.

Different behaviour of the phases within the initial steps of the process can be explained by considering the fact that the layer formation on specific surfaces is the consequence of reactions between metal ions and the solution anions. As the potential is applied, the metal ions are supplied by anodic dissolution process and the anions originating from the solution absorb the metal surface to form a film. These two processes, namely the "rate of anodic dissolution" and the "rate of film formation", are two opposing factors which reversely determine the final characteristics of the layer formed on the surface. Essentially the layer starts to form as the rate of the film formation gets higher than the dissolution rate of the substrate [4]. The α-Mg is mainly composed of Mg while a β phase consists of magnesium and aluminium. The reactivity of the magnesium is higher than that of aluminium and it dissolves much easier compared to the aluminium during the anodizing process [62,115]. So the formation of a layer containing higher Si and O forms on the β particle could be because of the higher rate of film formation compared to that of the α-Mg.

6.1.3.2 Formation process close to the breakdown voltage

The results showed that change of the solution concentration is the parameter influencing the formation process on the β-phase. The layer formation in the stages before breakdown ($V<V_{BD}$) showed that the layer in diluted solution (1g/l) was so thin that the particle could clearly be recognized (Fig. 5.12-Lb). The layer formed in the concentrated solution (20g/l) was so thick that it covers and hides the particle beneath (Fig. 5.12-Rb). The behaviour of the layer in medium concentration (10g/l) lay in between (Fig. 5.6-b). The layer is not too thin to be seen clearly, not too thick to be hard to recognize. This shows that the diluted solution obstructs the formation process while the concentrated solution facilitates the formation of the barrier layer. Essentially, formation of a layer during the PEO process is the consequence of the reactions between the constructive elements. These elements originate from both the electrolyte and substrate dissolution. As higher numbers of the species are beneficial for layer formation, any reason disturbing the supplement of the constructive species, deteriorates the formation process and vice versa. So the formation of a thicker layer

in the concentrated solution could be attributed to higher constructive species which are more available in higher concentration solutions.

The results of the next step namely ($V>V_{BD}$), for the diluted solution (1g/l) showed that unlike the 10 and 20g/l solutions, the barrier layer on the β-phase breaks down concurrent with that on the matrix (Fig. 5.12-Lc). Those of the 10 and 20 g/l however, indicated that the break down phenomenon on β particle and matrix area did not happen at the same time as the matrix. As Fig. 5.6 and 5.12-Rc showed the β surface has not been affected by the sparking phenomenon, even in the $V>V_{BD}$ condition. This indicates that the resistance of the barrier layer on the β surface is higher than that on the matrix areas. The potential which can break down the resistance of the barrier layer on the matrix is still insufficient for that on the β phase.

Essentially, the formation of a more stable barrier layer on β-phase could be attributed to higher aluminium content in the β-phase compared to that in the α-Mg. The aluminium contributes in the formation process of the layer which forms on the particle and produces a more stable barrier layer [61]. The data in Tables 5.4 and 5.5 indicated that more aluminium participates in the composition of the coating on the β phase compared to that on the matrix. This layer requires higher potential for breakdown and it happens when the voltage reaches higher values. The results obtained are in agreement with the studies of Khaselev et al. who stated that the breakdown voltage of the β-phase is higher than the α-Mg because the layer has higher aluminium and is more stable than that of the matrix area [72].

In addition to the composition of the layer, the rate of layer formation is another parameter that should be taken into consideration. The shortage of the constructive species in the diluted solution obstructs the rate of layer formation and a layer with lower stability forms. In more concentrated solutions with enough constructive species, the formation process get facilitated and the barrier layer on β phase shows higher rate of formation and more stability compared to that on the matrix.

6.1.3.3 Formation process over long duration

As the process proceeds and voltage reaches to higher values, enough energy for the breakdown of the barrier layer is supplied. Figs. 5.6-d, which is related to the coating after 750 seconds, give clear evidence on the formation of the pores and discharge tunnels on the β particle which are distinguishably bigger compared to the adjacent matrix. The bigger pores on the coating can be related to the breakdown phenomenon which happens on the β-phase at higher voltages compared to the matrix [72,73]. The need for higher breakdown voltage originates from the higher stability of the barrier layer compared to that of the matrix phase. Breakdown at higher voltages gives rise to bigger sparks carrying more energy and consequently results in bigger holes on the surface [48,71].

The results showed that long periods of treatment (1500 s) in diluted solutions (1g/l) resulted in a PEO coating containing bigger holes on β-phase than on the α-Mg (Fig. 5.12-Le). In solutions with higher concentration (10 and 20g/l), however, the long periods of treatment led to the formation of a PEO layer which has less thickness compared to the matrix area (Fig. 5.6-e and 5.12-Re)

The formation of the coating with bigger holes in diluted solution (1g/l) could be attributed to the higher Al content of the PEO coating on the β-phase. This produces a more stable layer which reduces the dissolution rate of the particle and lowers the reactivity of the β-phase compared to the α-Mg.[116] Therefore the concentration of the substrate ions (i.e. Mg^{2+}) locally reduces on the β-phase. This effect is intensified in diluted solutions by the shortage of constructive elements, namely silicate ions. Hence, the local shortage of the constructive ions (which are required for the formation process) together with stronger sparks resulted in the bigger holes on the β-phase [48,71].

The less thickness of the coating on β-phase in solutions of higher concentrations (10 and 20 g/l) can be explained in the following way. In solutions with higher silicate concentrations, the shortage of the solution species (i.e. silicate ions) is not what controls the formation process anymore. Instead, the formation of a more stable

barrier layer, which needs higher breakdown energy and postpones the sparking phenomenon, plays the dominant role. It was shown that a higher concentration solution facilitates development of the barrier layer and subsequently a thicker barrier layer forms on the β-phase. This layer requires higher potential for breakdown, which requires longer period of time compared to that of the α-Mg [92,95]. So the beginning of the formation process on the β-phase occurs with a delay compared to that of the α-Mg. This results in the lower thickness of the coating which becomes more distinguishable as the process proceeds [48,71].

Both of these effects, namely insufficient concentration of the constructive elements in low concentrations and postponed breakdown in high concentrations, result in the formation of a coating on the β-phase which displays different characteristics and introduce non-uniformity to the PEO coating formed on the surface.

6.1.4 Formation process on α-Mg Matrix

6.1.4.1 Formation process over short time

The results showed that the formation process on the α-matrix initially follows a net-like deposition behaviour (Fig 5.8-a). The results of the EDX mapping examination showed a higher concentration of oxygen and silicon in the composition of the nets (Fig.5.9). This gives a sign for the beginning of the coating formation on the matrix in a very short period of the process i.e. in 20s.

It is reported that the sub grains with a size of less than 10µm forms inside the original grains. This kind of arrangement specially forms in the microstructure of AM50 during the solidification process of the alloy [14]. So the nets are the traces of the sub grains which start forming by nucleation and the growth of the layer which shape a net-like deposition.

The formation of some tiny dendrites in a vertical direction to the nets shows the development mechanism of the layer on the surface. The layer spreads on the surface by the lateral growth of the nets. This kind of formation mechanism requires diffusion and the joining of the constructive elements to the growing tips of the

dendrites. The relation between time and thickness of the coating (Fig. 5.48) also showed that the weight gain and thickening of the coating depends on the time of the process. So the growth mechanism of the coating is a diffusion control process [86,117]. The development of the layer and surface coverage gets completed as the growing nets reach together and form the barrier layer.

The variation of atomic concentration within the thickness of the layer in Fig. 5.10 revealed that the outer free surface of the layer mainly consists of O and Si. As the etching process approaches the substrate the magnesium also participates in the structure of the layer. The descending trend of the silicon from the outer layer to the substrate, starting from ~25% to almost zero, leads to the conclusion that Si certainly participates in the formation process from the initial steps of the process and it originates mainly from the electrolyte. The EDAX data of the untreated sample in Table 5.2 also showed that α-matrix cannot be considered as a source for silicon. The importance of this conclusion can be realized when we consider some contradictions in the works which have studied the layer formation process in silicon solutions. Some of them claim that Si is involved in the coating process from the initial steps of the coating process [13,84] and others maintain that the primary layers are composed only of MgO [99,118].

The observations showed that diluted solution (1g/l) retards the formation process of the layer (Fig. 5.14-La) and that the formation process is faster in concentrated solution (Fig. 5.14-Ra). This shows that diluted solution obstructs the formation process while the concentrated solution facilitates the formation of the barrier layer. It was explained that the formation of a layer during the PEO process is a consequence of the reactions between the solution species and Mg^{2+} ions. As enough Mg^{2+} ions exist over the α-Mg, the concentration of the Mg^{2+} ions is not the parameter which controls the formation process; instead the solution species are the parameters controlling the rate of formation process. It is why the layer forms very quickly after 20 seconds in 20 g/l solution but in the 10 g/l solution only nets are under development and in the 1g/l solution no clear sign of layer formation can be seen.

6.1.4.2 Formation process close to breakdown

The results regarding the formation process very near to the breakdown (V<VBD) showed that different concentrations influence the development of the barrier layer. In diluted solution the surface of the matrix still needs time to be completed because of the shortage of the silicate ions (5.14-Lb).
In the case of the 10 g/l solution, the results showed the barrier layer was not only completed but some tiny pores could also be seen on some parts of the surface (Fig. 5.6-b). When a more highly concentrated solution (20 g/l) was used, the trace of the tiny pores could almost be seen on the whole of the surface (Fig. 5.14-Rb).

It was shown that the formation of the barrier layer is a gradual process which starts with the application of the voltage and is completed prior to the breakdown phenomenon. The breakdown phenomenon happens when the barrier layer has been completed and the potential reaches enough energy to overcome the resistance of the layer. So, the holes on the surface, as an indicator of the breakdown, show that unlike the 1g/l sample, the barrier layer is complete in the 10 and 20 g/l solutions.

In the 10g/l solution, the holes are seen only on some parts of the surface. This shows that the completion of the barrier layer has just finished. In the 20g/l solution, a higher proportion of the surface affected by the holes shows that the barrier layer was completed earlier and it was under the effect of the sparking phenomenon for a longer time compared to that of the 10g/l solution. It confirms that the higher concentration of the solution facilitates the layer formation during the PEO process.

The appearance of the tiny holes on the surface, even though the process is in the $V<V_{BD}$ condition, could be related to the occurrence of the micro sparks which are too small and tiny to be seen with bare eyes. This shows that the surface is affected by the sparks even before they get visualized.

In voltages beyond break down voltage ($V>V_{BD}$), the formation of smaller holes in diluted solution (1g/l) could be related to smaller sparks occurring during the process (Fig. 5.14-Lc). The barrier layer forming in the diluted solution is thinner and

subsequently requires less energy to be broken down. So some fine and tiny discharges happen on the surface. Under the same conditions in the middle concentration (10g/l), the holes have a non-uniform distribution and the pores are not in the circular shape (Fig. 5.8-c). This can be understood because the coating layer is still in the initial steps of the formation process. It is thin and the sparking temperature is easily able to disturb and melt the partition wall between the holes. In other words, the partition wall between two or three adjacent discharge tunnel is so thin that it can not resist against the discharge temperature. They merge and produce elongated holes.

In the case of the concentrated solution (20g/l), a finer surface morphology was obtained compared to the 10g/l solution (Figs. 5.8-c and 5.14-Lc). Based on the cross section images (Fig. 5.16), the coating prepared in 10g/l solution has a higher growth rate and results in thicker coating compared to that in the 20 g/l solutions. The thicker layer of the coating requires more powerful sparks to be broken down. So the size of the sparks and consequently the size of the discharge tunnels get bigger in 10 g/l coating compared to in the 20 g/l.

6.1.4.3 Formation process over long time

Fig. 5.14-Le shows a non-typical behaviour of the coating in which the discharge tunnels have joined together and produce an elongated structure of the pores. The reason for this behaviour can be understood by considering the initial steps of the formation process. It was explained that in initial steps, the formation process on the matrix area follows a net-like deposition (Fig. 5.9). The coating layer on the nets (i.e. the primary location on which the layer forms) becomes relatively thicker compared to the neighbours. The thicker layer of the coating not only requires stronger discharges for breakdown [92,95], but also lowers the dissolution rate of the substrate underneath [116]. The latter effect results in the local shortage of the constructive ions over the nets. The shortage of the ions is intensified in a diluted solution. As the process reaches the breakdown phenomenon, the sparks destroy the partition wall between two adjacent discharge tunnels. However the walls cannot

form again because of shortage of the constructive elements such as Mg ions. [48,71].

In 10 and 20 g/l solution, the elongated holes change to the more circular ones which grow bigger as the process proceeds (Fig. 5.8-d,e and 5.14R-d,e). The formation of more circular holes on the surface could be attributed to the growth of the coating layer which produces a more stable partition wall between the discharge tunnels. Furthermore, the increase of the hole size over the longer process duration could be related to the change of the spark size during the process. Within the shorter treatment time, the coating is still so thin that its resistance can be broken down by small sparks carrying low amounts of energy. The longer duration of treatment produces a thicker coating which requires higher amount of energy for breakdown. Increase of the voltage by time (Fig. 4.1) showed that the progress of the process requires higher energy. Therefore spark sizes get bigger and produce bigger holes.

6.1.5. Contribution of oxygen to PEO coating

The results indicated that from the composition point of view, the PEO coating is a non-homogeneous coating the chemical composition of which varies from one point to another point. Fig. 5.15 shows that independent of process duration or solution concentration, more oxygen was detected on the Al_8Mn_5 particles compared to on the β-phase or matrix regions. A higher percentage of oxygen on Al_8Mn_5 particles could be attributed to the type of the oxide layer forming on the surface. The anodic behaviour of manganese in alkaline mediums has been studied and it is reported that an oxide layer composed of MnO_2 covers the manganese surface [113]. It is also reported that a passive layer of Al_2O_3 rapidly forms on the aluminium surface during the first stages of the PEO process [19,114]. Therefore the protective layer on the Al-Mn phase might be composed of each or both of the manganese oxide and/or aluminium oxide. Thus corresponding to the constructive elements, the possible oxide layer on the Al_8Mn_5, β-phase and α-Mg could mainly be composed of Al_2O_3 + MnO_2, Al_2O_3 + MgO and MgO, respectively. However, it should be born in mind that an Al_8Mn_5 particle contains more aluminium compared to the β-phase. The β-phase has higher Mg compared to Al and the Al_8Mn_5 is composed of higher Al

compared to Mn. Thus formation of aluminium oxide on the Al_8Mn_5 surface is more possible than on a β-phase. So the detection of higher oxygen on Al_8Mn_5 particle could be related to the higher amount of oxygen in the stoicheiometry of the Al_2O_3 + MnO_2 structure compared to in that of Al_2O_3 + MgO.

The results showed that the Al_8Mn_5 curves experience a significant shift at the breakdown point. The involvement of more oxygen at the breakdown point confirms that the formation mechanism of the coating layer has changed. This could be expected because this is the point at which the discharges come into effect and give rise to the plasma environment which has higher energy and accelerates the rate of reactions. After breakdown, the high ramp of the curves slows down and it reaches an almost constant condition.

On the other hand, as β-phase and α-Mg are mainly made of magnesium, they show comparable behaviour especially before breakdown voltage. After breakdown voltage the oxygen content on the β-phase and matrix showed a slight and steady increase. However, it can be seen that in the 10g/l solution, the matrix contains higher oxygen compared to the β-phase. It was shown that the 10g/l solution produces a thicker coating compared to the 1 and 20 g/l solutions (Fig. 5.16). The XPS study also showed that the distribution of MgO/SiO_2 and Mg_2SiO_4 phases in the 10g/l coating is more uniform compared to that in the 1 and 20g/l coatings (Fig. 5.20). Detection of higher oxygen in the structure of the coating prepared in the 10 g/l solution could be attributed to the greater thickness of the coating in which MgO and Mg_2SiO_4 phases have formed more uniformly compared to in the 1 and 20 g/l solutions.

6.1.6 Structure of the coatings

6.1.6.1 Rate of layer formation

Fig. 5.16 showed that the coating generated in the middle concentration (10g/l) was thicker than those prepared in 1 or 20 g/l solutions. Both the diluted and concentrated solutions deteriorated the rate of the coating formation and resulted in the lower

thickness of the coating. This shows that the rate of layer formation in a middle concentration solution is higher than in diluted or concentrated solutions.

The adverse influence of the diluted solution is understandable and it seems logical. Shortage of the constructive elements which participate in the coating structure reduces the rate of the formation process. A thinner barrier layer forms on the surface which offers lower resistance. Breakdown of this layer requires lower energy and subsequently finer discharges with lower energy takes place on the surface. Lower energy of the sparks reduces the formation rate of the PEO coating.

In the case of the concentrated solution a lower thickness is also obtained. The results showed that the barrier layer forms more quickly in high concentrations of solution. Early formation of the barrier layer reduces the dissolution rate of the substrate which leads to the shortage of the Mg^{2+} ions. The latter effect reduces the rate of layer formation and gives raise to the lower thickness of the coating.

6.1.6.2 Phase evaluation

The XRD patterns was showing that the intensity of MgO main peak with 2θ=43° and Mg_2SiO_4 with 2θ=40° changes due to different concentration of the solution (Fig. 5.17). It is also reported that increase in concentration of sodium silicate leads to gradual diminish of the MgO peaks [119]. To determine the fraction of the phases, the intensities of the main peak of MgO and Mg_2SiO_4 were calculated. The $I_{Mg_2SiO_4} / I_{MgO}$ ratios of the 1, 10, 20 g/l coatings are about 0.34, 0.87 and 1.17, respectively. The ratios vary in such a way that reduction of concentration results in higher intensity of MgO but lower intensity of Mg_2SiO_4. Higher ratio of the 20g/l solution can be related to the higher concentration of the silicate ions. In concentrated solution more silicate species involve in the plasma reactions than those in the diluted solution. It indicates that concentration of the solution has a direct effect on fraction of the phases forming in the PEO process.

6.1.6.3 Phase distribution

XPS analysis of the layer formed in 20sec (Figs. 5.19) showed that even in very short durations and in voltages far below the breakdown point, a very thin layer forms on the surface. The appearance of the 155 ev (Si 2s) and 533eV (O 1s) spectra in the most outer layer shows that the layer is composed of SiO_2. In the middle stages, the peaks with 51.5eV (Mg 2p) and 532ev (O 1s) show that the layer is composed of MgO. This layer forms directly over the Mg substrate. In the final stages, the spectra of 50eV (Mg 2p) appears without detecting the spectra of O1s or Si 2S. So the spectra could be related to Mg [121].

Fig. 5.20 showed that independent of solution concentration, the peaks with binding energies of 48, 50, 51.5 eV (Mg 2p), 528.5, 532.5 eV (O 1s) and 150.5 eV, 155eV (Si 2s) appeared in the structure of the coatings prepared over long periods (1500s). The same peaks, except 48ev (Mg 2p), were also detected in structure of the layer prepared in a short duration of the process (20 s). The detected peaks could be related to different phases distributed in the coating structure.

As the results showed, the peaks with binding energy of 48 eV (Mg 2p) followed a common trend in solutions with different concentrations. It had higher intensity in the most outer layer of the coating (i.e. the initial steps of the etching process) and was reduced by approaching the middle thickness of the coatings. Similar trends also happened in the intensity of the peaks with a binding energy of 528.5 eV (O 1s) and 150.5 eV (Si 2s). This suggests that the latter peaks originated from Mg_2SiO_4 phase which are mainly distributed in the outer layers of the coatings. Formation of Mg_2SiO_4 in the outer layers of the PEO coating is in agreement with the literature. It is reported that the Mg_2SiO_4 starts to form when bigger sparks with higher energy appear on the surface, because Mg_2SiO_4 is a stable phase and needs more energy to form [95,118]. Behaviour of the sparks during the PEO process also indicated that the bigger sparks appear on the surface when the coating gets thicker and offers higher resistance (fig 5.1). So the latter spectra can be related to the Mg_2SiO_4 phase which is mainly distributed in the outer layers of the coatings.

As the etching process proceeded, the intensity of the 48 eV peaks got lower but another peaks with a binding energy of 51.5 eV (Mg 2p) emerged. At the same time, new peaks with respective binding energies of 532.5 eV(O 1s) and 155 eV (Si 2s) also emerged in the spectra of the oxygen and silicon patterns. The latter peaks mainly appeared in the middle thickness of the coatings and continue to the substrate. This indicates, the formation of new phases very close to the substrate/coating interface. It is reported that the formation reactions on the magnesium substrate in alkaline solutions can start at low voltages. [84]. These reactions during the initial steps of the coating process can lead to the formation of MgO and/or SiO_2 [24,120]. The values indexed in the data base also indicate that the latter peaks can be representative of the MgO/SiO_2 phases [121]. Examination of the passive layer formed over a short time (20 s) showed that the latter spectra namely also appeared in the structure of the layer (Fig.5.19). This indicates that the passive layer is composed of MgO/SiO_2 phases and it remains in the structure of the coating. Formation of MgO, SiO_2 and Mg_2SiO_4 could be considered by following reactions.

$Mg \rightarrow Mg^{2+} + 2e^-$ (anodic dissolution)	[48,13]
$Mg^{2+}(aq) + 2OH^-(aq) \rightarrow Mg(OH)_2$ (s) subsequently $\rightarrow MgO + H_2O$	[71]
$2Mg^{2+} + 2SiO_3^{2-} \rightarrow Mg_2SiO_4 + SiO_2$	[48,13]
$2Mg^{2+} + SiO_3^{2-} + 2OH^- \rightarrow Mg_2SiO_4 + H_2O$	[48,13]
$SiO_3^{2-} + 2e \rightarrow SiO_2 + 1/2O_2$	[122]
$Mg + SiO_3^{2-} + 2H_2O \rightarrow MgO.SiO_2 + 2OH^- + H_2$	[122]
$SiO_3^{2-} + 2H^+ + (n\text{-}1)H_2O \rightarrow SiO_2 + n\ H_2O$	[123]

Figs. 5.19 and 5.20 showed that, apart from solution concentration or process duration, the peaks with 50 eV (Mg 2p) came up when the etching process reached the substrate/coating interface. However, the absence of any corresponding peak in O1s and Si 2s patterns indicated that the emerging peak is representative of pure Mg. [121,124,125].

The emerging sequence of the XPS spectra in Fig. 5.20 showed that MgO and/or SiO_2 mostly form in the initial steps of the coating process. The formation of the

Mg_2SiO_4 however, is a subsequent process which starts in the next stage. So the phases are distributed non-uniformly through the coating thickness from outer to inner layers. In the case of 1 and 20g/l samples, the spectra showed sharp changes. This suggests that the 1 and 20g/l coatings have a more non-homogeneous structure compared to the 10g/l solution. Like in the 1 and 20 g/l solutions, the first layer over the substrate in the 10g/l solution is mainly composed of just MgO/SiO_2. However unlike in the 1 and 20g/l solutions, the formation of MgO/SiO_2 phase in the 10g/l solution continues parallel with Mg_2SiO_4 to the final steps of the coating and it shows a more uniform structure compared to that in the 1 and 20g/l solutions.

6.1.6.4 Corrosion resistance of the coatings

Fig 5.21 showed that the coatings produced in the diluted (1 g/l) and concentrated (20g/l) solutions, have lower ability to resist against corrosion compared to that of the intermediate (10g/l) solution. In order to explain different corrosion resistance of the coatings, the parameters determining the performance of the coating were taken into account. The surface morphology [8-10], thickness [6,7] and phases [11-13], are the parameters which effectively influence the performance of the PEO coating and determine the ability of the coatings to resist against the corrosion. The following lines explain how these parameters form during the PEO process in different concentrations.

The *surface morphology* of the coatings can be seen in the Figs. 5.14-Le, 5.14-Re, 5.8-e. The first picture shows a non-typical behaviour of the coating in which the discharge tunnels have joined together and produced an elongated structure of the pores. The pores by it self are known as an unfavourable parameter in the structure of the PEO coatings. The pores are undesirable because they provide easy routs for the corrosive electrolyte towards the substrate [20,98]. The negative effect of the pores intensifies when they join together and form an elongated structure. In this case, the corrosive medium reaches more easily to the substrate and the coating is not able to resist effectively against the corrosion. This kind of elongated structure of the pores, however, has not formed in the coatings prepared in medium (Fig. 5.8-e) and concentrated (Fig. 5.14-Re) solutions.

Another parameter is the *thickness* of the coating. An optimum thickness is a parameter which can improve the performance of the coating against corrosion. In comparison of two different thicknesses, the corrosive medium reaches faster to the substrate in a thinner layer of coating .Based on the results shown in the Figs. 5.16, the thickness of the coating prepared in 1g/l solution has the lowest and the 10 g/l solution has the greatest value. Thus, more corrosion resistance can be expected from the coatings prepared in 10g/l solution.

The next parameter is *phases* existing in the coating. The phase evaluation of the coatings in Fig. 5.17 showed that the coatings are composed of MgO and Mg_2SiO_4. However, the XPS studies (Fig. 5.20) showed that the phases distribute differently in the structure of the coatings. In the case of 1 and 20g/l samples, the XPS spectra showed sharp changes which suggest a non-uniform structure of the coatings compared to the 10g/l sample. The more uniform distribution of the phases and the chemical composition of the phases through PEO coating are among the parameters which influence the corrosion resistance of the final coating [11,12].

Thus, the lower corrosion resistance of the coating prepared in 1g/l solution compared to the 10g/l solution can be related to the less thickness, formation of an elongated structure of the pores and non uniform distribution of the phases. In case of 20 g/l coating, however, the less thickness of the coating and non uniform distribution of the phases are the parameters which result in the poorer corrosion resistance of the coating compared to the 10g/l coating.

6.2 Influence of the electrolyte composition on stability of the passive layer and corrosion resistance of the PEO coating

6.2.1 Passive behaviour

6.2.1.1 Salt solutions

Study of the passive layer by different salt solutions showed that the solution composition directly influences the stability of the passive layer. The passive layer produced by sodium silicate, sodium phosphate and potassium phosphate showed higher impedance value and lower current density in their own group (Figs. 5.22 and 5.23). These imply that the passive layer formed on these solutions is comparatively more stable. Low impedance value and breakdown in the polarization curve of the sodium aluminate solution also showed that its passive layer was not able to offer stable behaviour.

Fukuda et al studied the anodic behaviour of Mg alloy under low potential in a solution containing Na_2SiO_3. According to the results, silicon participates in the formation process and silicate phases form in the structure of the anodic film [13]. The contribution of the solution species in the passive layer is also reported by Wang et al who applied a passive layer on magnesium in alkali-silicate solution. The XRD analysis of the layer showed that magnesium silicate phases form in the layer which can only be due to the deposition of particles from the treatment solution [1]. The phosphorous species also contributes to the formation process during the anodizing process. The characteristics of the anodic film on magnesium alloy in phosphate solution showed the layer is mainly contained of magnesium, oxygen and phosphorus species [126]. The formation of a thin passive film on magnesium substrate is reported during the anodizing process in aluminium containing solution. It is shown that aluminium can penetrate into the film from the electrolyte because the elements in crystalline film are mainly magnesium, aluminium, and oxygen. This indicates that $MgAl_2O_4$ has formed in the layer. [72,127]. So, the composition of the passive layers is the parameter which determines the final stability of the layers in different solutions. In solutions with similar elements (e.g. sodium phosphate or potassium phosphate groups), however, the higher values of pH and conductivity are

two parameters resulting in a more stable passive layer. For example; the pH and conductivity of Na_3PO_4 solution are 12.12, 11.77 mS/cm, respectively (Table 5.6). These values are higher than those of the $Na_5P_3O_{10}$ and $Na_2H_2P_2O_7$ solutions i.e. 9.42, 6.40 mS/cm and 4.33, 5.53 mS/cm, respectively. Consequently a more stable passive layer forms in the Na_3PO_4 solution compared to the rest solutions of this group. The data of the impedance test and passive current which are indicator of the stability of the passive layer are listed in Fig 5.22 and table5.7, respectively. It is seen that the corresponding data of Na_3PO_4 are about 5.2×10^3 $\Omega\cdot cm^2$ and 4×10^{-3} mA/cm^2, respectively. However those of $Na_5P_3O_{10}$ are just about 1.4×10^3 $\Omega\cdot cm^2$, 1.8 mA/cm^2 and those of $Na_2H_2P_2O_7$ are about 0.6×10^3 $\Omega\cdot cm^2$ and 6.7 mA/cm^2, respectively. Another example is K_3PO_4 solution which has higher value of pH and conductivity compared to the $K_4P_2O_7$ solution. As a result, the passive layer in the former solution is more stable than the latter. The same trend is followed by Na_2SiO_3 and K_2SiO_3 solutions where the stability of the passive layer in the former solution is higher than the latter because of higher value of pH and conductivity.

6.2.1.2 Hydroxide solutions

Thermodynamics and the E-pH (Pourbaix) diagram predict that $Mg(OH)_2$ film forms on the surface in solutions with a pH of more than 10.5. This is the pH value required for the $Mg(OH)_2$ to precipitate on the magnesium surface. The passivation study of the hydroxide solutions presented in Fig. 5.36 showed that a passive layer forms on the substrate in $Al(OH)_3$ and $Mg(OH)_2$ solutions while the pH value of these solutions is about 8.7 and 10.5, respectively.

The electrochemical behaviour of magnesium alloy is significantly influenced by the pH of the solution. The passive or active behaviour of the magnesium substrate is essentially governed by the characteristics of the film forming on the surface [115]. At low pH values, even though the surface film is not thermodynamically stable, the dissolution kinetics may be slow and a surface film may be formed, provided the dissolution kinetics is slower than the formation kinetics [63]. This could explain essentially how the passive layer in solutions with pH equal or lower than 10.5 forms. Unstable formation behaviour of the passive layer can justify the variations

occurring in the $Mg(OH)_2$ solution in different potentials. The variations could be related to the changes in the stability of the passive layer. The passive layer forming on the substrate exhibits stable conditions between OCP and -700 mV. However the layer breaks down when more positive potentials are applied. Application of potentials over -700 mV lead to the reformation of a passive layer but at a lower level of stability.

The results showed that a more stable passive layer forms in KOH compared to NaOH solution. This could be related to the higher activity of the KOH solution compared to that of the NaOH solution. The measured data listed in the literature show that KOH solution has a higher activity coefficient than the NaOH solution [107]. More active species in the KOH solution increase the rate of reactions and facilitate the formation process of the passive layer.

6.2.2 Influence of the electrolyte composition on PEO process

6.2.2.1 Elements in the PEO process

Figs 5.25 and 5.26 showed the result of the OES examinations. Based on the results it appears that most of the electrolyte species get excited and involved in the plasma environment of the discharges. However, existence of the magnesium peaks shows that the substrate also takes part in the discharge phenomenon which could originate from the dissolution of the substrate. Presence of the K and Na peaks in the patterns showed that the cations also get excited in the plasma environment. This is interesting because participation of the cations in an anodizing process is not essentially expected. Based on the results it can be concluded that the discharges happening during the PEO process provide the requisite energy for the melting of the magnesium surface and activate the reactions and not necessarily all the elements get involved in the coating process [98].

The results show that the peak with wavelength of 589.3 nm appears in all the patterns. Based on the consideration of the data base this is a common wavelength for both of the Na and H_2O. However the intensity of the peak is lower when no Na is introduced to the solution. The latter results show that H_2O is another component

participating in the sparking process in addition to the chemical elements originated from the solutions or substrate. Fig 5.25 shows that even without the addition of any hydroxide, an OH peak of 309.7 nm appears in the spectra patterns. The appearance of the peak which just could be raised from the H_2O is an additional support showing that H_2O is involved in the PEO process.

As expected, the potassium peaks are absent in the patterns of the Na_3PO_4, Na_2SiO_3 and $NaAlO_2$ solutions. On the other hand, in K_3PO_4 and K_2SiO_3 solutions potassium peaks can still be detected, but at a lower intensity. Comparison of the results with the results of the solutions plus KOH shows that the elements originated from the salt and hydroxide part, and both participate in the coating process. The results revealed that the role of hydroxide in the coating process is not limited only to the adjustment of the pH and conductivity of the solution. Instead, the elements introduced to the solution directly participate in the plasma environment.

6.2.2.2 Thickness

The thickness of the coatings listed in Table 5.8 shows that under the application of similar current density and duration, the silicate coatings result in a greater thickness than the phosphate or aluminate coatings. The average growth rate of the silicates (2 coatings), phosphates (five coatings) and aluminate (1 coatings) is about 1.5, 0.8 and 0.2 µm/min, respectively. The passive layer formed in the silicate solution also showed higher stability compared to the phosphate and aluminate solutions. This provides evidence that the silicate species facilitate and increase the rate of the formation reactions compared to the phosphate or aluminate species. It is also reported that the anions contribute in the formation process and influence the characteristics of the PEO coating [20]. This is in agreement with the studies pointing to the beneficial influence of the silicate anions on the growth rate of the PEO coating compared to that of phosphate or aluminate anions. [77,82,92].

The effect of conductivity on the rate of film formation process should also be considered. Guo et al. reported that the rate of film formation increased when anions with higher conductivity were introduced to the coating solution [83]. This is in

agreement with the solution conductivities measured in this study. Table 5.8 show that in each group, the thickness of the PEO coating is directly influenced by the conductivity of the solutions.

6.2.2.3 Surface morphology

Figs 5.27, 5.29, 5.31 and 5.33 showed that depending on the type of the solutions, different kind of morphologies forms on the surface of a PEO coating. It was seen that the surface morphologies contained pores and/or cracks. The main reason for getting various surface morphologies could be attributed to the dissimilar characteristics of the sparks, such as size and number of sparks occurring during the PEO process. Continuous and intense sparking discharges with a small life time (limited to about 10 μs), together with the gas formation on the surface, produce many micro channels and a porous morphology. Based on the literature, a porous morphology may form as a consequence of oxygen entrapment in molten material in the vicinity of localized electrical discharges during PEO coating formation [91,105]. The results showed that the pores in the surface morphology of different coatings are different in size and quantity. This is in agreement with the works reporting that different numbers of sparks during the PEO process in different solutions (e.g. phosphate and silicate) result in a higher number of pores after the cooling of the discharge channels [12].

It was reported that the surface of the coating gets coarser and rougher as the process proceeds and the oxide layer gets thicker [12,58,95]. The same trend was also observed for the silicate coatings which have a greater thickness compared to the phosphate or aluminate coatings. Essentially in a thicker layer of the coating, higher energy is required for the current to pass through the coating. Under this condition, the current localizes at weak points of the layer to find its way through the coating. This is the reason why the number of sparks decreases but their size increases in thicker layers. In fact, an increase in the diameter of the discharge channels is the way in which the process compensates for the reduction in number of the channels [92]. Hence, the size and the number of sparks are affected by the thickness of the layer.

The cracks observed in the structure of the coatings could be the result of sparks at temperatures higher than a thousand degrees in the vicinity of the cool electrolyte during the PEO process [19,69,108]. These conditions lead to rapid solidification of molten oxides which are formed in the plasma environment. The nature of this process imposes high thermal stresses which provide enough driving force for cracks to be initiated on the coating surface [83].

6.2.2.4 Chemical phases

Another important parameter influencing the corrosion resistance of the coating is the chemical composition of the PEO coating [10,11,12,]. The XRD results showed that the anions are involved in the formation process and produce different phases in the coatings. Apart from MgO which is commonly detected in the coatings, specific phases form during the coating process depending on the electrolyte type. The phases which could form in silicate, phosphate and aluminate solutions are Mg_2SiO_4, $Mg_3(PO_4)_2$ and $MgAl_2O_4$ respectively. The formation of the phases could be based on the following reactions:

$$Mg^{2+} + 2OH^- \rightarrow MgO + H_2O \quad [57]$$

$$2Mg^{2+} + SiO_3^{2-} + 2OH^- \rightarrow Mg_2SiO_4 + H_2O \quad [48]$$

$$3Mg^{2+} + 2PO_4^{3-} \rightarrow Mg_3(PO_4)_2 \quad [71]$$

$$Mg^{2+} + 2AlO_2^- \rightarrow MgAl_2O_4 \quad [6]$$

Liang et al. compared the corrosion resistance of two coatings. The first was mainly composed of MgO and Mg_2SiO_4, and the second one of MgO. Although the results showed that both coatings provided effective corrosion protection, the coating containing Mg_2SiO_4 showed a better corrosion resistance [12]. A comparison of the corrosion resistance of the coatings which are composed of MgO and $MgAl_2O_4$ also showed that a higher amount of $MgAl_2O_4$ increased the corrosion resistance of the PEO coating [69]. Other studies have additionally reported the beneficial effect of stable phases such as Mg_2SiO_4 [13,10] $Mg_3(PO_4)_2$ [20] and $MgAl_2O_4$ [6,9] to improve the corrosion resistance of PEO coatings. Therefore, one of the major roles

of the solution species seems to be an influence on the chemical composition of the coatings leading to different corrosion performance of the coatings.

In the case of sodium aluminate solution, however, low thickness and uneven morphology of the coating provide such adverse conditions that a very weak coating is obtained. The unfavourable effect of thickness and morphology puts a non-beneficial influence on the performance of the coating that even formation of the $MgAl_2O_4$ cannot improve corrosion resistance of the coating.
The formation of different chemical phases in the potassium phosphate coatings compared to the sodium phosphate coatings showed that changes of the cations also influence the chemical phases. This is interesting because in an anodizing process, it is not essentially expected that the cations play a determining role in the process. However, the Figs. 5.30-d and 5.32-d showed that when solutions contain both of Na^+ and K^+ cations the MgO and $Mg_3(PO_4)_2$ phases form in the coating. The existence of only K^+ cations in the solution, however, resulted in the formation of the MgO. The result of the optical emission spectroscopy study also confirms that the cations also participate in the plasma environment.

The phase determination of the hydroxide coatings showed that MgO forms in the structure of the coatings produced by different hydroxides (Fig 5.35). The Mg_2SiO_4 phase is an additional phase which is formed only in KOH solution. This could be attributed to the low conductivity of the aluminium hydroxide and magnesium hydroxide electrolytes and the higher thickness of the KOH coating compared to the rest of the hydroxides solutions. It is stated that the distribution of the elements and chemical composition of the coating differs within the cross section of the coating [95,118]. Some literature has shown that the composition of the coating is affected by the intensity of the sparks [2,48,118]. The coating produced by intensive sparks is mainly enriched of the anions originating from the solution. In contrast, a coating formed by weak and tiny sparks is mainly composed of the base metal. Wang et al believes that the sparks accelerate the migration process of the SiO_3^{2-} ions to the anode substrate in a silicate solution [118]. Owing to the higher temperature of the intensive spark discharges, the transfer process as well as the combination of SiO_3^{2-}

ions with the magnesium substrate is accelerated which results in the enrichment of Si in the intensive spark regions. It means that Mg_2SiO_4 forms mostly after the coating layer reaches a great enough thickness, giving rise to more powerful sparks. This could be attributed to the temperature of the sparks in the final stage of the process when the sparks are bigger and carry more energy [118]. Therefore, after reaching to a critical thickness, the more stable phases like Mg_2SiO_4 form in the coating in addition to the MgO.

6.2.2.5 Corrosion resistance

Different characteristics of the PEO coating namely thickness, morphology and chemical phases, have been discussed above. It is reported that thickness [6,7], morphology [8,41] and chemical phases [10,11,12] are the effective parameters influencing the final corrosion resistance of the PEO coatings. The results indicated that the coatings in each group showed different corrosion properties although they have comparable thickness, phases and surface morphology. Different corrosion performance of the coatings in this case could be related to the stability of the passive layer, different cross section appearance and the existence of the defects and pores inside the layers.

It was seen that the cross section of the potassium silicate had more defects in the form of pores and crakes compared to the sodium silicate coating. Moreover, it was shown that the stability of the passive layer formed in the potassium silicate solution is lower than that in the sodium silicate. In the sodium phosphate group, very low stability of the passive layer and uneven structure of $Na_2H_2P_2O_7$ coating (fig 5.29-b) points to the poor quality of the coating. It is clear that the coating cannot effectively resist against the corrosion attack. So the corrosion resistance of the $Na_2H_2P_2O_7$ coating shows the lowest value compared to the other coating in the group. On the other hand the coating produced in the Na_3PO_4 solution showed the highest corrosion resistance compared to the other coatings. This could be attributed to the more compact structure of the coating (fig 5.29-d) and higher stability of the passive layer.

In the potassium phosphate group, the poor cross section of the $K_4P_2O_7$ coating with a lot of interconnected pores in the structure of the coating resulted in lower corrosion resistance compared to the K_3PO_4 coating. On the contrary, the cross section of the K_3PO_4 coating shows lower defects and its passive layer is more stable. These conditions lead to the higher corrosion resistance of the coating. In the case of $NaAlO_2$ coating, the weak performance of the layer would be expected because the coating is so thin and non uniform. So the coating cannot provide proper protection for the magnesium substrate.

A corrosion evaluation of the coatings which have higher corrosion resistance in their own group, i.e. Na_2SiO_3, Na_3PO_4, K_3PO_4 and $NaAlO_2$ coatings, showed that the Na_2SiO_3 and $NaAlO_2$ solutions produced the highest and the lowest corrosion resistance coatings, respectively. The coatings produced by Na_3PO_4 and K_3PO_4 solutions showed comparable corrosion properties. The corrosion resistance of the latter coatings is higher than $NaAlO_2$ but lower than Na_2SiO_3 coatings. Different corrosion resistance of the coatings could be explained by considering the effective parameters which are stability of the passive layer, thickness, phases and structure (cross section) of the coating. It is worth mentioning that a passive layer forms over the surface before the breakdown phenomenon [19,104,128]. It is also reported that characteristics of the passive layer on the metal surface show a direct relationship with corrosion resistance of the PEO coating [3,98,101].

In spite of what is expected, no relationship can be seen between the open pores data listed in Table 5.8 and the corrosion resistance of the coatings. This could be explained by considering the experimental method which is based on the immersion of the coatings in acidic solution. The acidic solution can dissolve the passive layer acting as a barrier against the corrosion. So, those parts of the substrate which are protected by the passive layer are designated as an open pore, which is incorrect. The time required for the acidic solution to reach the substrate is another parameter which makes the method unreliable. Different thicknesses of the coatings require different penetration times. So the thinner coatings are more affected by acidic solutions compared to the thicker ones.

In order to find out if any relation exists between the passive layer and the PEO coatings, the corrosion resistance data of the PEO coatings (Figs. 5.28, 5.30, 5.32, 5.34) were compared with the passive layer stability data (Figs. 5.22, 5.23, 5.37). The results showed that the more stable passive layer results in a PEO coating with higher corrosion resistance. For example, it is seen that in silicate group the sodium silicate solution produces more stable passive layer. The PEO coating produced in the same solution also shows the higher corrosion resistance. This trend can be seen in the other groups as well. For example, the stability of the passive layers in the sodium phosphate group is as Na_3PO_4 >$Na_5P_3O_{10}$>$Na_2H_2P_2O_7$. The corrosion resistance data also show the same trend. In other words, the PEO coating prepared in Na_3PO_4 solution has higher corrosion resistance than $Na_5P_3O_{10}$ and that of the latter is higher than $Na_2H_2P_2O_7$.

It is seen that where a more stable passive layer forms on the surface, a more corrosion resistant coating obtains. This suggests that a correlation exists between the passive layer and the properties of the PEO coating. It seems that a more stable passive layer formed in the initial steps of the coating process provides a more effective barrier layer on the surface which consequently improves the corrosion performance of the PEO coating. The results of the XPS study in the previous section also showed that the passive layer formed during the initial stages of the PEO process keep surviving on the surface even after the formation of the PEO coating. Therefore the stability of the passive layer is an effective parameter which directly influences on the corrosion resistance of the PEO coatings.

The corrosion evaluation of the coatings prepared by different hydroxides (Fig. 5.36) showed that the addition of KOH resulted in a more corrosion resistant coating compared to the others. Higher corrosion resistance of the KOH coating could be attributed to the greater thickness of the coating. The greater thickness of coating provided a more effective barrier against the passing current. Therefore the sparks became lower in number but more powerful in intensity in order to pass through the thick barrier. The bigger sparks provide enough energy for the stable phases such as Mg_2SiO_4 to develop during the coating process and contribute to the coating

structure. The thicker layer and the presence of more stable phases in the structure of coating are the parameters improving the corrosion performance of the coating prepared in the KOH solution.

6.2.3 Corrosion process of the PEO coating

The corrosion behaviour of the PEO coating in Fig. 5.38 showed that local corrosion mechanism controls the corroding behaviour of the PEO coating. It means that when a weak point of the coating breaks down and starts corroding, the main corrosion process concentrates on the point and the corroding pattern propagates and covers all the sample from the point.

A more detailed study of the coating by the curve fitting method showed that the resistance of the outer layer (R_1 value) follows a descending trend in the first 3.5h of the immersion period (Fig. 5.42). This could be related to the penetration of the electrolyte into the pores of the outer layer and the gradual degradation of the inner layer. Fig. 5.38-b also showed that small bubbles appear on the surface of the coating shortly after immersion in the test solution. Appearance of the bubbles in this stage could be attributed to the penetration of the solution into the outer layer which replaces with the gas existing inside the pores.

Within the first 2.5h, the resistance of the inner layer (R_2) remains almost unchanged and then starts decreasing. This is the period in which the electrolyte reaches the inner/outer interface and degradation of the inner layer starts. The R_2 value showed a reduction trend after 2.5h of immersion which lasts until 7.5h. This indicates that the NaCl solution has started to affect the inner layer. The inner layer gets thinner and/or some new tiny pores and cracks forms in the layer [129]. Fig. 5.38-c,d also showed that in longer immersion periods, the bubbles got bigger in size but fewer in number. As the electrolyte has reached the substrate in this stage, the appearance of the bubbles could be related to the corrosion reactions. Reduction in the number of the bubbles and the bubbles getting restricted to only a few points is also in agreement with local corrosion mechanisms of the magnesium.

The R1 showed a shift in value after 3.5h of the immersion. The shift of R_1 could be interpreted as hydration of the MgO. It is known that the MgO is not thermodynamically stable in neutral salt solutions and it gets hydrated to produce $Mg(OH)_2$. The molar volume of $Mg(OH)_2$ is higher than MgO, therefore it fills the pores and prevents easy penetration of the electrolyte inside the coating. However, the $Mg(OH)_2$ is a poor corrosion resistant material in nature and yields in periods of exposure longer than 4.5h [129].

After 7.5h of immersion, the R_1 and R_2 follow an ascending trend. A sudden shift also occurs in the impedance curves after 7.5h of immersion (Fig. 5.41). This kind of behaviour could be related to the formation of a passive layer on the magnesium surface. As it was explained; the inner layer is deteriorated by contact with the electrolyte and gets thinner and/or forms some defects e.g. tiny pores or cracks. The electrolyte passes through the defected layer and touches the substrate. However the pH of the electrolyte in narrow positions like the bottom of the pores increases and provides proper conditions for the formation of a stable passive film [34,98]. The R1 and R2 show degradation again because the passive layer breaks down in longer exposure periods and some pits appear on the surface. Fig 5.38-d also shows that the first sign of corrosion products appear on the surface almost after almost 10h. The pitting mechanism is what happens during the corrosion process of the PEO coating. Morphology of a typical corroded area in Fig 5.43 showed that the coating was deteriorated and some cracks formed in the pit area. The formation of the cracks could be attributed to hydration of MgO to $Mg(OH)_2$. The volume expansion occurring during the transformation could change the mechanical stress within the coating layers, which leads to the development of cracks [129].

6.3 The role of thickness in the corrosion resistance of the PEO coating

This section discusses how thickness influences the corrosion performance of the coating and what would be the optimal thickness in which the higher corrosion resistance of the PEO coating obtains.

It was explained that the surface morphology (e.g. holes and pores) [8,9,10], phase composition [11,12,13] and thickness [6,7] are effective parameters which influence the final corrosion performance of the PEO coating. However, study of the thickness is more important because the surface morphology and phase composition by themselves are influenced by thickness. But thickness is not influenced by surface morphology or phase composition.

Morphology of the PEO coating e.g. the size and number of pores is directly related to the characteristics of the sparks. However, as Fig. 5.1 showed, the size and number of the sparks changes as the process proceeds and the coating layer becomes thicker [12,58,96].

The *phase composition* of the PEO coating is also influenced by the thickness of the coating. It was also explained that greater thicknesses of the coating requires more powerful sparks and more powerful sparks produces the phases which needs higher energy to form. Thus, the thickness of the coating layer influence the type of the phases in the coating [48,95,118].

In order to study the influence of thickness on corrosion resistance of the coating, the main parameters determining the final thickness of the PEO coatings, namely current density, time and concentration of the coating solution, have been varied to generate different thicknesses. Subsequently, the corrosion resistance of the coatings were evaluated and behaviour of the coatings was studied. It can be stated that the thickness directly and current density, time and concentration indirectly determine the final corrosion properties of the PEO coatings.

6.3.1 Constant voltage treatments

Fig. 5.46 shows that in the potential range between the breakdown and 270 V the growth rate of the coating is almost constant. Beyond this value, however, both parameters, i.e. weight gain and coating thickness, show sudden increase. In order to study the growth behaviour of the PEO coating the voltage-weight gain & voltage-thickness curves were considered in three stages. In the primary stage, i.e. the potentials below V_{BD}, the rate of layer formation is much less than dissolution of the metal. So, dissolution of the metal is the dominant mechanism which controls the process in this stage.

The second stage of the curves covers the voltages over V_{BD} to about 270V. In this range, the curves show a steady state condition. It shows that the both factors, i.e. formation and dissolution mechanisms are active and it seems that they have reached equilibrium condition. In this range, although the weight gain shows almost constant values, the thickness curve shows a slight increase rate. It means that in spite of coating formation, the total weight of the sample remains constant. This confirms that in this stage two mechanisms are active simultaneously and the coating grows inward from the original surface of the substrate [28].

In the third stage, over 270V, the coating is thick enough to prevent high rates of metal dissolution. The coating behaves as a barrier between the electrolyte and metal surface and the growth process is mainly controlled by formation of the coating. It is why the thickness and weight gain show quick rises in the third stage of the curves.

6.3.2 Influence of the current density on thickness and corrosion resistance

Fig 5.47 and Table 5.13 show the results regarding variation of thickness and corrosion resistance in different current densities. The results show that the coating period of the 72.5 mA/cm^2 coating is shorter than that of 36.2 mA/cm^2. However, the thicknesses of both coatings are comparable. In the case of the 72.5 mA/cm coating, the specimen even starts losing weight. This could be related to the over heated arcs produced during the burning effect. It is seen when the process reaches the burning point, independent of the duration of the coating process, the thickness of the

coatings reaches an almost equal value. It shows that over certain amounts of the current density, the process reaches the burning effect, which does not allow the coating to grow any more. The application of the higher value of the current densities just shortens the time required to get to the burning effect. The obtained results emphasize that it is not possible to obtain thick layers on the surface just by using higher current densities. Producing greater thicknesses is possible when combination of low current densities and longer period of process is applied. The latter results show consistency with the fact that the growth of the PEO coating is a diffusion control process.

On the other hand, the use of very low, i.e. 3.6 mA/cm^2, and very high current densities, i.e. 36.2 or 72.5 mA/cm^2, produces the coatings whose corrosion resistance is not good enough to protect the underlying substrate. The weakness of the 3.6 mA/cm^2 and 36.2 and 72.5 mA/cm^2 coatings originates from insufficient thickness and burning damage in the coatings, respectively.

6.3.3 Influence of process duration on thickness and corrosion resistance

Table 5.14 shows that the growth rate of the coating reaches a maximum in about 900 seconds and subsequently it declines until the end of the process. This behaviour of the growth rate could be related to the “anodic dissolution” and “layer formation” processes which are acting reversely during the process [4]. Lower growth rate of the 225s coating compared to that of the 900s happens because what has formed on the surface is still a thin layer which cannot provide an effective barrier against the dissolution process. As the coating gets thicker, a more effective barrier develops on the surface which reduces the speed of the anodic dissolution process.

As the coating gets thicker, it can plays a more effective role to reduce the speed of the “anodic dissolution” process. This leads to the lower concentration of the Mg^{2+} ions which are the constructive species contributing in the coating process [48,71]. So the rate of the “layer formation” slows down and results in lower growth rate. It is why after reaching a maximum value, the rate of growth shows a descending trend.

.

The thickness and weight gain data in Figs. 5.48 and 5.49 shows that the samples gain weight concurrent with the thickening of the coatings. Synchronized increase of the thickness and weight gain could be related to the higher rate of "layer formation" compared to that of the "anodic dissolution" [4]. It shows that the layer formed on the surface effectively decreases the rate of anodic dissolution compared to the rate of the layer formation process.

Table 5.14 shows the data related to the corrosion resistance of the coatings. The data shows that middle thicknesses have higher corrosion resistance compared to those with very thin or very thick coatings. The low corrosion resistance of very thin coatings makes sense because of insufficient material formed on the surface. However, despite typical expectations that a thicker layer of coating provides a more effective barrier against corrosion [6,7], thicknesses greater than a particular value deteriorate the corrosion properties of the coatings. This could be attributed to the stronger sparks appearing in the process when the coating reaches to a certain level of thickness. The stronger sparks create bigger holes on the coating surface and also damage the barrier layer formed directly on the metal surface. [92,95]

6.3.4 Influence of solution concentration on thickness and corrosion resistance

It was explained that from the beginning steps of the coating process in the 20 g/l solution, the sparks were larger in size, fewer in numbers, slower in mobility and orange in colour compared to the lower concentrations. These conditions are similar to the final steps of the coating process explained previously in Table 5.1. So it is obvious that the coating process reaches the burning point in a short time when the 20 g/l solution is used. The burning effect in high concentration of the solution could be attributed to high rate of thickening. In a comparable period, higher concentrations of the solution increase the growth rate of the coating. And a thicker coating can more effectively act as a barrier against the current passing. This is exactly what leads to the focusing of the current on local points and subsequently burning effect.

Fig. 5.50 showed that an intermediate thickness of the coating provides higher corrosion resistance. The low corrosion resistance of the thin layers (< 3.2µm) could be understood because it is not able to provide an effective barrier against the corrosive species and they can simply pass through the coating and reach the substrate. The resistance of the thin layer quickly diminishes and the corrosion process starts.

The thick coatings (>13.3 µm) also showed low corrosion resistance. This could be attributed to the size of the sparks which get bigger and produce higher temperatures in thicker layers of the coatings. Essentially, the charges require higher energy to pass through a thicker layer of coating. Under this condition, the current concentrates on some weak points of the coating layer to find a way to discharge. This is why the number of the sparks decrease but their size increases as the layer gets thicker. In fact, an increase in the diameter of the discharge channels is the way in which the passing current overcomes the resistance of the layer [92]. In this way, size and number of the sparks are by themselves affected by the thickness of the coating layer. It is believed that a PEO coating is composed of an inner compact layer and an outer layer [3,24,90] and the main corrosion resistance of the PEO coating originates from the inner layer [85,104]. Nevertheless, it is reported that the compactness of the inner layer deteriorates as the coating get thicker. The development of such structures could be attributed to the thermal stresses during the evolution of the coating as a result of the melting and solidification of hard ceramic compounds like magnesium oxide and magnesium silicate [130]. This could explain the poor corrosion resistance of the thick layers. A little improvement in corrosion resistance, which is seen in the 36.6 and 54.8 µm coatings, could be related to the intricate path through which the corrosive species should diffuse to reach the substrate.

7 Conclusions

1- The coating formation on substrate phases, namely Al_8Mn_5, β-phase and α-Mg was studied. The results showed that the formation process on each phase followed a particular behaviour. The formation process on Al_8Mn_5 particle was initiated from the particle/matrix interface. Initially, a ring with higher content of oxygen and silicon formed around the particle. Later on, the surface of the particle involved in the coating process concurrent with the breakdown phenomenon.

2- The formation process on the β-phase showed that the coating formed on the β-particle, had different composition and characteristics depending on the solution concentration. In a low concentration solution (i.e. 1g/l), big holes formed in the morphology of the layer. However, in higher concentrations (i.e. 10 and 20g/l), the break down phenomenon occurred with a delay which results in a lower thickness of coating on the β-phase.

3- The layer formation on the α-Mg matrix initiated with a net like deposition pattern. The nets are locations with higher percentage of silicon and oxygen which cover the whole area as the process proceeds. As the surface is covered, the breakdown phenomenon takes place and subsequently the PEO coating starts to form. The PEO coating formed in the low concentration solution (i.e. 1 g/l) showed an elongated structure of the pores on the surface. This kind of structure, however, cannot be seen in solutions with higher concentration (i.e. 10 or 20 g/l).

4- The solution species such as silicate ions participate in the formation process from the very initial stages of the PEO process to produce a passive layer on the surface. The XPS examination revealed that under the conditions used, the passive layer was composed of magnesium oxide and/or silicon dioxide.

5- The study of the phase distribution through cross section of the PEO coating showed that the initial layer which forms on the surface is composed of MgO/SiO_2 phases. As the PEO process proceeds, the Mg_2SiO_4 phase also forms in the structure of the coating. This effect generates a non-homogeneous coating with different

layers. The non-homogeneous distribution of the phases is intensified in diluted (1g/l) or concentrated (20g/l) solutions.

6- The stability of the passive layer forming on AM50 in different salt solutions and hydroxides solutions were determined. Based on the results, the passive layer formed in a sodium silicate solution is more stable than that in a phosphate or aluminate solution. The results also showed that the stability of the layer produced by KOH is greater than that of the NaOH, $Al(OH)_3$ and $Mg(OH)_2$ solutions.

7- It was found out that the stability of the passive layer is the parameter influencing the corrosion resistance of the PEO coating. Based on the results, more stable passive layer results in the higher corrosion resistance of the PEO coating. Under the conditions employed, combination of the Na_2SiO_3 and KOH was the proper solution which resulted in more stable passive layer and consequently more corrosion resistant PEO coating compared to the rest of the solutions tested.

8- The results showed that the solution composition influenced the thickness, morphology and phases of the PEO coatings. The silicate solution produced a coating composed of MgO and Mg_2SiO_4 with greater thickness compared to the phosphate and aluminate solutions. The least thickness of the coating was produced by aluminate solution.

9- Optical emission spectroscopy results showed that cations participate in the sparking process. Participation of the ions originating from the hydroxides (e.g. K^+) revealed that the hydroxide part added to the coating solution, not only adjusts the pH and conductivity, but also participates directly in the sparking phenomenon.

10- Based on the curve fitting results, the PEO coating produced by Na_2SiO_3+KOH solution consists of an inner and an outer layer. The inner layer has a more compact structure and demonstrates higher corrosion resistance, while the outer layer has a porous structure and shows poor resistance.

11-The results showed that the corrosion process of the PEO coating follows the local (pitting) corrosion mechanism. In other worlds, when a weak point of the coating is corroded, the main corrosion process concentrates in this point and propagates from this point to cover the whole sample.

12- The results showed that the thickness is the parameter which directly affect on the corrosion resistance of the coating. Moreover, the solution concentration, current density and time are the parameters which influence the thickness of the coating. As a result, the thickness directly and the latter parameters indirectly influence the corrosion resistance of the coating.

13- The results showed that under conditions used, an intermediate thickness of the coating resulted in the enhanced corrosion resistance of the coating. The optimum range of coating thickness was about 3-13 µm. The coatings thicker or thinner than this optimum range resulted in lower corrosion resistance of the coating.

8 References

[1] Y. Wang, J.Wang, J. Zhang and Z. Zhang, *Characteristics of anodic coatings oxidized to different voltage on AZ91D Mg alloy by micro-arc oxidization technique*, Mater. Corros. 56 (2005) 88-92.

[2] Q. Cai, L. Wang, B. Wei and Q. Liu, *Electrochemical performance of microarc oxidation films formed on AZ91D magnesium alloy in silicate and phosphate electrolytes*, Surf. Coat. Tech. 200 (2006) 3727-3733.

[3] A. Ghasemi, V.S. Raja, C. Blawert, W. Dietzel and K.U. Kainer, *Study of the structure and corrosion behavior of PEO coatings on AM50 magnesium alloy by electrochemical impedance spectroscopy*, Surf. Coat. Tech. 202 (2008) 3513-3518.

[4] L.O. Snizhko, A.L. Yerokhin, A. Pilkington, N.L. Gurevina, D.O. Misnyankin, A. Leyland and A. Matthews, *Anodic processes in plasma electrolytic oxidation of aluminium in alkaline solutions*, Electrochim. Acta 49 (2004) 2085-2095.

[5] A. Ghasemi, N. Scharnagl, C. Blawert, W. Dietzel, K.U. Kainer, *Influence of electrolyte constituents on corrosion behaviour of PEO coatings for magnesium alloys*, Surface Eng. in press.

[6] Y. Ma, X. Nie, D.O. Northwood and H. Hu, *Systematic study of the electrolytic plasma oxidation process on a Mg alloy for corrosion protection*, Thin Solid Films 494 (2006) 296-301.

[7] Y. Ma, H. Hu, D. Northwood and X. Nie, *Optimization of the electrolytic plasma oxidation processes for corrosion protection of magnesium alloy AM50 using the Taguchi method*, Journal of Materials Processing Technology 182 (2007) 58–64

[8] W. Dietzel, M. Klapkiv, H. Nykyforchyn, V. Posuvailo and C. Blawert, *Porosity and corrosion properties of plasma coatings on magnesium alloys*, Mater. Sci. 40, (2004) 585-590.

[9] O. Khaselev, D. Weiss and J. Yahaloma, *Anodizing of Pure Magnesium in KOH-Aluminate Solutions under Sparking*, J. Electrochem. Soc. 146 (1999) 1757-1761.

[10] H. Luo, Q. Cai, B. Wei, B. Yu, D. Li, J. He and Z. Liu, *Effect of $(NaPO_3)_6$ concentrations on corrosion resistance of plasma electrolytic oxidation coatings formed on AZ91D magnesium alloy*, J. Alloy. Compd. 464 (2008) 537-543.

[11] H.Y. Hsiao, H.C. Tsung and W.T. Tsai, *Anodization of AZ91D magnesium alloy in silicate-containing electrolytes*, Surf. Coat. Tech. 199 (2005) 127-134.

[12] J. Liang, L. Hu and J. Hao, *Characterization of microarc oxidation coatings formed on AM60B magnesium alloy in silicate and phosphate electrolytes*, Appl. Surf. Sci. 253 (2007) 4490-4496.

[13] H. Fukuda and Y. Matsumoto, *Effects of Na_2SiO_3 on anodization of Mg-Al-Zn alloy in 3 M KOH solution*, Corros. Sci. 46 (2004) 2135-2142.

[14] Y. Ma, J. Zhang and M. Yang, *Research on microstructure and alloy phases of AM50 magnesium alloy,* J. Alloy. Compd. 470 (2009) 515-521.

[15] G. Chadha, J. E. Allison, and J. W. Jones, *The Role of Microstructure on Ductility of Die-Cast AM50 and AM60 Magnesium Alloys,* Metallurgical and Materials Transactions A, Vol. 38A, (2007) 286-297

[16] H.E. Kadiri, Y. Xue, M.F. Horstemeyer, J.B. Jordon and P.T. Wang, *Identification and modeling of fatigue crack growth mechanisms in a die-cast AM50 magnesium alloy,* Acta Mater.a 54 (2006) 5061-5076.

[17] R.M. Wang, A. Eliezer and E.M. Gutman, *An investigation on the microstructure of an AM50 magnesium alloy,* Mater. Sci. Eng. A355 (2003) 201-207.

[18] H. Guo, M. An, S. Xu and H. Huo, *Formation of oxygen bubbles and its influence on current efficiency in microarc oxidation process of AZ91D magnesium alloy,* Thin Solid Films 485 (2005) 53 – 58

[19] A.L. Yerokhin, X. Nie, A. Leyland, A. Matthews and S.J. Dowey, *Plasma electrolysis for surface engineering,* Surf. Coat. Tech. 122 (1999) 73-93.

[20] H. Duan, C. Yan and F. Wang, *Effect of electrolyte additives on performance of plasma electrolytic oxidation films formed on magnesium alloy AZ91D,* Electrochim. Acta 52 (2007) 3785-3793.

[21] R.K. Rude, *Magnesium deficiency: A cause of heterogeneous disease in human,* J Bone Miner Res, 13 (1998) 749-758.

[22] M.Avedesian, H.Baker, Magnesium and Magnesium alloys, ASM Specialty Handbook, 1999, ISBN: 0-87170-657-1

[23] J.E. Gray and B. Luan, *Protective coatings on magnesium and its alloys-a critical review,* J. Alloy. Compd. 336 (2002) 88-113.

[24] V. Birss, S. Xia, R. Yue and R.G. Rateick Jr., *Characterization of Oxide Films Formed on Mg-Based WE43 Alloy Using AC/DC Anodization in Silicate Solutions,* J. Electrochem. Soc. 151 (2004) B1-B10.

[25] X. P. Zhang, Z.P. Zhao, F.M. Wu, Y.L. Wang and J. Wu, *Corrosion and wear resistance of AZ91D magnesium alloy with and without microarc oxidation coating in Hank's solution,* J. Mater. Sci. 42 (2007) 8523-8528.

[26] M. Abdellatif, M. Freeman, *Mintek Thermal Magnesium Process: Status and Prospective,* Advanced Metals Initiative, Gold Reef City, Johannesburg, South Africa (2008) 1-13

[27] M. Jonsson, D. Thierry and N. LeBozec, *The influence of microstructure on the corrosion behaviour of AZ91D studied by scanning Kelvin probe force microscopyand scanning Kelvin probe,* Corros. Sci. 48 (2006) 1193-1208.

[28] W. Xue, Z. Deng, R. Chen and T. Zhang, *Growth regularity of ceramic coatings formed by microarc oxidation on Al/Cu/Mg alloy,* Thin Solid Film. 372 (2000) 114-117.

[29] J. Tian, Z. Luo, S. Qi and X. Sun, *Structure and antiwear behavior of micro-arc oxidized coatings on aluminum alloy,* Surf. Coat. Tech. 154 (2002) 1-7.

[30] N.P. Sluginov, J. Russ. Phys. Chem. Soc., 12 (1880) 193.

[31] A.Gunterschultze and H. Betz, *Electrolytkondensatoren* (1937) Berlin: Krayn.

[32] K. Huber, *Anodic Formation of Coatings on Magnesium, Zinc and Cadmium*, J. Electrochem. Soc., 100 (1953) 376-382.

[33] Dow Chemical Company, G.B. Pat. 762,195 (1956).

[34] Z Shi, G. Song and A. Atrens, *Influence of the beta phase on the corrosion performance of anodised coatings on magnesium-aluminium alloys*, Corros. Sci. 47 (2005) 2760-2777.

[35] H.A. Evangelides, US Patent 2,723,952. (1955) U.S.A.

[36] W. McNeill and L.L. Gruss, *Anodic spark reaction processes and articles*, US Patent 3,293,158. (1966) U.S.A.

[37] G.R. Kotler, D.L. Hawke, E.N. Aqua and G.L.Kotler, 33rd Annual Meeting-International Magnesium Association Proc., Montreal, Canada, 33 (1976) 45-48.

[38] G.L. Kotler, D.L. Hawke and E.N. Aqua, Light Met. Age 34 (1976), p. 20.

[39] Technology Application Group Incorporation, http://www.tagnite.com/.

[40] D.E Barak, B.E. Lemieux and E.R. Woolsey, US patent: 5470664, (1995)

[41] C. Blawert, W. Dietzel, E. Ghali, and G. Song, *Anodizing Treatments for Magnesium Alloys and Their Effect on Corrosion Resistance in Various Environments*, Adv. Eng. Mat. (2006), *8*, No. 6

[42] T.F. Barton, US Patent: 5792335,1998

[43] Keronite International Ltd,.http://www.keronite.com.

[44] AHC Oberflächentechnik GmbH, http://www.ahc-surface.com.

[45] Luke Engineering & Mfg. Co., http://www.lukeeng.com.

[46] S.Hutchins, S.Shrestha, A.Sturgeon,P.Shashkov and A.Shatrov, *The corrosion performance of sealed KERONITE coating on AZ91D magnesium alloys*, Magnesium: Proceeding of the 6th international conference magnesium and their application, ISBN:9783527309757

[47] A.L. Yerokhin, A. Shatrov, V. Samsonov, P. Shashkov, A. Leyland, A. Matthews, *Fatigue properties of Keronite coatings on a magnesium alloy*, Surf. and Coat. Tech. 182 (2004) 78–84

[48] H. Duan, C. Yan and F. Wang, *Growth process of plasma electrolytic oxidation films formed on magnesium alloy AZ91D in silicate solution,* Electrochim. Acta 52 (2007) 5002-5009.

[49] G.C. Wood and C. Pearson, *The theory of avalanche breakdown in solid dielectrics,* Corros. Sci. 7 (1967) 119-125.

[50] A. G. Rakoch, V.V. Khokhlov, V.A. Bautin, N.A. Lebedeva, Y.V. Magurova, and I.V. Bardin, *Model Concepts on the Mechanism of Microarc Oxidation of Metal Materials and the Control over This Process,* Prot. Met. 42 (2006) 158-169.

[51] A.K. Vijh, *Sparking voltages and side reactions during anodization of valve metals in terms of electron tunneling,* Corros. Sci. 11 (1971) 411-417.

[52] S. Ikonopisov, *Theory of electrical breakdown during formation of barrier anodic films,* Electrochim. Acta 22 (1977) 1077-1082.

[53] J.M. Albella, I. Montero and J.M.M. Duart, *A theory of avalanche breakdown during anodic oxidation,* Electrochim. Acta 32 (1987) 255-258.

[54] J.M. Albella, I. Montero, M.F. Bndez, C. G. Aleixandre and J.M.M. Duart, *Double anodization experiments in tantalum,* Electrochim. Acta 30 (1985) 1361-1364.

[55] M.D. Klapkiv, *Simulation of synthesis of oxide-ceramic coatings in discharge channels of a metal-electrolyte system,* Mater. Sci. 35 (1999) 279-282.

[56] A.L. Yerokhin, L.O. Snizhko, N.L. Gurevina, A. Leyland, A. Pilkington and A. Matthews, *Discharge characterization in plasma electrolytic oxidation of aluminium,* J. Phys. D. Appl. Phys. 36 (2003) 2110-2120.

[57] G. H. Lv, H. Chen, W. C. Gu, L. Li, E.W. Niu, X. H. Zhang, S. Yang, *Effects of current frequency on the structural characteristics and corrosion property of ceramic coatings formed on magnesium alloy by PEO technology***,** Journal of Materials Processing Technology, Volume 208, 21 (2008) 9-13

[58] B.H. Long, H.H. Wu, B.Y. Long, J.B. Wang, N.D. Wang, X.Y. Lu, Z.S. Jin and Y.Z. Bai, *Characteristics of electric parameters in aluminium alloy MAO coating process,* Appl. Phys. 38 (2005) 3491-3496.

[59] V.M. Posuvailo, *Analysis of the radiation spectra in the process of synthesis of zirconium oxide in an electrolytic plasma,* Mater. Sci. 37 (2001) 677-679.

[60] R.F. Zhang, D.Y. Shan, R.S. Chen and E.H. Han, *Effects of electric parameters on properties of anodic coatings formed on magnesium alloys,* Mater. Chem. Phys. 107 (2008) 356-363.

[61] G. Song and A. Atrens, Corrosion Mechanisms of Magnesium Alloys, Adv. Eng. Mat. 1 (1999) 11-33.

[62] A. Pardo, M.C. Merino, A.E. Coy, R. Arrabal, F. Viejo and E. Matykina, *Corrosion behaviour of magnesium/aluminium alloys in 3.5 wt.% NaCl,* Corros. Sci. 50 (2008) 823-834.

[63] M.C. Zhao, M. Liu, G. L. Song, A. Atrens, *Influence of pH and chloride ion concentration on the corrosion of Mg alloy ZE41*, Corrosion Science 50 (2008) 3168–3178

[64] *S. Bender, J. Goellner* and *A. Atrens, Corrosion of AZ91 in 1N NaCl and theMechanism of Magnesium Corrosion,* Advanced Engineering Materrials, 10, No. 6 (2008) 583-587

[65] H. Hoche, H. Scheerer, D. Probst, E. Broszeit, C. Berger, *Development of a plasma surface treatment for magnesium alloys to ensure sufficient wear and corrosion resistance,* Surface and Coatings Technology 174 –175 (2003) 1018–1023

[66] P. Schmutz, V. Guillaumin, R.S. Lillard, J.A. Lillard, G.S. Frankel, J. Electrochem. Soc. 150 (4) (2003) B99.

[67] ASM Handbook Vol.13 Corrosion, ASM International, 2005

[68] N. Hara, Y. Kobayashi, D. Kagaya and N. Akao, *Formation and breakdown of surface films on magnesium and its alloys in aqueous solutions*, Corros. Sci. 49 (2007) 166-175.

[69] J. Liang, B. Guo, J. Tian, H. Liu, J. Zhou, W. Liu and T. Xu, *Effects of $NaAlO_2$ on structure and corrosion resistance of microarc oxidation coatings formed on AM60B magnesium alloy in phosphate-KOH electrolyte,* Surf. Coat. Tech. 199 (2005) 121-126.

[70] R. Arrabal, E. Matykina, F. Viejo, P. Skeldon and G.E. Thompson, *Corrosion resistance of WE43 and AZ91D magnesium alloys with phosphate PEO coatings,* Corros. Sci. 50 (2008) 1744-1752.

[71] G.H. Lv, H. Chen, L. Li, E.W. Niu, H. Pang, B. Zou and S.Z. Yang, *Investigation of plasma electrolytic oxidation process on AZ91D magnesium alloy,* Current Applied Physics 9 (2009) 126-130.

[72] O. Khaselev and J. Yahalom, *The anodic behaviour of binary Mg-Al alloys in KOH Aluminate solutions,* Corros. Sci. 40 (1998) 1149-1160.

[73] O. Khaselev, D. Weiss and J. Yahalom, *Structure and composition of anodic films formed on binary Mg-Al alloys in KOH-Aluminate solutions under continuous sparking,* Corros. Sci. 43 (2001) 1295-1307.

[74] Y. Ma, X. Nie, D.O. Northwood and H. Hu, *Corrosion and erosion properties of silicate and phosphate coatings on magnesium*, Thin Solid Films 469-470 (2004) 472-477.

[75] Y. Mizutani, S.J. Kim, R. Ichino and M. Okido, *Anodizing of Mg alloys in alkaline solutions,* Surf. Coat. Tech. 169-170 (2003) 143-146.

[76] X. Nie, E.I. Meletis, J.C. Jiang, A. Leyland, A.L. Yerokhin and A. Matthews, *Abrasive wear/corrosion properties and TEM analysis of Al_2O_3 coatings fabricated using plasma electrolysis,* Surf. Coat. Tech. 149 (2002) 245-251.

[77] A.A. Voevodin, A.L. Yerokhin, V.V. Lyubimov, M.S. Donley and J.S. Zabinski, *Characterization of wear protective Al-Si-0 coatings forrned on Al-based alloys by micro-arc discharge treatment,* Surf. Coat. Tech. 86-87 (1996) 516-521.

[78] A.L. Yerokhin, A.A. Voevodin, V.V. Lyubimov, J.S. Zabinski and M.S. Donley, *Plasma electrolytic fabrication of oxide ceramic surface layers for tribotechnical purposes on aluminium alloys,* Surf. Coat. Tech. 110 (1998) 140-146.

[79] S. Verdier, M. Boinet, S. Maximovitch and F. Dalard, *Formation, structure and composition of anodic films on AM60 magnesium alloy obtained by DC plasma anodising,* Corros. Sci. 47 (2005) 1429-1444.

[80] M. Boinet, S. Verdier, S. Maximovitch and F. Dalard, *Plasma electrolytic oxidation of AM60 magnesium alloy Monitoring by acoustic emission technique electrochemical properties of coatings,* Surf. Coat. Tech. 199 (2005) 141-149.

[81] Die Casting Engineer. Vol. 47, no. 3, pp. 50-51. May 2003

[82] A.L. Yerokhin, A. Shatrov, V. Samsonov, P. Shashkov, A. Pilkington, A. Leyland and A. Matthews, *Oxide ceramic coatings on aluminium alloys produced by a pulsed bipolar plasma electrolytic oxidation process,* Surf. Coat. Tech. 199 (2005) 150-157.

[83] H.F. Guo and M.Z. An, *Growth of ceramic coatings on AZ91D magnesium alloys by micro-arc oxidation in Aluminate-fluoride solutions and evaluation of corrosion resistance,* Appl. Surf. Sci. 246 (2005) 229-238.

[84] Y. Zhang and C. Yan, *Development of anodic film on Mg alloy AZ91D,* Surf. Coat. Tech. 201 (2006) 2381-2386.

[85] R. Arrabal, E. Matykina, P. Skeldon, G. E. Thompson and A. Pardob, *Transport of Species during Plasma Electrolytic Oxidation of WE43-T6 Magnesium Alloy, Journal of The Electrochemical Society,* 155 (2008) C101-C111.

[86] G. Lv, W. Gu, H. Chen, W. Feng, M.L. Khosa, L. Li, E. Niu, G. Zhang and S.Z. Yang, *Characteristic of ceramic coatings on aluminum by plasma electrolytic oxidation in silicate and phosphate electrolyte,* Appl. Surf. Sci. 253 (2006) 2947-2952.

[87] C. Blawert, V. Heitmann, W. Dietzel, H.M. Nykyforchyn, M.D. Klapkiv, *Influence of electrolyte on corrosion properties of plasma electrolytic conversion coated magnesium alloys,* Surface & Coatings Technology 201 (2007) 8709–8714.

[88] A.V. Timoshenko and Y.V. Magurova, *Investigation of plasma electrolytic oxidation processes of magnesium alloy MA2-1 under pulse polarisation modes,* Surf. Coat. Tech. 199 (2005) 135-140.

[89] M.R. Ok, E.Y. Kang, J.H. Kim, Y.S. Ji, C. W. Lee, Y.J. Oh and K.T. Hong, *Analysis on the microstructure of ceramic coating layer fabricated by plasma electrolytic oxidation*, Mater. Sci. Forum 539-543 (2007) 1258-1263.

[90] C.S. Lin and Y.C. Fu, *Characterization of Anodic Films on AZ31 Magnesium Alloys in Alkaline Solutions Containing Fluoride and Phosphate Anions*, J. Electrochem. Soc. 153 (2006) B417-B424

[91] J.A. Curran and T.W. Clyne, *Porosity in plasma electrolytic oxide coatings*, Acta Mater. 54 (2006) 1985-1993.

[92] G. Sundararajan and L.R. Krishna, *Mechanisms underlying the formation of thick alumina coatings through the MAO coating technology*, Surf. Coat. Tech. 167 (2003) 269-277.

[93] Y.M. Wang, F.H. Wang, M.J. Xu, B. Zhao, L.X. Guo, J.H. Ouyang, *Microstructure and corrosion behavior of coated AZ91 alloy by microarc oxidation for biomedical application,* Applied Surface Science 255 (2009) 9124–9131

[94] J. Y. Cho, D.Y.Hwang, D. H. Lee, B. Yoo, D. Shin, *Influence of potassium pyrophosphate in electrolyte on coated layer of AZ91 Mg alloy formed by plasma electrolytic oxidation*, Trans. Nonferrous Met.Soc. China 19(2009) 824-828

[95] W.C. Gu, G.H. Lv, H. Chen, G.L. Chen, W.R. Feng and S.Z. Yang, *Characterisation of ceramic coatings produced by plasma electrolytic oxidation of aluminum alloy,* Mater. Sci. Eng. A 447 (2007) 158-162.

[96] Y.M. Wang, T.Q. Lei, B.L. Jiang and L.X. Guo, *Growth, microstructure and mechanical properties of microarc oxidation coatings on titanium alloy in phosphate-containing solution,* Appl. Surf. Sci. 233 (2004) 258-267.

[97] J. Liang, B. Guo, J. Tian, H. Liu, J. Zhou and T. Xu, *Effect of potassium fluoride in electrolytic solution on the structure and properties of microarc oxidation coatings on magnesium alloy,* Appl. Surf. Sci. 252 (2005) 345-351.

[98] J. Liang, P. Bala Srinivasan, C. Blawert, M. Störmer, W. Dietzel, *Electrochemical corrosion behaviour of plasma electrolytic oxidation coatings on AM50 magnesium alloy formed in silicate and phosphate based electrolytes* Electrochimica Acta, 54 (2009) 3842-3850

[99] R. Arrabal, E. Matykina, T. Hashimoto, P. Skeldon, G.E. Thompson, *Characterization of AC PEO coatings on magnesium alloys,* Surface & Coatings Technology, 203 (2009) 2207–2220

[100] R. Arrabal, E. Matykina, P. Skeldon,G. E. Thompson, *Incorporation of zirconia particles into coatings formed on magnesium by plasma electrolytic oxidation*, J. mater sci 43(2008) 1532-1538

[101] A. Ghasemi , V.S. Raja, C. Blawert, W. Dietzel, K.U. Kainer, *The role of anions in the formation and corrosion resistance of the plasma electrolytic oxidation coatings,* Surface & Coatings Technology 204 (2010) 1469–1478

[102] H. Ardelean, I. Frateur, S. Zanna, A. Atrens, P. Marcus, *Corrosion protection of AZ91 magnesium alloy by anodizing in niobium and zirconium-containing electrolytes*, Corrosion Science, 51 (2009), 3030-3038

[103] D. Y. Hwang, Y. M. Kima, D.Y. Park, B.Yoo,, D. H. Shin, *Corrosion resistance of oxide layers formed on AZ91 Mg alloy in KMnO4 electrolyte by plasma electrolytic oxidation*, Electrochimica Acta 54 (2009) 5479–5485

[104] N. Sato, *A theory for breakdown of anodic oxide films on metals,*Electrochemica Acta, 16 (1971) 1683 -1692

[105] H. Duan, K. Duc, C. Yan and F. Wang, *Electrochemical corrosion behaviour of composite coatings of sealed MAO film on magnesium alloy AZ91D*, Electrochim. Acta 51 (2006) 2898-2908.

[106] L.O. Snizhko, A.L. Yerokhin, N.L. Gurevina a, V.A. Patalakha, A. Matthews, *Excessive oxygen evolution during plasma electrolytic oxidation of aluminium*, Thin Solid Film. 516 (2007) 460-464.

[107] David R. Lide, *CRC Handbook of Chemistry and Physics*, 85th Edition.

[108] C. Blawert, V. Heitmann, W. Dietzel, H.M. Nykyforchyn, M.D. Klapkiv, *Influence of process parameters on the corrosion properties of electrolytic conversion plasma coated magnesium alloys*, Surf. Coat. Tech. 200 (2005) 68-72.

[109] R. Baboian, *Corrosion tests and standards*, 1995 ASTM manual series

[110] R.Cottis, S.Turgoose, Electrochemical impedance and noise, 1999, Nace international

[111] Z.R. Chang, Z. Jin**,** H.W. Jiu, W. Dietzel, K.U. Kainer, C. Blawert and K. Wei, *Review of studies on corrosion of magnesium alloys*, T. Nonferr. Metal. Soc. 16 (2006) s763-s771.

[112] M. Jonsson, D. Persson and D. Thierry, *Corrosion product formation during NaCl induced atmospheric corrosion of magnesium alloy AZ91D*, Corros. Sci. 49 (2007) 1540-1558.

[113] B. Messaoudi, S. Joiret, M. Keddam and H. Takenouti, *Anodic behaviour of manganese in alkaline medium*, Electrochim. Acta 46 (2001) 2487-2498.

[114] G. Y. Jun and X.Yuan, *Correlation between discharging property and coatings microstructure during plasma electrolytic oxidation*, T. Nonferr. Metal. Soc. 16 (2006) 1097-1102.

[115] G. Song, A. Atrens, X. Wu, Z. Bo and B. Zhang, *Corrosion behaviour of AZ21, AZ501 and AZ91 in sodium chloride*, Corros. Sci. 40 (1998) 1769-1971.

[116] M. Anik, G. Celikten, *Analysis of the electrochemical reaction behavior of alloy AZ91 by EIS technique in H3PO4/KOH buffered K2SO4 solutions*, Corrosion Science 49 (2007) 1878–1894

[117] L.J. Zhang, J.J. Fan, Z. Zhang, F.H. Cao, J.Q. Zhang, C.N. Cao, *Study on the anodic film formation process of AZ91D magnesium alloy*, Electrochimica Acta 52 (2007) 5325–5333

[118] Y. Wang, J. Wang, J. Zhang and Z. Zhang, *Effects of spark discharge on the anodic coatings on magnesium alloy*, Mater. Lett. 60 (2006) 474–478.

[119] L. Chai, X. Yu, Z. Yang, Y. Wang and M. Okido, *Anodizing of magnesium alloy AZ31 in alkaline solutions with silicate under continuous sparking*, Corros. Sci. 50 (2008) 3274-3279.

[120] M. Santamaria, F.D Quarto, S. Zanna and P. Marcus, *Initial surface film on magnesium metal: A characterization by X-ray photoelectron spectroscopy (XPS) and photocurrent spectroscopy (PCS)*, Electrochim. Acta 53 (2007) 1314-1324.

[121] http://srdata.nist.gov/xps/

[122] Q. Dong, L. Xiao and Q. Luo, *Preparation of Ceramic Membrane by Micro Arc Oxidation on Mg-Alloy*, Mater. Sci. Forum 488-489 (2005) 677-680.

[123] F. Monfort, A. Berkani, E. Matykina, P. Skeldon,G.E. Thompson, H. Habazaki and K. Shimizu, *Development of anodic coatings on aluminium under sparking conditions in silicate electrolyte*, Corros. Sci. 49 (2007) 672-693.

[124] V. Fournier, P. Marcus and I. Olefjord, *Oxidation of magnesium*, Surf. Interface Anal. (2002), 494–497

[125] Y. Bouvier , B. Mutel and J. Grimblot, *Use of an Auger parameter for characterizing the Mg chemical state in different materials*, Surf. and Coat. Tech 180 –181 (2004) 169–173

[126] F. A. Bonilla,A. Berkani,Y. Liu, P. Skeldon, G. E. Thompson, H. Habazaki, K. Shimizu, C. John, K. Stevensd, *Formation of Anodic Films on Magnesium Alloys in an Alkaline Phosphate Electrolyte*, *Journal of The Electrochemical Society*, 149 (2002) B4-B13

[127] O. Khaselev, J. Yahalom, *Constant Voltage Anodizing of Mg-Al Alloys in KOH-Al(OH)3 Solutions*, J. Electrochem. Soc., 145,(1998) 191

[128] H.F. Guo, M.Z. An, H.B. Huo, S. Xu and L.J. Wu, *Microstructure characteristic of ceramic coatings fabricated on magnesium alloys by micro-arc oxidation in alkaline silicate solutions*, Applied Surface Science 252 (2006) 7911–7916

[129] S. J. Xia, R. Yue, R. G. Rateick, Jr., V. I. Birss, *Electrochemical Studies of AC/DC Anodized Mg Alloy in NaCl Solution*, Journal of The Electrochemical Society, 151 (2004) B179-B187

[130] P. B. Srinivasan, J. Liang, C. Blawert, M. Stormer, W. Dietzel, *Effect of current density on the microstructure and corrosion behaviour of plasma electrolytic oxidation treated AM50 magnesium alloy*, Applied Surface Science 255 (2009) 4212–4218.

Eidesstattliche Erklärung

Hiermit erkläre ich an Eides statt, dass ich die vorliegende Arbeit selbständig ohne unerlaubte Hilfe verfasst und die benutzten Hilfsmittel vollständig angegeben habe und noch keine früheren Promotionsversuche unternommen habe.

Alireza Ghasemi Abyazani

Lebenslauf

Alireza Ghasemi Abyazani

Geburtstag: 20.09.1974
Geburtsort: Teheran / Iran

Studium

10/2007-06/2011 **Promotionsabschluss** in Materialwissenschaft (Ph.D.)
Technische Universität Clausthal, Deutschland
Schwerpunkt:
Entwicklung und Prozessoptimierung von Plasma Electrolytic Oxidation um Magnesiumteile vor Korrosion zu schützen.

10/1998-01/2001 **Masterabschluss** in Materialwissenschaft (M.Sc.)
Technischen Universität Sharif, Teheran, Iran
Schwerpunkt:
Verbindungen zwischen Mikrostruktur und mechanischen Eigenschaften der A-356 Aluminium-Legierungen

10/1993-06/1998 **Bachelorabschluss** in Werkstofftechnik (B.Sc.)
Shiraz Universität, Shiraz, Iran
Schwerpunkte:
Mikrostruktur und Eigenschaften der Werkstoffe, Werkstoffauswahl, Korrosionsprozess des Metalls.

Beruflicher Werdegang

10/2005-10/2009 **Wissenschaftlicher Mitarbeiter**
GKSS-Forschungszentrum Geesthacht GmbH, Deutschland
Institut für Werkstoffforschung, Korrosion Abteilung
Schwerpunkt:
Oberflächenbeschichtung und Korrosionsschutz metallischer Werkstoffe durch elektrochemische Prozesse

05/2001-07/2005 **Projektleiter**
Forschungs- und Entwicklungsabteilung, IKCompany (Autoproduzent), Iran
Schwerpunkte:
Gefügeanalyse, Verbesserung der mechanischen Eigenschaften von Autoteilen, Aluminiumlegierung, Magnesiumlegierung

Publikationen

1. **A. Ghasemi**, N. Scharnagl, C. Blawert, W. Dietzel, K.U.Kainer, "Influence of electrolyte constituents on corrosion behaviour of PEO coatings for magnesium alloys", Surface Engineering 26 (2010) 321-327
2. **A. Ghasemi**, V.S. Raja, C. Blawert, W. Dietzel, K.U. Kainer, "The role of anions in the formation and corrosion resistance of the plasma electrolytic oxidation coatings" Surface and Coatings Technology, 204 (2010) 1469–1478
3. **A. Ghasemi**, V.S. Raja, C. Blawert, W. Dietzel, K.U. Kainer, "Study of the structure and corrosion behaviour of PEO coatings on AM50 magnesium alloy by EIS" Surface and Coatings Technology, Vol. 202, 2008, 3513-3518.
4. **A.Ghasemi,** F.Khomamizadeh, "Quantitative microstractural analysis of A-356 aluminium alloy and its effect on mechanical properties" Sharif Journal of Sci. & Tech., No.28, 2005, 38-42.
5. F.Khomamizadeh, **A.Ghasemi**, "Evaluation of quality index of aluminium alloy by microstructure analysis" Scientia Iranica, Vol.11, No.4, 2004, 386-391.

Vorträge

1. **A. Ghasemi**, N. Scharnagl, C. Blawert, W. Dietzel, K.U.Kainer, "Effect of hydroxides on the corrosion properties of magnesium alloys coated by PEO process", 21st Int. conf. on Surf. Modification Tech., Paris, France, Sep. 2007.
2. **A.Ghasemi,** C. Blawert, W. Dietzel, K.U.Kainer "Corrosion protection of magnesium alloys by PEO process", DFG-SPP 1168 (InnoMagTec), Sonnenberg International House, St. Andreasberg, Germany, Dec. 2006.
3. **A.Ghasemi**, F.Khomamizadeh "Microstructure and mechanical properties of aluminium alloy" 13th Foundry Seminar, Iran Uni. of Sci. & Tech., Jun. 2001.

Projekte

1. "Qualitätsverbesserung der metallische Gußteile durch Modifizierung des Sandgusses"- Forschung und Entwicklung Organisation, Teheran-Iran (2004)
2. "Verbesserung der maschinelle Bearbeitbarkeit von Aluminiumlegierung A-319 durch Modifizierung des Gefüges " IKCompany, Teheran-Iran, (2003)
3. "Gefügeanalyse und mechanischen Eigenschaften von Autoteile aus Magnesiumlegierung AZ-91", IKCompany, Teheran-Iran (2002)
4. "Verbesserung der mechanische Eigenschaften von Auto Zylinderkopf durch Gefügemodifizierung", IKCompany, Teheran-Iran (2001)

Sprachkenntnisse

Englisch: fließend in Wort und Schrift
Deutsch: sehr gut in Wort und gut in Schrift
Persisch: Muttersprache

Anwendungssoftware

Microsoft Office, Z-view, Image Analyzer

Veröffentlichungsliste

Zeitschriften

1. **A. Ghasemi**, N. Scharnagl, C. Blawert, W. Dietzel, K.U.Kainer, “Influence of electrolyte constituents on corrosion behaviour of PEO coatings for magnesium alloys”, Surface Engineering 26 (2010) 321-327

2. **A. Ghasemi**, V.S. Raja, C. Blawert, W. Dietzel, K.U. Kainer, “The role of anions in the formation and corrosion resistance of the plasma electrolytic oxidation coatings” Surface and Coatings Technology, 204 (2010) 1469–1478

3. **A. Ghasemi**, V.S. Raja, C. Blawert, W. Dietzel, K.U. Kainer, “Study of the structure and corrosion behaviour of PEO coatings on AM50 magnesium alloy by EIS” Surface and Coatings Technology, Vol. 202 (2008) 3513-3518.

Konferenzen

4. **A. Ghasemi**, N. Scharnagl, C. Blawert, W. Dietzel, K.U.Kainer, “Effect of hydroxides on the corrosion properties of magnesium alloys coated by PEO process", 21st Int. conf. on Surf. Modification Tech., Paris, France, Sep. 2007.

5. **A. Ghasemi,** C. Blawert, W. Dietzel, K.U.Kainer “Corrosion protection of magnesium alloys by PEO process”, DFG-SPP 1168 (InnoMagTec), Sonnenberg International House, St. Andreasberg, Germany, Dec. 2006.